Design, Construction and Reactivity of Porous Frameworks with Substitution-Labile Sites

ITOH TAKAHIRO

Doctor of Philosophy

Department of Structural Molecular Science
School of Physical Sciences
SOKENDAI (The Graduate University for Advanced Studies)

Design, Construction and Reactivity of Porous Frameworks with Substitution-Labile Sites

置換活性サイトを有する多孔性フレームワークの設計・構築ならびに反応性

Takahiro Itoh

March 2017
Department of Structural Molecular Science
School of Physical Sciences
The Graduate University for Advanced Studies

Contents

General Introduction

Porous frameworks constructed by molecular assembly

Porous materials are of interest not only for academia but also for industry because of their characteristic properties utilized for adsorbates, separation or purification of chemicals and heterogeneous catalysts. Among those materials, porous frameworks constructed by molecular assembly have an advantage in functionalization compared to other porous materials such as zeolites, carbon-based materials and so on because the pore structures of molecular porous frameworks are well-defined and modification of the pore surface at the molecular level can be achieved. Those porous frameworks can be classified into three categories (Figure 1): metal-organic frameworks (MOFs) or porous coordination polymers (PCPs), porous organic frameworks (POFs) including covalent organic frameworks (COFs), and supramolecular organic frameworks (SOFs).

MOFs or PCPs are constructed by connecting inorganic secondary building units (SBUs) with organic linker and synthesized under mild conditions compared to zeolites and carbon-based materials. Due to the infinite combination of them, more than 20,000 different MOFs have been reported for past decades. The network topologies can be designed by consideration of the geometry of organic linker and inorganic SBUs which is so called as reticular chemistry.[1] Since they are crystalline materials, there is one of the advantages of these materials that atomic level analysis can be achieved by X-ray diffraction. In addition, MOFs have a characteristic feature for design-ability to afford functionalization of pore surfaces. Not only inherent porosity, but also incorporation of Lewis acidic/basic or open metal sites enables MOFs to be applied for broad applications[2-8] (e.g., gas adsorption/storage,[2,3] sensing,[2b,4] drug delivery, [2b,5] conductive materials,[2b,6] magnetic materials, [2b,7] heterogeneous catalysts, [2,8] etc.).

Recently, POFs have emerged as a new family of porous materials to show attractive features such as high surface area, design-abilities and high thermal and chemical stabilities and so on. POFs are synthesized by polymerization of organic monomer and the properties or structures of POFs are strongly depending on the choice of monomers and polymerization reactions. The monomers with special geometry, for example, linear pattern, planar triangle, square, tetrahedron, octahedron, etc. determines

resulting POF structure.[9] In terms of polymerization reaction, the reversibility decides the fate of resulting POFs. From the perspective, POFs can be divided in two classes: amorphous POFs and crystalline POFs. While, for the synthesis of amorphous POFs, irreversible covalent bonds formation reactions such as coupling reactions are used, reversible reactions which are thermodynamically controlled reactions are necessary for the synthesis of crystalline POFs. In 2005, O. M. Yaghi and coworkers achieved a breakthrough for syntheses of crystalline POFs, so called COFs to change the traditional concept that POFs are amorphous rather than crystalline.[10] Since then, the chemistry of POFs have developed drastically and special applications of POFs in a wide range of areas such as gas adsorption/storage,[9,11] catalyst,[9,12] optical and electronic materials[9] have also been reported.

SOFs in this context mean crystalline SOFs formed through non-covalent interactions such as hydrogen bonds, halogen bonds, π-π interaction, or van der Waals forces. As well as POFs, SOFs have recently been paid considerable attention as promising porous materials due to their soft and flexible nature. Additionally, crystalline nature of those materials enables us not only to determine the precise structures by X-ray crystallography but also to investigate the relationships between crystal packings and properties. However, SOFs are mostly not enough robust to maintain their porosity upon guest removal because non-covalent interaction is relatively weak and the removal of included guest typically causes phase change to give denser-packed structures. Therefore, there are relatively few reports of SOF materials possessing permanent porosity confirmed with gas sorption property.[13] In order to avoid such collapse, judicious choice of organic modules of which packing favors the formation of spatial voids is important. This field is still challenging but it should be worth exploring as we can see in several applications of these materials for such as gas adsorption/storage,[13] drug delivery,[14] molecular recognition,[15] fluorescence sensing,[16] separation of toxic chemical[17] and so on.

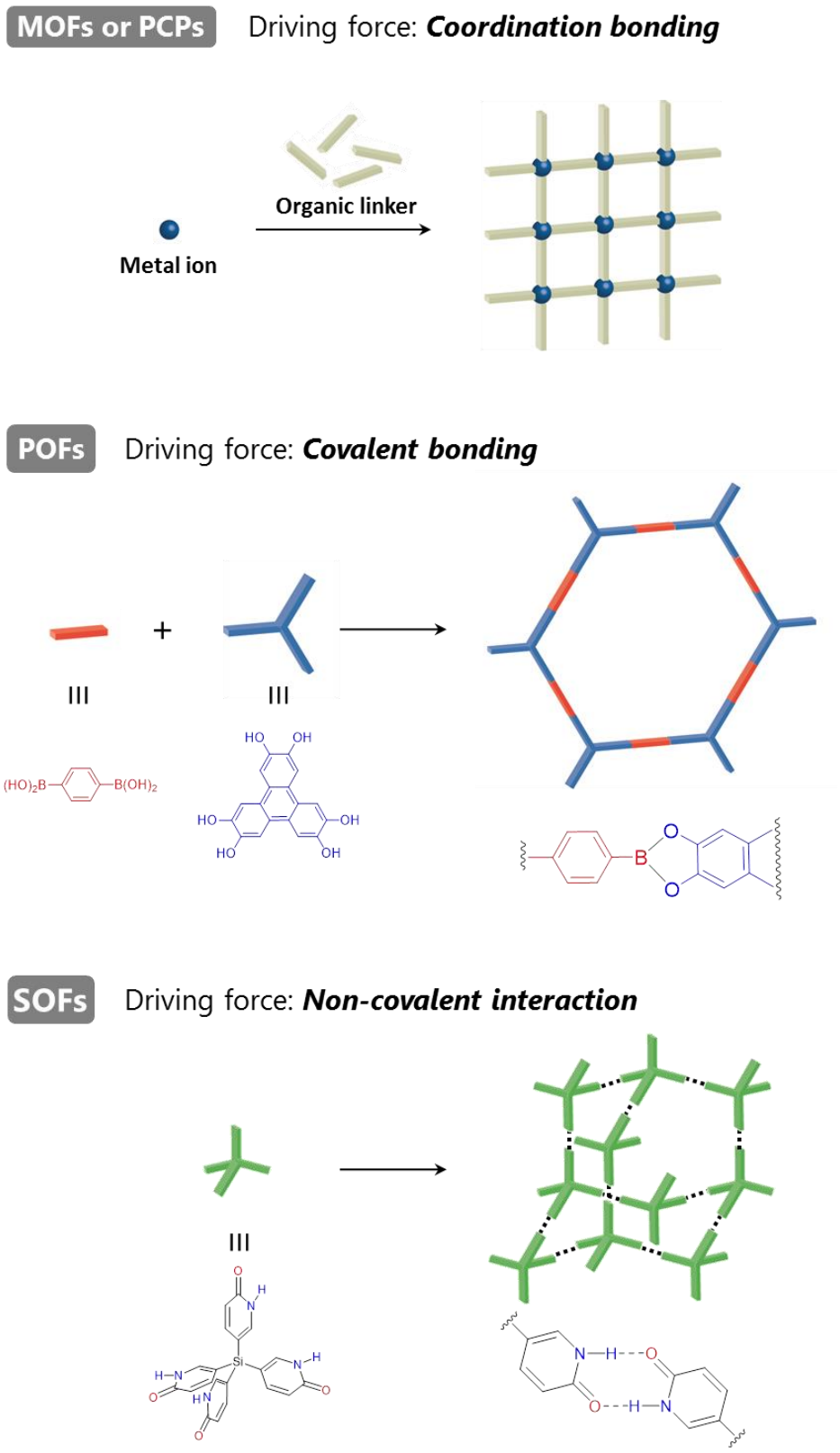

Figure 1. Synthesis of MOF or PCPs, POFs, and SOFs

Porous frameworks with open metal sites

In 2000, O. M. Yaghi and co-workers firstly used the term *open metal sites*[18] (also called as *unsaturated metal centers, accessible metal sites, exposed metal sites)* which refers to a metal center with coordinatively unsaturated sites or labile solvent molecules. Immobilization of open metal sites which can be a molecular recognition sites is one of the ways to functionalize the pore surfaces of porous frameworks. Porous frameworks in this context mean MOFs or PCPs because there are relatively few reports on other porous frameworks with open metal sites[19] By incorporating open metal sites, a diversity of unique MOFs have been developed and resulted in enhanced activity or giving new functions for example, gas storage/adsorption,[20] heterogeneous catalysts,[21] magnetic properties,[22] sensing (Figure 2).[23] In parallel, methods to incorporate open metal sites have been also pursued as mentioned in the next section.

Functionalization of porous frameworks by incorporation of open metal sites should be explored further to develop practically useful porous materials accompanied with the development of MOFs or PCPs and supramolecular frameworks.

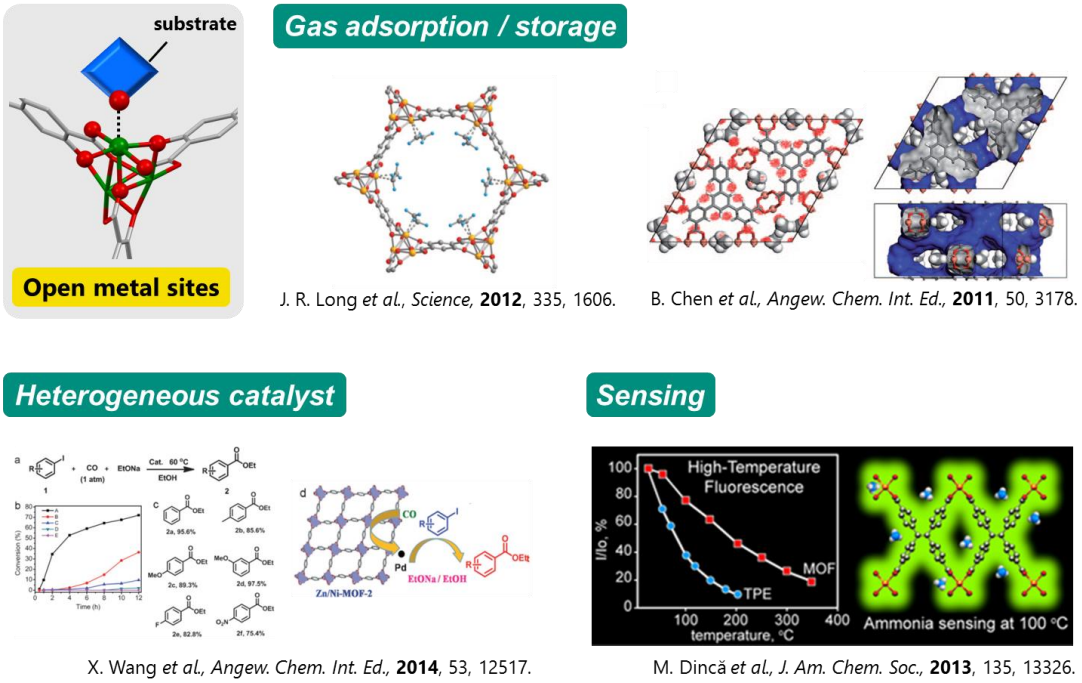

Figure 2. Applications of MOF or PCPs with open metal sites. Reproduced with permission from J R. Long Iet *al.*,[20c] B. Chen *et al.*,[20g] X. Wang *et al.*,[21c] and M. Dincă *et al.*[23b]

Methods for incorporation of open metal sites into porous frameworks

There seem to be three prominent ways for the incorporation of open metal sites. As first approach, secondary building units (SBUs) with unsaturated coordination sites such as paddle-wheel complex $[M_2(O_2CR)_4]$,[24a] trigonal prismatic clusters $[M_3O(O_2CR)_6]$[24b] are utilized (Figure 3a). In second approach, metal centers mainly as catalytic sites are directly incorporated into the linker ligands to form metalloligand before construction of framework (Figure 3b).[25] Third one is post-synthetic modification which means incorporation of another metal center into the chelating ligands after the framework synthesis (Figure 3c).[26]

However, in spite of these developments, it is still difficult to obtain single-crystalline materials and the problem prevents the precise determination of the local environment around open metal sites.

One of the solutions for the problem is the utilization of non-covalent interactions (e.g., hydrogen bonds, π-π interactions, van der Waals interactions and host-guest interactions) which enable to assemble units in ambient condition as described in the explanation of SOFs of first section.[13-16] This strategy can be one of the promising tools to construct porous framework as previously reported.[19] Compared to covalent bonding, these forces are weaker and less directional, but increase of interaction sites can overcome these disadvantages. Self-assembly of metal complexes via intermolecular interaction should extend unexplored porous materials which are difficult to construct by coordination-driven self-assembly.

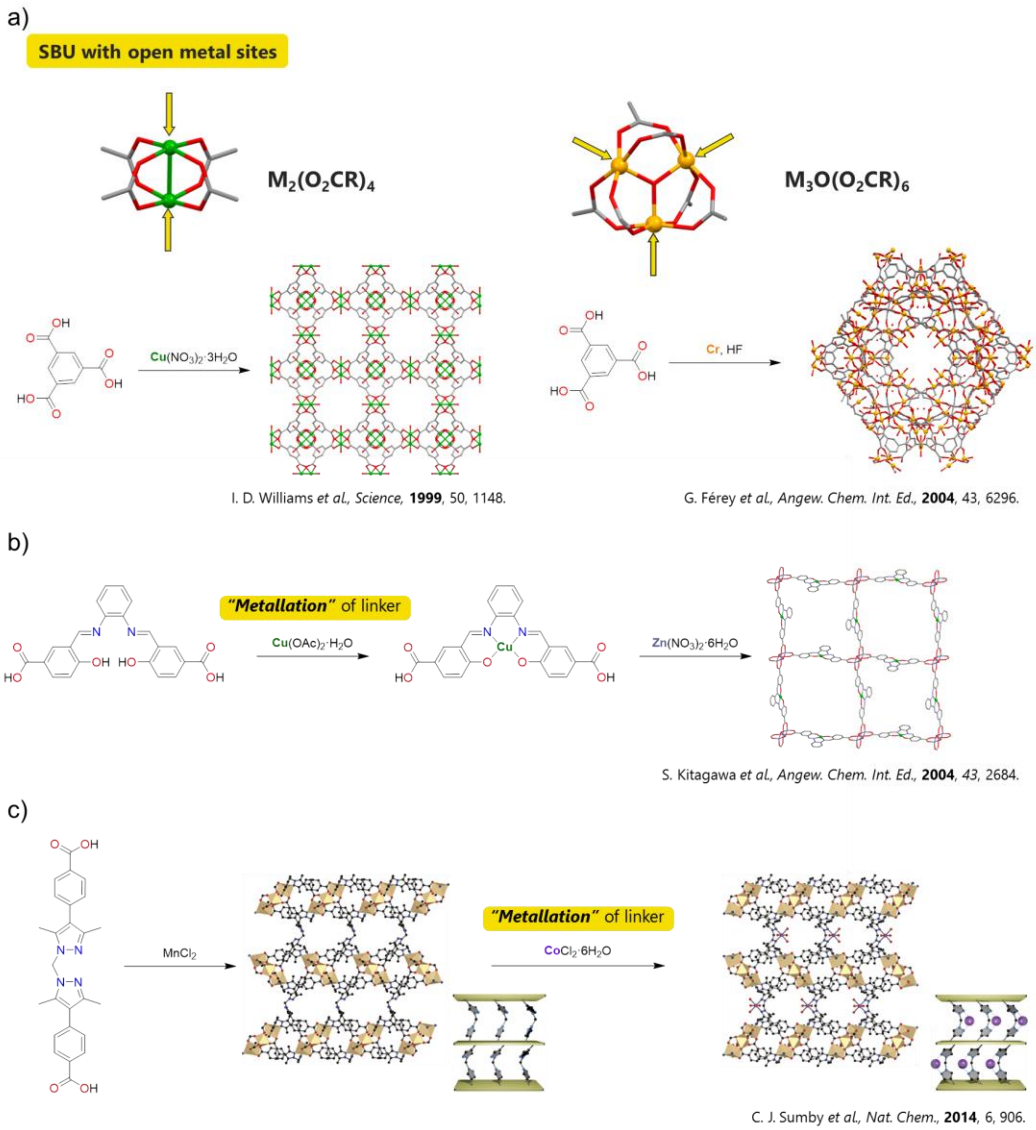

Figure 3. Methods for incorporation of open metal sites into MOFs or PCPs: (a) utilization of SBUs with open metal sites (b) utilization of metalloligand (c) post-synthetic modification. Reproduced with permission from C. J. Sumby *et al.*[26c]

Arene-perfluoroarene (Ar-Ar^F) interaction as a tool for controlled self-assembly

In 1960, Patrick and co-workers reported a co-crystal of benzene and hexafluorobenzene which comes from firstly observed arene-perfluoroarene interactions.[27] Unlike arene-arene interaction, which can usually exhibit both face-to-face (π-π) and edge-to-face (CH-π) interactions, face-to-face interaction is dominantly observed between arene and perfluoroarene due to the van der Waals and quadrupole-quadrupole interactions.[28] By utilization of this interaction as a tool for molecular assembly, several interesting researches have been reported as shown below.

For the construction of closely arranged metal-metal systems, A. Hori and co-workers reported co-crystals of two different β-diketonate metal complexes thorough Ar-Ar^F interaction.[29a] Two different metal complexes in arene- and perfluoroarene-functionalized ligands successfully arranged alternately to give one-dimentional structures by columnar stacking.

Compared to rare applications for assembly of metal complexes using Ar-Ar^F interaction,[29] there are relatively a large number of examples for assembly of organic molecules.[30] The applications began with crystal engineering[31] possibly due to the discovery of the interaction in co-crystal of benzene and hexafluorobenzene. Concomitantly, topochemical polymerization or dimerization has also been developed by the control of the distance between reactive chemical bonds.[32] As other applications, construction of porous frameworks can be listed. T.-H. Chen and co-workers reported porous non covalent organic framework by combination of hydrogen bonds and Ar-Ar^F interactions.[33] This framework is thermally robust and stable up to 250°C and exhibits high affinity for the adsorption of hydrocarbons and their halogenated derivatives, which are potent greenhouse species.

From these reports, it is apparent that Ar-Ar^F interaction is definitely an efficient supramolecular synthon. Considerable broad applications of this interaction might be attributed to the facility of introducing phenyl and perfluorophenyl ring moiety into molecules to be assembled. As indicated in recent studies,[33,34] utilization of this interaction still knows no boundaries.

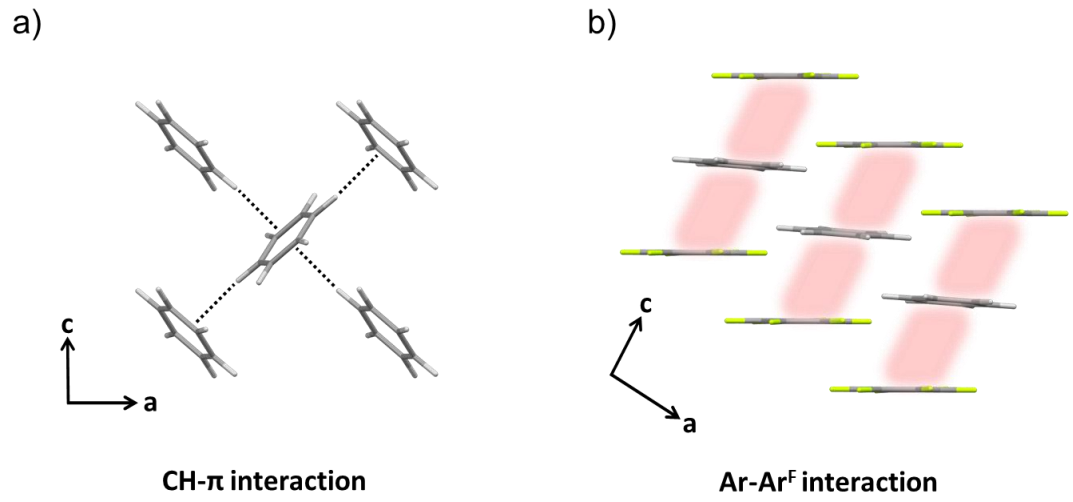

Figure 4. Crystal packing of (a) benzene and (b) co-crystal of benzene and hexafluorobenzene.

Rh(II) paddle-wheel complexes

The first paddle-wheel structure of Rh(II) complex, $Rh_2(OAc)_4(H_2O)_2$ has been reported by A. S. Antsyshkina *et al*. in 1962,[35] and since then, the related compounds obtained by mainly ligand exchange reaction of $Rh_2(OAc)_4(H_2O)_2$ have been extensively investigated.[36] The complexes consists of dinuclear Rh(II) with a Rh- Rh bond and four bridging ligands and possess D_{4h} symmetrical structure (Figure 5). Two axial sites of rhodium center can serve as substrate binding sites or catalytic sites to lead to numerous applications in many different research fields. They have been extensively utilized to develop antitumor agents,[37] NMR shift agents, [38] gas adsorbate,[39] sensors[40] and catalysts.[41] Nonetheless, most applications were focused on catalysts which make it possible to perform a variety range of reactions[41] (e.g., oxidation, H_2 production, hydrogenation, cyclopropanation, C-H insertion, C-H amination, and so on). In terms of organic transformations, metal-carbenoid intermediate is important for tuning the reactivity of the carbene and mechanistic studies have been reported.[42]

In spite of the rarity of rhodium metal on the earth, much attention is still paid due to the unique reactivity of the substitution-labile axial sites and high stability arising from the substitution-inert bridging ligands which is considered to be very important for catalytic reaction.

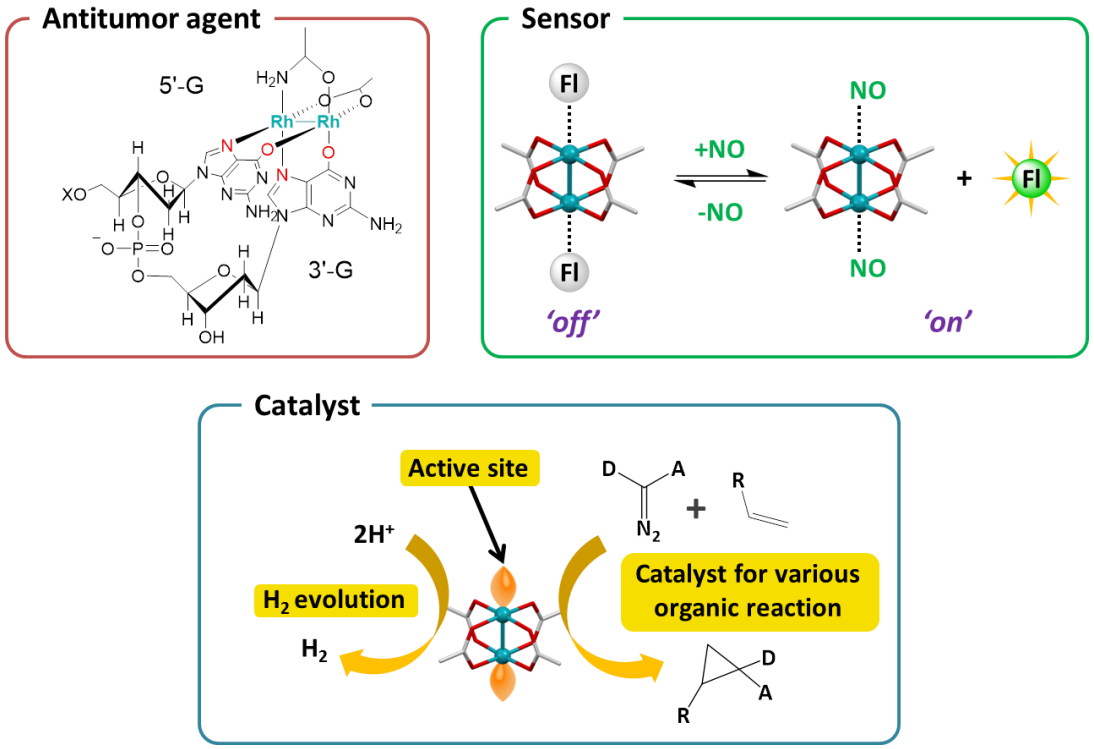

Figure 5. Applications of Rh(II) paddle-wheel complexes.

The aim of this thesis

As mentioned above, porous frameworks composed of organic or organic and inorganic building units have been developed tremendously so far. These materials can be functionalized further by the incorporation of open metal sites for many applications based on metal ions. Although, methodologies for the incorporation of open metal sites have been pursued, incorporation of open metal sites of substitution-inert complexes are still difficult and challenging topic.

In this study, a new strategy to assemble substitution-inert Rh(II) paddle wheel dimers to construct novel porous frameworks is described. As referred in previous section, Rh(II) paddle-wheel complexes has been paid much attention because of their unique properties and catalytic activities for various reactions. Thus, I aimed to assemble the complexes by using multipoint Ar-Ar^{F} interaction as a tool for controlled molecular arrangements. Through the combination of D_{4h} symmetrical Rh(II) paddle-wheel complex and unidirectional multipoint Ar-Ar^{F} interaction, the construction of porous framework without interfering active sites of Rh(II) dimer units can be expected. Moreover, investigation of the porous properties and reactivities of obtained porous framework should be important for development of a new class of porous materials.

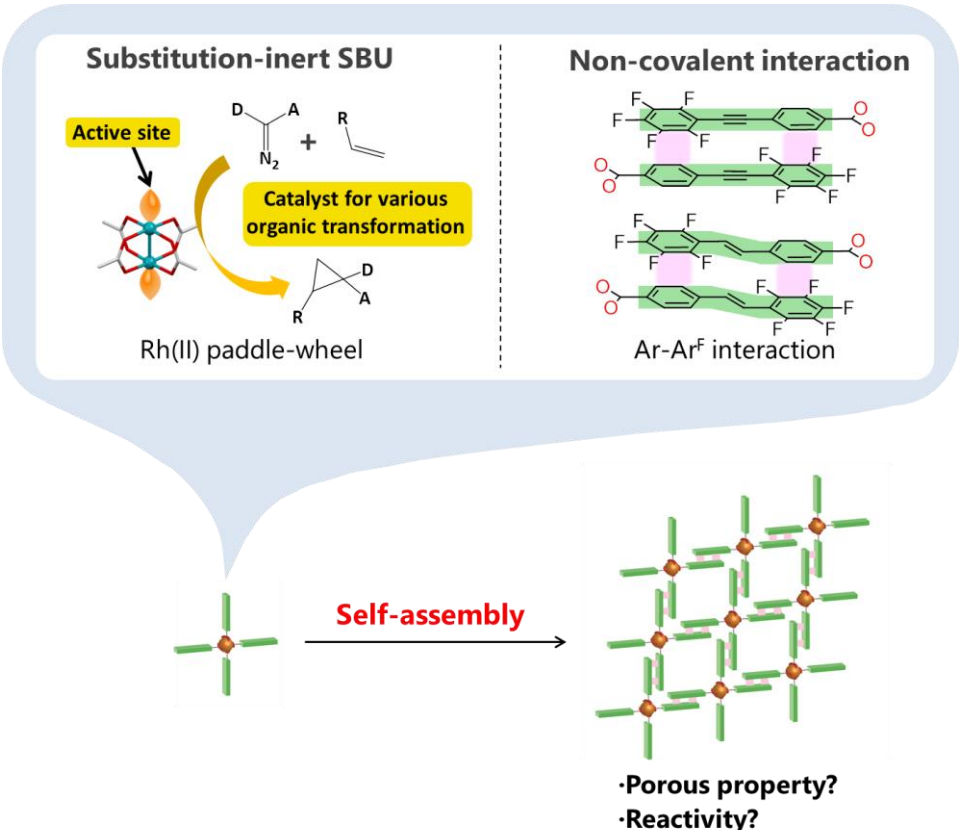

Survey of this thesis

Chapter 1 describes utility of Ar-Ar^F interactions for self-assembly of paddle-wheel complexes. I succeeded in controlling the self-assembly of paddlewheel dimers by intermolecular multipoint arene–perfluoroarene (Ar-Ar^F) interactions. A ligand with multipoint arene-perfluoroarene interaction sites, Hppeb = 4-[(perfluorophenyl)ethynyl]benzoic acid) was newly designed and synthesized. Then, two types of complexes, I-shaped $Rh_2(O_2CCF_3)_2(ppeb)_2$ (3-pentanone)$_2$ (**1**) and cross-shaped $Cu_2(ppeb)_4(THF)_2$ (**2**) were successfully synthesized to afford 1D chain and 2D square-grid sheet structures, respectively.

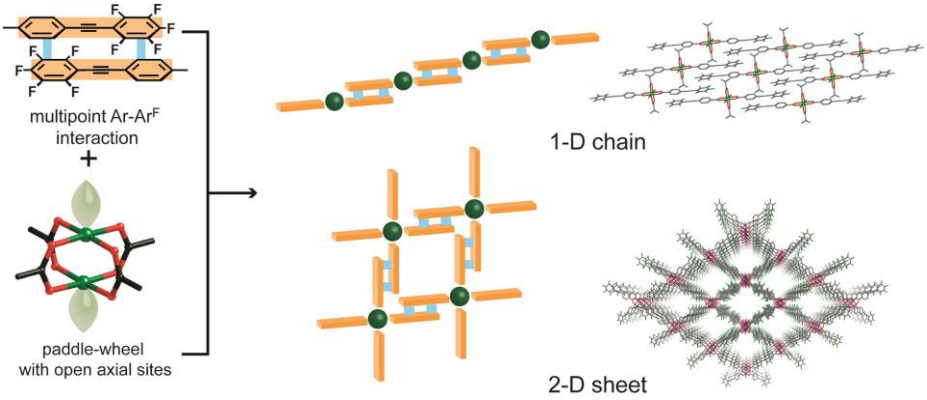

Chapter 1

Chapter 2 describes the methodology to organize substitution-inert metal-based secondary building units (SBUs) with active sites to form porous frameworks. In this study, I successfully assembled substitution-inert paddle-wheel Rh(II) dimers to afford three novel porous frameworks, $Rh_2(ppeb)_4(THF)_2$ (**3-THF**), $Rh_2(ppeb)_4(3\text{-pentanone})_2$ (**3-PN**) and $Rh_2(ppeb)_4(1\text{-adamantylamine})_2$ (**3-AD**) (ppeb = 4-[(perfluorophenyl)ethynyl]benzoate), by using non-covalent interactions. Multipoint arene-perfluoroarene ($Ar\text{-}Ar^F$) interactions, which allow in the unidirectional face-to-face interaction mode of aromating rings, were used to assemble substitution-inert paddle-wheel Rh(II) dimers. The obtained frameworks were structurally characterized by single crystal X-ray diffraction, and it is found that all strucures exhibited a one-dimensional channel with active axial sites exposed to the pores. The porous properties of the obtained frameworks were also investigated by thermogravimetric analysis, gas adsorption and powder X-ray diffraction measurements. Moreover, the ligand substitution reaction at the active axial sites was examined at the crystalline state and the flexible structural transformation with the change of channel shapes and sizes was observed.

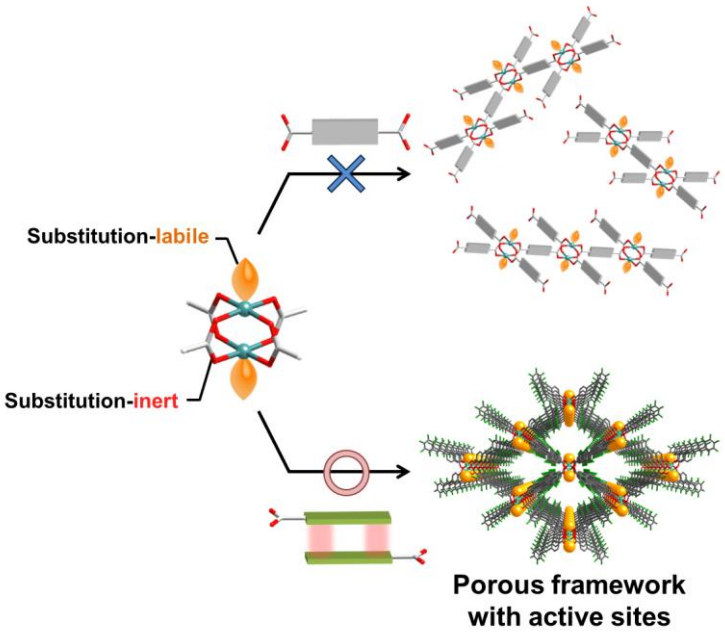

Chapter 2

Chapter 3 describes an attempt to convert noncovalent linking of porous framework into covalent linking by the use of [2+2] photodimerization reaction. As a ligand with Ar-Ar^F interaction sites and photo chemically reactive site, (*E*)-Hppvb was newly designed and synthesized. By UV-light irradiation to the crystal of (*E*)-Hppvb obtained from DMF solution, photodimerization proceeded quantitatively. Subsequently, the synthesis of Rh(II) complex was performed to afford Rh_2((*E*)-ppvb)$_4$. In the crystal packing structure of Rh_2((*E*)-ppvb)$_4$(X)$_2$ (X=THF, 2-butanone) obtained from recrystallization, 1-D channel structure was successfully constructed to show the effectiveness of Ar-Ar^F interaction. However, almost no photo polymerization proceeded even irradiation of UV-light for 48 hours, possibly due to the deactivation of the excited state of the ligand by Rh center.

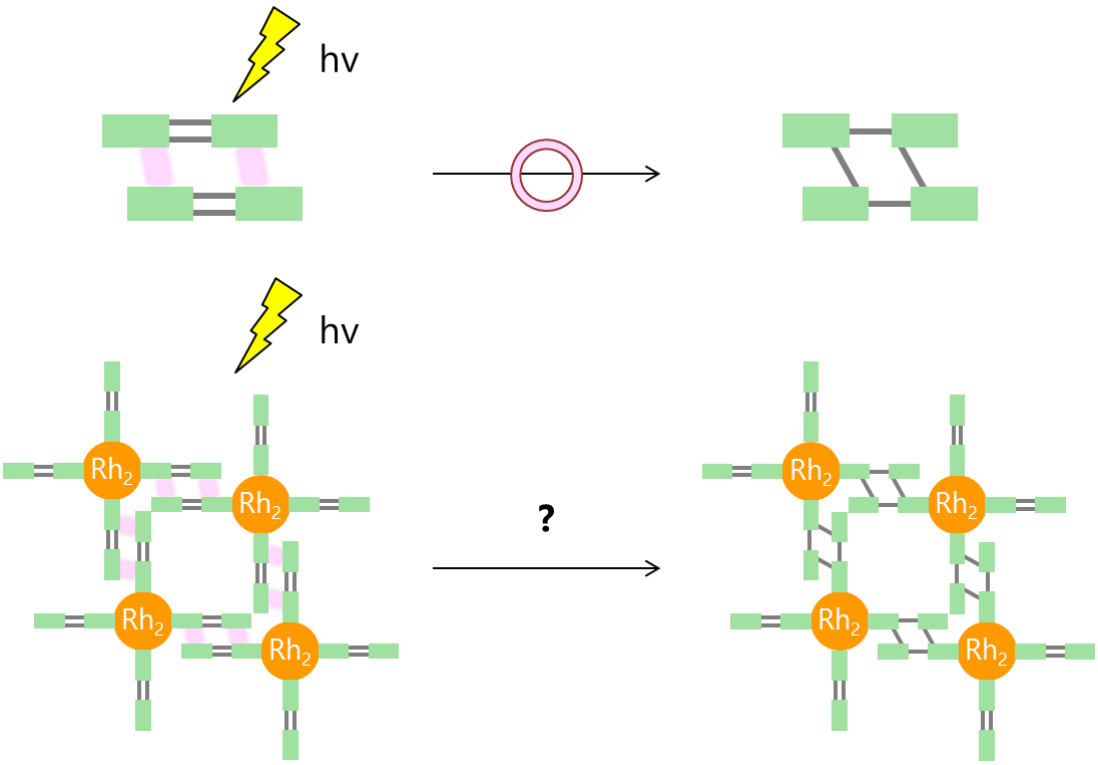

Chapter 3

Chapter 4 describes the reactivity of $Rh_2(ppeb)_4$ with diazo compounds and the construction of triazole-incorporated porous frameworks. $Rh_2(ppeb)_4$ showed moderate reactivities for cyclopropanation of styrene and C-H insertion into allyl or benzylic positions. However, $Rh_2(ppeb)_4$ could not be used as heterogeneous catalyst because it can be dissolved in allyl or aromatic substrates. Then, alternative carbene precursors, triazoles which shows diazo-azomethine/1,2,3-triazole tautomerism were chosen because prospective incorporation of triazoles before construction of porous frameworks was anticipated. While $Rh_2(ppeb)_4$ with two [1,2,3]triazolo[1,5-a]pyridine-3-carboxylate (**TR2**) showed 0 dimensional pore due to interfering multipoint Ar-Ar^F interaction by π- π interaction between triazole 2 and equatorial ligand, adducts of **TR3** which has *tert*-butyl ester afforded 1-D cahnnel structure as reported in chapter 2.

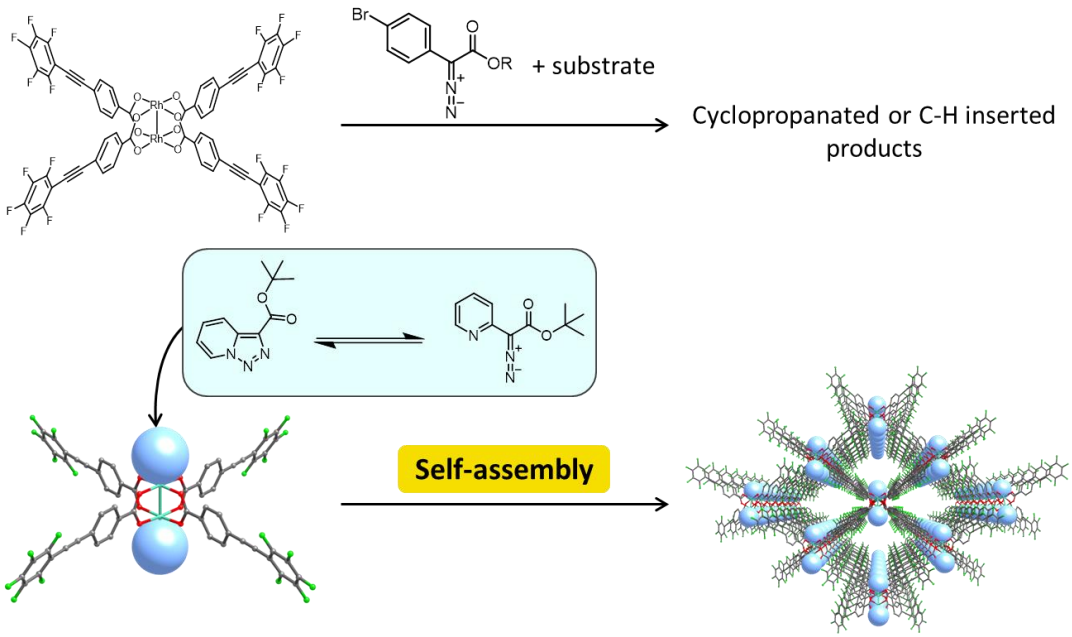

Chapter 4

References

1 (a) O. M. Yaghi, M. O'keeffe, N. W. Ockwig, H. K. Chae, M. Eddaoudi and J. Kim, *Nature*, **2003**, *423*, 705–714; (b) M. O'Keeffe, M. A. Peskov, S. J. Ramsden and O. M. Yaghi, *Acc. Chem. Res.*, **2008**, 41, 1782–1789. (c) M. Li, D. Li, M. O'Keeffe and O. M. Yaghi, *Chem. Rev.*, **2014**, *114*, 1343–1370.

2 (a) H. Furukawa, K. E. Cordova, M. O'Keeffe and O. M. Yaghi, *Science*, **2013**, *341*, 974–986; (b) R. J. Kuppler, D. J. Timmons, Q.-R. Fang, J.-R. Li, T. A. Makal, M. D. Young, D. Yuan, D. Zhao, W. Zhuang and H.-C. Zhou, *Cood. Chem. Rev.*, **2009**, *253*, 3042–3066.

3 (a) K. Sumida, D. L. Rogow, J. A. Mason, T. M. McDonald, E. D. Bloch, Z. R. Herm, T.-H. Bae and J. R. Long, *Chem. Rev.*, **2012**, *112*, 724–781; (b) S. Kitagawa, R. Kitaura and S. Noro, *Angew. Chem., Int. Ed*., **2004**, *43*, 2334–2375; (c) J.-R. Li, J. Sculley and H.-C. Zhou, *Chem. Rev.*, **2012**, *112*, 869–932; (d) Y. He, W. Zhou, G. Qian and B. Chen, *Chem. Soc. Rev.*, **2014**, *43*, 5657–5678.

4 (a) M. D. Allendorf, C. A. Bauer, R. K. Bhakta and R. J. T. Houk, *Chem. Soc. Rev.*, **2009**, *38*, 1330–1352; (b) L. E. Kreno, K. Leong, O. K. Farha, M. Allendorf, R. P. V. Duyne and J. T. Hupp, *Chem. Rev.*, **2012**, *112*, 1105–1125; (c) D. Banerjee, Z. Hu and J. Li, *Dalton Trans.*, **2014**, *43*, 10668.

5 (a) Z. Ma and B. Moulton, *Cood. Chem. Rev.*, **2011**, *255*, 1623–1641; (b) R. C. Huxford, J. D. Rocca and W. Lin,"*Current Opinion in Chemical Biology*", **2010**, *14*, 262–268; (c) P. Horcajada, R. Gref, T. Baati, P. K. Allan, G. Maurin, P. Couvreur, G. Férey, R. E. Morris and C. Serre, *Chem. Rev.*, **2012**, *112*, 1232–1268.

6 (a) V. Stavila, A. A. Talin and M. D. Allendorf, *Chem. Soc. Rev.*, **2014**, *43*, 5994–6010; (b) G. Givaja, P. Amo-Ochoa, C. J. Gómez-García and F. Zamora, *Chem. Soc. Rev.*, **2012**, *41*, 115–147; (c) A. Morozan and F. Jaouen, Energy & Environmental Science, **2012**, *5*, 9269.

7 (a) D. Maspoch, D. Ruiz-Molina and J. Veciana, *J. Mater. Chem.*, **2004**, *14*, 2713; (b) E. Coronado and G. M. Espallargas, *Chem. Soc. Rev.*, **2013**, *42*, 1525–1539.

8 (a) J. Lee, O. K. Farha, J. Roberts, K. A. Scheidt, S. T. Nguyen and J. T. Hupp, *Chem. Soc. Rev.*, **2009**, *38*, 1450–1459; (b) M. Yoon, R. Srirambalaji and K. Kim, *Chem. Rev.*, **2012**, *112*, 1196–1231; (c) J. Liu, L. Chen, H. Cui, J. Zhang, L. Zhang and C.-Y. Su, *Chem. Soc. Rev.*, **2014**, *43*, 6011–6061; (d) A. H. Chughtai, N. Ahmad, H. A. Younus, A. Laypkov and F. Verpoort, *Chem. Soc. Rev.*, **2015**, *44*, 6804–6849: (e) M. Ranocchiari and J. A. V. Bokhoven, *Phys. Chem. Chem. Phys.*, **2011**, *13*, 6388; (f) D. Farrusseng, S. Aguado and C. Pinel, *Angew. Chem. Int. Ed.*, **2009**, *48*, 7502–7513; (g) M. Yoon, R. Srirambalaji and K. Kim, *Chem. Rev.*, **2012**, 112, 1196–1231; (h) J. Gascon, A. Corma, F. Kapteijn and F. X. L. I. Xamena, *ACS Catal.*, **2014**, *4*, 361–378.

9 (a) G. Zhu and H. Ren, "*Porous organic frameworks: design, synthesis and their advanced applications*", Springer, **2015**; (b) U. Díaz and A. Corma, *Cood. Chem. Rev.*, **2016**, *311*, 85–

124; (c) J. C. A. L. Segura, M. J. Mancheño and F. Zamora, *Chem. Soc. Rev.*, **2016**, *45*, 5635–5671; (d) S.-Y. Ding and W. Wang, *Chem. Soc. Rev.*, **2013**, *42*, 548–568: (e) X. Feng, X. Ding and D. Jiang, *Chem. Soc. Rev.*, **2012**, *41*, 6010.

10 A. P. Cote, *Science*, **2005**, *310*, 1166–1170.

11 (a) Y. Zeng, R. Zou and Y. Zhao, *Adv. Mater.*, **2016**, *28*, 2855–2873; (b) A. A. Olajire, *Journal of CO_2 Utilization*, **2017**, *17*, 137–161.

12 Y. Zhang and J. Y. Ying, *ACS Catal.*, **2015**, *5*, 2681–2691.

13 Selected examples: (a) W. Yang, A. Greenaway, X. Lin, R. Matsuda, A. J. Blake, C. Wilson, W. Lewis, P. Hubberstey, S. Kitagawa, N. R. Champness and Schröder Martin, *J. Am. Chem. Soc.*, **2010**, *132*, 14457–14469, and references references therein; (b) Sozzani, P; Bracco, S; Comotti, A; Ferretti, L; Simonutti, R. *Angew. Chem., Int. Ed*. **2005**, *44*, 1816; (c) *Adv. Mater.* **2014**, 26, 7027–7031 (d) *J. Am. Chem. Soc.* **2014**, *136*, 12828−12831; (e) P. Li, Y. He, H. D. Arman, R. Krishna, H. Wang, L. Weng and B. Chen, *Chem. Commun.*, **2014**, *50*, 13081–13084; (f) Y. B. He, S. C. Xiang and B. L. Chen, *J. Am. Chem. Soc.*, **2011**,*133*, 14570 (g) P. Li, Y. B. He, J. Guang, L. H. Weng, J. C. G. Zhao, S. C. Xiang and B. L. Chen, *J. Am. Chem. Soc.*, **2014**, *136*, 547. (h) R. S. Patil, D. Banerjee, C. Zhang, P. K. Thallapally and J. L. Atwood, *Angew.Chem. Int.Ed.*, **2016**, *55*,4523–4526.

14 Selected examples: (a) D. L. Wang, Y. Su, C. Y. Jin, B. S. Zhu, Y. Pang, L. J. Zhu,J. Y. Liu, C. L. Tu, D. Y. Yan and X. Y. Zhu, *Biomacromolecules*, **2011**, *12*, 1370; (b) Q. P. Duan, Y. Cao, Y. Li, X. Y. Hu, T. X. Xiao, C. Lin, Y. Panand L. Y. Wang, *J. Am. Chem. Soc.*, **2013**, *135*, 10542.

15 Selected examples: (a) C. Michael´a Drain, *Chem. Commun.*, **1996**, *337*. 37 S. Hanessian, M. Simard and S. Roelens, *J. Mater. Chem. A*, **1995**, *117*, 7630. 38 F. W. Zeng and S. C. Zimmerman, *Chem. Rev.*, **1997**, *97*, 1681.

16 X. F. Ji, Y. Yao, J. Y. Li, X. Z. Yan and F. H. Huang, *J. Am. Chem. Soc.*, **2012**, *135*, 74.

17 B. Li, C. Bai, S. Zhang, X. Zhao, Y. Li, L. Wang, K. Ding, X. Shu, S. Li and L. Ma, *J. Mater. Chem. A*, **2015**, *3*, 23788–23798.

18 B. Chen, M. Eddaoudi, T. M. Reineke, J. W. Kampf, M. O'keeffe and O. M. Yaghi, *J. Am. Chem. Soc.*, **2000**, *122*, 11559–11560.

19 Selected examples: (a) C. G. Bezzu, M. Helliwell, J. E. Warren, D. R. Allan and N. B. Mckeown, *Science*, **2010**, *327*, 1627–1630; (b) N. B. Mckeown, S. Makhseed, K. J. Msayib, L.-L. Ooi, M. Helliwell and J. E. Warren, *Angew. Chem. Int. Ed.*, **2005**, *44*, 7546–7549; (c) R. D. Zorzi, N. Guidolin, L. Randaccio and S. Geremia, *CrystEngComm*, **2010**, *12*, 4056; (d) K. S. Suslick, P. Bhyrappa, J.-H. Chou, M. E. Kosal, S. Nakagaki, D. W. Smithenry and S. R. Wilson, *Acc. Chem. Res.*, **2005**, *38*, 283–291. (e) I. Goldberg, *Chem. Commun.*, **2005**, 1243.

20 Selected examples: (a) A. Biswas, M.-B. Kim, S.-Y. Kim, T.-U. Yoon, S.-I. Kim and Y.-S. Bae, *RSC Adv.*, **2016**, *6*, 81485–81490; (b) D. Britt, H. Furukawa, B. Wang, T. G. Glover and O. M.

Yaghi, *Proc. Natl. Acad. Sci. USA*, **2009**, *106*, 20637–20640; (c) E. D. Bloch, W. L. Queen, R. Krishna, J. M. Zadrozny, C. M. Brown and J. R. Long, *Science*, **2012**, *335*, 1606–1610; (d) S. Xiang, Z. Zhang, C. Zhao, K. Hong, X. Zhao, D. Ding, M. Xie, C. Wu, M. C. Das, R. Gill, K. M. Thomas and B. Chen, *Nat. Commun.*, **2011**, *2*, 204; (e) E. D. Bloch, M. R. Hudson, J. A. Mason, S. Chavan, V. Crocellà, J. D. Howe, K. Lee, A. L. Dzubak, W. L. Queen, J. M. Zadrozny, S. J. Geier, L.-C. Lin, L. Gagliardi, B. Smit, J. B. Neaton, S. Bordiga, C. M. Brown and J. R. Long, *J. Am. Chem. Soc.*, **2014**, 136, 10752–10761; (f) Y.-S. Bae, C. Y. Lee, K. C. Kim, O. K. Farha, P. Nickias, J. T. Hupp, S. T. Nguyen and R. Q. Snurr, *Angew. Chem., Int. Ed*., **2012**, *51*, 1857–1860; (g) Z. Guo, H. Wu, G. Srinivas, Y. Zhou, S. Xiang, Z. Chen, Y. Yang, W. Zhou, M. O'Keeffe and B. Chen, *Angew. Chem., Int. Ed*., **2011**, *50*, 3178–3181; (h) J. Pang, F. Jiang, M. Wu, C. Liu, K. Su, W. Lu, D. Yuan and M. Hong, *Nat. Commun.*, **2015**, *6*, 7575; (i) J.-M. Lin, C.-T. He, Y. Liu, P.-Q. Liao, D.-D. Zhou, J.-P. Zhang and X.-M. Chen, *Angew. Chem., Int. Ed.*, **2016**, *55*, 4674–4678; (j) J. L. C. Rowsell, O. M. Yaghi, B. Chen, N. W. Ockwig, A. R. Millward and D. S. Contreras, *Angew. Chem., Int. Ed.*, **2005**, *44*, 4647–4647; (k) X.-S. Wang, S. Ma, P. M. Forster, D. Yuan, J. Eckert, J. J. López, B. J. Murphy, J. B. Parise and H.-C. Zhou, *Angew. Chem., Int. Ed*., **2008**, *47*, 7263–7266; (l) J. Zhang, T. Wu, S. Chen, P. Feng and X. Bu, *Angew. Chem., Int. Ed*., **2009**, *48*, 3486–3490; (m) K. Gedrich, I. Senkovska, N. Klein, U. Stoeck, A. Henschel, M. R. Lohe, I. A. Baburin, U. Mueller and S. Kaskel, *Angew. Chem., Int. Ed*., **2010**, *49*, 8489–8492; (n) X. Zhao, C. Mao, K. T. Luong, Q. Lin, Q.-G. Zhai, P. Feng and X. Bu, *Angew. Chem., Int. Ed*., **2016**, *55*, 2768–2772; (o) W. Zhou, H. Wu and T. Yildirim, *J. Am. Chem. Soc*., **2008**, *130*, 15268–15269; (p) K. Lee, W. C. Isley, A. L. Dzubak, P. Verma, S. J. Stoneburner, L.-C. Lin, J. D. Howe, E. D. Bloch, D. A. Reed, M. R. Hudson, C. M. Brown, J. R. Long, J. B. Neaton, B. Smit, C. J. Cramer, D. G. Truhlar and L. Gagliardi, *J. Am. Chem. Soc.*, **2014**, *136*, 698–704; (q) B. Chen, X. Zhao, A. Putkham, K. Hong, E. B. Lobkovsky, E. J. Hurtado, A. J. Fletcher and K. M. Thomas, *J. Am. Chem. Soc.*, **2008**, *130*, 6411–6423; (r) X. Zhao, X. Bu, Q.-G. Zhai, H. Tran and P. Feng, *J. Am. Chem. Soc*., **2015**, *137*, 1396–1399.

21 (a) C.-D. Wu, A. Hu, L. Zhang and W. Lin, *J. Am. Chem. Soc.*, **2005**, *127*, 8940–8941; (b) W. Xuan, C. Ye, M. Zhang, Z. Chen and Y. Cui, *Chem. Sci.*, **2013**, *4*, 3154; (c) Z. Zhang, Y. Chen, S. He, J. Zhang, X. Xu, Y. Yang, F. Nosheen, F. Saleem, W. He and X. Wang, *Angew. Chem., Int. Ed.*, **2014**, 126, 12725–12729; (d) G. Akiyama, R. Matsuda, H. Sato and S. Kitagawa, *Chem.-Asian J.*, **2014**, *9*, 2772–2777; (e) J. Juan-Alcañiz, R. Gielisse, A. B. Lago, E. V. Ramos-Fernandez, P. Serra-Crespo, T. Devic, N. Guillou, C. Serre, F. Kapteijn and J. Gascon, *Catal. Sci. Technol.*, **2013**, *3*, 2311; (f) N. T. Phan, T. T. Nguyen, K. D. Nguyen and A. X. Vo, Applied Catalysis A: General, **2013**, *464-465*, 128–135; (g) Y. E. K. Hwang, D.-Y. Hong, J.-S. Chang, S. H. Jhung, Y.-K. Seo, J. Kim, A. Vimont, M. Daturi, C. Serre and G. Férey, *Angew. Chem., Int. Ed.*, **2008**, *120*, 4144–4418; (h) A. Henschel, K. Gedrich, R. Kraehnert and S.

Kaskel, *Chem. Commun.*, **2008**, 4192-4194; (i) J.-P. Ma, S.-Q. Wang, C.-W. Zhao, Y. Yu and Y.-B. Dong, Chemistry of Materials, **2015**, *27*, 3805–3808; (j) J. Lee, O. K. Farha, J. Roberts, K. A. Scheidt, S. T. Nguyen and J. T. Hupp, *Chem. Soc. Rev.*, **2009**, *38*, 1450-1459; (k) S. Meng, X. Zou, C. Liu, H. Ma, N. Zhao, H. Ren, M. Jia, J. Liu and G. Zhu, ChemCatChem, **2016**, *8*, 2393–2400; (l) Y. Kataoka, K. Sato, Y. Miyazaki, K. Masuda, H. Tanaka, S. Naito and W. Mori, Energy & Environmental *Science*, **2009**, *2*, 397; (m) S. Horike, Dincă Mircea, K. Tamaki and J. R. Long, *J. Am. Chem. Soc.*, **2008**, *130*, 5854–5855; (n) M. Banerjee, S. Das, M. Yoon, H. J. Choi, M. H. Hyun, S. M. Park, G. Seo and K. Kim, *J. Am. Chem. Soc.*, **2009**, *131*, 7524–7525; (o) S. Biswas, M. Maes, A. Dhakshinamoorthy, M. Feyand, D. E. D. Vos, H. Garcia and N. Stock, *J. Mater. Chem.*, **2012**, *22*, 10200; (p) L.-J. Zhang, C.-Y. Han, Q.-Q. Dang, Y.-H. Wang and X.-M. Zhang, *RSC Adv.*, **2015**, *5*, 24293–24298.

22 (a) G. Agustí, R. Ohtani, K. Yoneda, A. B. Gaspar, M. Ohba, J. F. Sánchez-Royo, M. C. Muñoz, S. Kitagawa and J. A. Real, *Angew. Chem. Int. Ed.*, **2009**, *48*, 8944–8947; (b) R. Ohtani, K. Yoneda, S. Furukawa, N. Horike, S. Kitagawa, A. B. Gaspar, Muñoz M. Carmen, Real José A. and M. Ohba, *J. Am. Chem. Soc.*, **2011**, *133*, 8600–8605; (c) Q. Zhang, B. Li and L. Chen, Inorganic Chemistry, **2013**, *52*, 9356–9362; (d) Jee, K. Eisinger, F. Gul-E-Noor, M. Bertmer, M. Hartmann, D. Himsl and Pöppl Andreas, *J. Phys. Chem. C*, **2010**, *114*, 16630–16639; (e) Y. Y. Sun, Y.-H. Kim, K. Lee, D. West and S. B. Zhang, *Phys. Chem. Chem. Phys.*, **2011**, *13*, 5042.

23 (a) B. Chen, Y. Yang, F. Zapata, G. Lin, G. Qian and E. B. Lobkovsky, *Adv. Mater.*, **2007**, *19*, 1693–1696; (b) N. B. Shustova, A. F. Cozzolino, S. Reineke, M. Baldo and M. Dincă, *J. Am. Chem. Soc.*, **2013**, *135*, 13326–13329; (c) L. E. Kreno, K. Leong, O. K. Farha, M. Allendorf, R. P. V. Duyne and J. T. Hupp, *Chem. Rev.*, **2012**, *112*, 1105–1125; (d) Y.-W. Li, J.-R. Li, L.-F. Wang, B.-Y. Zhou, Q. Chen and X.-H. Bu, J. Mater. Chem. A, **2013**, *1*, 495–499.

24 Selected examples: (a) S. S.-Y. Chui, S. M.-F. Lo, J. P. H. Charmant, A. G. Orpen and I. D. Williams, *Science*, **1999**, *283*, 1148–1150; (b) G. C. A. Férey, C. Serre, C. Mellot-Draznieks, F. Millange, S. Surblé, J. Dutour and I. Margiolaki, *Angew. Chem. Int. Ed.*, **2004**, *43*, 6296–6301.

25 Selected examples: (a) B. Chen, X. Zhao, A. Putkham, K. Hong, E. B. Lobkovsky, E. J. Hurtado, A. J. Fletcher and K. M. Thomas, *J. Am. Chem. Soc.*, **2008**, *130*, 6411–6423; (b) . F. Song, C. Wang, J. M. Falkowski, L. Ma and W. Lin, *J. Am. Chem. Soc.*, **2010**, *132*, 15390–15398; (c) R. Kitaura, G. Onoyama, H. Sakamoto, R. Matsuda, S.-I. Noro and S. Kitagawa, *Angew. Chem. Int. Ed.*, **2004**, *43*, 2684–2687.

26 Selected examples: (a) K. K. Tanabe and S. M. Cohen, *Chem. Soc. Rev.*, **2011**, *40*, 498–519; (b) Z. Wang and S. M. Cohen, *Chem. Soc. Rev.*, **2009**, *38*, 1315; (c) J. D. Evans, C. J. Sumby and C. J. Doonan, *Nat. Chem.*, **2014**, *6*, 906–912.

27 C. R. Patrick and G. S. Prosser, *Nature*, **1960**, *187*, 1021.

28 J. H. Williams, *Acc. Chem. Res.*, **1993**, *26*, 593–598.

29 (a) A. Hori, A. Shinohe, M. Yamasaki, E. Nishibori, S. Aoyagi and M. Sakata, *Angew. Chem., Int. Ed.*, **2007**, 46, 7617–7620; (b) A. S. Batsanov, J. C. Collings and T. B. Marder, Acta Crystallographica Section C Crystal Structure Communications, **2006**, 62, m229–m231.

30 K. Reichenbächer, H. I. Süss and J. Hulliger, *Chem. Soc. Rev.*, **2005**, 34, 22–30.

31 (a) C. Dai, P. Nguyen, T. B. Marder, T. B. Marder, A. J. Scott, W. Clegg, C. Viney and C. Viney, *Chem. Commun.*, **1999**, 2493–2494; (b) J. C. Collings, K. P. Roscoe, E. G. Robins, A. S. Batsanov, L. M. Stimson, J. A. K. Howard, S. J. Clark and T. B. Marder, New J. Chem., **2002**, *26*, 1740–1746; (c) J. C. Collings, A. S. Batsanov, J. A. Howard, D. A. Dickie, J. A. Clyburne, H. A. Jenkins and T. B. Marder, *J. Fluorine Chem.*, **2005**, *126*, 513–517; (d) T. M. Fasina, J. C. Collings, D. P. Lydon, D. Albesa-Jove, A. S. Batsanov, J. A. K. Howard, P. Nguyen, M. Bruce, A. J. Scott, W. Clegg, S. W. Watt, C. Viney and T. B. Marder, *J. Mater. Chem.*, **2004**, *14*, 2395; (e) V. R. Vangala, A. Nangia and V. M. Lynch, *Chem. Commun.*, **2002**, 1304–1305.

32 (a) G. W. Coates, A. R. Dunn, L. M. Henling, D. A. Dougherty and R. H. Grubbs, *Angew. Chem., Int. Ed.*, **1997**, *36*, 248–251; (b) R. Xu, V. Gramlich and H. Frauenrath, *J. Am. Chem. Soc.*, **2006**, *128*, 5541–5547; (c) P. Kissel, D. J. Murray, W. J. Wulftange, V. J. Catalano and B. T. King, *Nat. Chem.*, **2014**, *6*, 774–778.

33 T.-H. Chen, I. Popov, W. Kaveevivitchai, Y.-C. Chuang, Y.-S. Chen, O. Daugulis, A. J. Jacobson and O. Š. Miljanić, *Nat. Commun.*, **2014**, *5*, 5131.

34 (a) T. Okamoto, K. Nakahara, A. Saeki, S. Seki, J. H. Oh, H. B. Akkerman, Z. Bao and Y. Matsuo, Chemistry of Materials, **2011**, *23*, 1646–1649; (b) K. Kishikawa, T. Inoue, Y. Sasaki, S. Aikyo, M. Takahashi and S. Kohmoto, Soft Matter, **2011**, *7*, 7532.

35 M. A. Porai-Koshits and A. S. Antsyshkina, *Dokl. Akad. Sauk SSSR*, 1962, 146, 1102.

36 F. A. Cotton, C. A. Murillo, and R.A Walton,"*Multiple Bonds Between Metal Atoms*", 3rd ed., Springer Science and Business Media, New York, **2005**.

37 Selected examples: (a) A. Erck, L. Rainen, J. Whileyman, I.-M. Chang, A. P. Kimball and J. Bear, *Exp. Biol. Med.*, **1974**, *145*, 1278–1283; (b) H. T. Chifotides and K. R. Dunbar, *Acc. Chem. Res.*, **2005**, *38*, 146–156; (c) A. R. de Souza, E. P. Coelho and S. B. Zyngier, Eur. J. Med. Chem., **2006**, *41*, 1214–1216.

38 Selected examples: (a) Z. Rozwadowski and B. Nowak-Wydra, Magn. Reson. Chem., **2008**, *46*, 974–978. (b) J. T. Mattiza, N. Harada, S. Kuwahara, Z. Hassan and H. Duddeck, Chirality, **2009**, *21*, 843–849; (c) H. Duddeck, Chem. Rec., **2005**, *5*, 396–409; (d) Z. Rozwadowski, Magn. Reson. Chem., **2007**, *45*, 605–610; (e) H. Duddeck and E. Díaz Gómez, Chirality, **2009**, *21*, 51–68.

39 S. Furukawa, N. Horike, M. Kondo, Y. Hijikata, A. Carné-Sánchez, P. Larpent, N. Louvain, S. Diring, H. Sato, R. Matsuda, R. Kawano and S. Kitagawa, Inorganic Chemistry, **2016**, *55*, 10843–10846.

40 Selected examples: (a) S. A. Hilderbrand, M. H. Lim and S. J. Lippard, *J. Am. Chem. Soc.*, **2004**, *126*, 4972–4978; (b) M. H. Lim and S. J. Lippard, *Acc. Chem. Res.*, **2006**, *40*, 41–51; (c) R. C. Smith, A. G. Tennyson and S. J. Lippard, *Inorg. Chem.*, **2006**, *45*, 6222–6226; (d) A. Gulino, T. Gupta, M. Altman, S. Lo Schiavo, P. G. Mineo, I. L. Fragala, G. Evmenenko, P. Dutta and M. E. van der Boom, *Chem. Commun.*, **2008**, 2900–2902.

41 Selected examples: (a); M. H. Lim and S. J. Lippard, *Acc. Chem. Res.*, **2006**, *40*, 41–51; (b) R. C. Smith, A. G. Tennyson and S. J. Lippard, *Inorg. Chem.*, **2006**, *45*, 6222–6226; (c) A. Gulino, T. Gupta, M. Altman, S. Lo Schiavo, P. G. Mineo, I. L. Fragala, G. Evmenenko, P. Dutta and M. E. van der Boom, *Chem. Commun.*, **2008**, 2900–2902. Oxy (d) M. O. Ratnikov, L. E. Farkas, E. C. McLaughlin, G. Chiou, H. Choi, S. H. El-Khalafy and M. P. Doyle, *J. Org. Chem.*, **2011**, *76*, 2585–2593, and references therein; Hydrogenation (e) T. Sato, W. Mori, C. N. Kato, T. Ohmura, T. Sato, K. Yokoyama, S. Takamizawa and S. Naito, *Chem. Lett.*, **2003**, *32*, 854–855; (f) S. Naito, T. Tanibe, E. Saito, T. Miyao and W. Mori, *Chem. Lett.*, **2001**, *30*, 1178–1179; (g) W. Mori, T. Sato, T. Ohmura, C. N. Kato and T. Takei, *J. Solid State Chem.*, **2005**, *178*, 2555–2573; (h) T. Sato, W. Mori, C. Kato, E. Yanaoka, T. Kuribayashi, R. Ohtera and Y. Shiraishi, *J. Catal.*, **2005**, *232*, 186–198; (i) G. Nickerl, U. Stoeck, U. Burkhardt, I. Senkovska and S. Kaskel, *J. Mater. Chem. A*, **2014**, 2, 144–148. (j) S. Tanaka,S. Masaoka, K. Yamauchi, M. Annaka and K. Sakai, *Dalton Trans.*, **2010**, *39*, 11218–11226; Y. Kataoka, K. Sato, Y. Miyazaki, Y. Suzuki, H. Tanaka, Y. Kitagawa, T. Kawakami, M. Okumura and W. Mori, *Chem. Lett.*, **2010**, *39*, 358–359. Cyclo (k) H. M. L. Davies and C. Venkataramani, *Org. Lett.*, **2003**, *5*, 1403–1406; (l) S. Negretti, C. M. Cohen, J. J. Chang, D. M. Guptill and H. M. Davies, *Tetrahedron*, **2015**, *71*, 7415–7420; (m) S. Hashimoto, T. Washio, R. Yamaguchi, T. Abe,H. Nambu and M. Anada, *Tetrahedron*, **2007**, *63*, 12037–12046; (o) M. P. Doyle, M. Valenzuela and P. L. Huang, Proc. Natl. Acad. Sci. U. S. A., **2004**, *101*, 5391–5395; (p) M. Anada, T. Washio, N. Shimada, S. Kitagaki, M. Nakajima, M. Shiro and S. Hashimoto, *Angew. Chem., Int. Ed.*, **2004**, *43*, 2665–2668; (q) R. E. Forslund, J. Cain, J. Colyer and M. P. Doyle, Adv. Synth. Catal., **2005**, *347*, 87–92; (r) M. P. Doyle, R. Duffy, M. Ratnikov and L. Zhou, *Chem. Rev.*, **2010**, *110*, 704–724; H. M. L. Davies and J. R. Manning, *Nature*, **2008**, *451*, 417–424; (s) F. Collet, R. H. Dodd and P. Dauban, *Chem. Commun.*, **2009**, 5061–5074; (t) D. A. Colby, R. G. Bergman and J. A. Ellman, *Chem. Rev.*, **2009**, *110*, 624–655;

42 Selected examples: (a) J. F. Berry, *Dalton Trans.*, **2012**, *41*, 700–713; (b) K. P. Kornecki, J. F. Briones, V. Boyarskikh, F. Fullilove, J. Autschbach, K. E. Schrote, K. M. Lancaster, H. M. L. Davies, J. F. Berry, *Science*, **2013**, *342*, 351-354; (c) C. Werlé, R. Goddard and A. Fürstner, *Angew. Chem., Int. Ed.*, **2015**, *51*, 15452–15456; (d) C. Werlé, R. Goddard, P. Philipps, C. Farès and A. Fürstner, *J. Am. Chem. Soc.*, **2016**, *138*, 3797–3805.

Chapter 1

Construction of porous frameworks via Ar-Ar^{F} interaction

CrystEngComm, 2013, 15, 6122–6126.

Introduction

Control over the self-assembling process of metal complexes is of key importance to construct supramolecular materials in which desirable bulk properties emerge as a consequence of specific intermolecular orientations.[1] Paddle-wheel complexes which are described as M_2L_4 (M = metal ion, L = monoanionic bidentate ligand) attract much attention because of their highly symmetric (D_{4h}) structures suitable for the construction of continuous structures. Moreover, the existence of free coordination sites at the axial positions (open axial sites) and their Lewis acidity play a crucial role in catalysis or selective guest recognition. For example, Rh(II) carboxylates are very efficient catalysts for many reactions[2a-e] and also used for the sensor of toxic molecules,[2f] and Cu(II) carboxylates can be utilized for the gas separation.[2g,h] Therefore, the construction of continuous structures of paddle-wheel units with open axial sites is of significance to develop functional materials. There have been several reports which succeeded to assemble paddle-wheel units with open axial sites via the combination of arene-arene[3] or haloarene-haloarene[4] moieties. However, the coexistence of more than

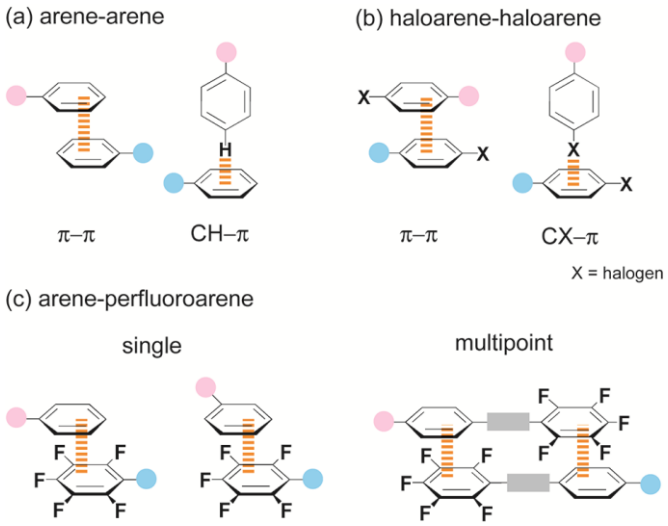

Scheme 1. Schematic illustration of intermolecular interactions. Multipoint arene-perfluoroarene interaction exhibits *unidirectional* arrangement, whereas other interactions show multidirectional arrangements.

two kinds of interaction modes makes intermolecular interactions multidirectional and the molecular arrangements are hard to predict (Scheme 1a, 1b). Therefore, the development of paddle-wheel units with *unidirectional* interaction sites is essential for the construction of supramolecular architectures with desired topologies.

Here we firstly report the self-assembly of Rh(II) and Cu(II) paddle-wheel complexes with open axial sites controlled via unidirectional interaction (Scheme 2). Two kinds of paddle-wheel dimers, the I-shaped complex, which has only two unidirectional interaction sites and is expected to have one-dimensional chain assembly, and the cross-shaped complex, which has four unidirectional interaction sites in one molecule and is expected to have two-dimensional sheet structure, are chosen to examine the molecular arrangements in the crystalline state (Scheme 2).

One of the promising ways to obtain *unidirectional* interaction is to exploit multipoint arene-perfluoroarene interaction. Whereas more than two kinds of interaction modes are exhibited in arene-arene interaction, arene-perfluoroarene interaction dominantly exhibits face-to-face interaction mode[5,6] arising from the van der Waals and quadrupole-quadrupole interactions[7] (Scheme 1). Moreover, the incorporation of multipoint interactive sites would inhibit the free rotation of arene rings to afford the unidirectional arrangement (Scheme 1c). Based on the strategy mentioned above, a novel ligand, 4-[(perfluorophenyl)ethynyl]benzoic acid (H**L**, Chart 1) was designed. Arene and perfluoroarene moieties of H**L** are bridged by ethyne moiety to keep planar configuration in the crystalline state,[8] and thus, robust and multipoint arene-perfluoro arene interactions can be expected.

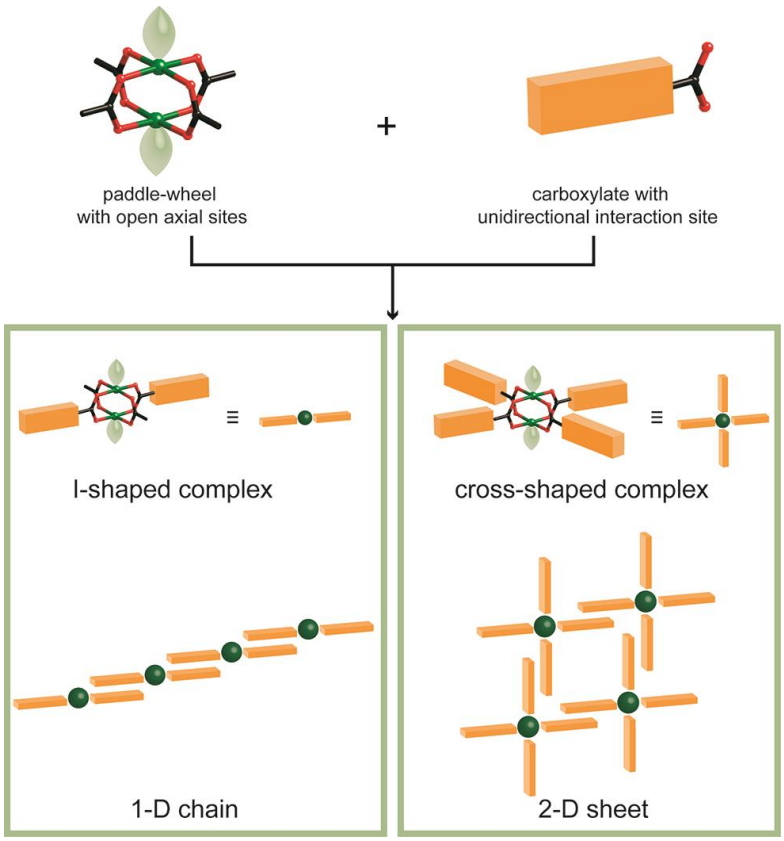

Scheme 2. Schematic illustration of I- and cross-shaped paddle-wheel complexes with open axial sites and their self-assembled structures.

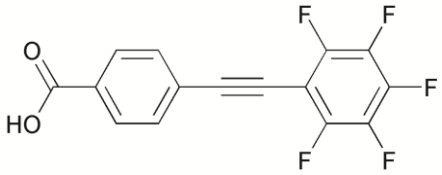

Chart 1. Chemical structure of H**L**.

Syntheses of ligand HL and paddle-wheel complexes

The synthesis of H**L** is summarized in Scheme 3. Methyl 4-[(perfluorophenyl)ethynyl]benzoate as an ester precursor was synthesized via Sonogashira cross coupling reaction[9] of pentafluoroiodobenzene and methyl 4-ethynylbenzoate.[10,11] The ester precursor obtained was hydrolyzed by BBr_3 to give H**L**, which was characterized by ^{1}H NMR, ^{19}F NMR and elemental analysis. The total synthetic yield for H**L** was 10%.

The synthesis of I-shaped Rh(II) complex was carried out by the reaction of $Rh_2(O_2CCF_3)_4(acetone)_2$ with 8 equivalent of H**L** at 110 °C in digylme for 2 h. Single crystals of $Rh_2(O_2CCF_3)_2(\mathbf{L})_2(3\text{-pentanone})_2$ (**1**) were obtained by the slow evaporation of 3-pentanone-Et_2O mixed solution and were suitable for X-ray crystallography. The synthesis of cross-shaped Cu(II) complex was performed by layering the acetone solution of H**L** (5 eq.) on the THF solution of $Cu(OAc)_2{\cdot}H_2O$. Blue solution was obtained after 2 days and the slow evaporation of solvent afforded single crystals of $Cu_2(\mathbf{L})_4(THF)_2$ (**2**) suitable for X-ray crystallography. It should be noted that the suppression of ligand scrambling reaction is essential to obtain the I-shaped complex. Therefore, Rh(II) was selected as a metal centre because Rh(II) paddle-wheel dimer has relatively strong M-carboxylate bonds and is known to form stable disubstituted complex.[12]

The crystal structure of **1** comprises Rh(II) paddle-wheels with 3-pentanone molecules coordinated at the axial sites (Figure 1). In the case of **1**, the paddle-wheel sits on an inversion centre and two $\mathbf{L}^-$ ligands occupy the *trans* position in the equatorial plane of each rhodium atom. The Rh1-Rh1' distance is 2.404(2) Å in the range found for previously reported Rh(II) paddle-wheel dimers (2.316 to 2.486 Å).[13] Although **1** has two types of carboxylate ligands, there is no significant difference in bond lengths between Rh and O: Rh1-O1 and Rh1-O2' distances are 2.041(4) and 2.025(7) Å, respectively, and Rh1-O3 and Rh1-O4' distances are 2.035(5) and 2.028(7) Å, respectively. The angle between phenylene and perfluorophenyl rings is estimated to be 9.4°. An ORTEP drawing of **2** is shown in Figure 1b. The crystal structure of **2** comprises Cu(II) paddle-wheels with mirror symmetry and THF molecules are coordinated at the axial sites. The Cu1-Cu2 distance is 2.6131(7) Å and is in the range found for previously reported Cu(II) paddle-wheel dimers (2.563 to 2.886 Å).14 The averaged angle between phenylene and perfluorophenyl rings is estimated to be 20.0°.

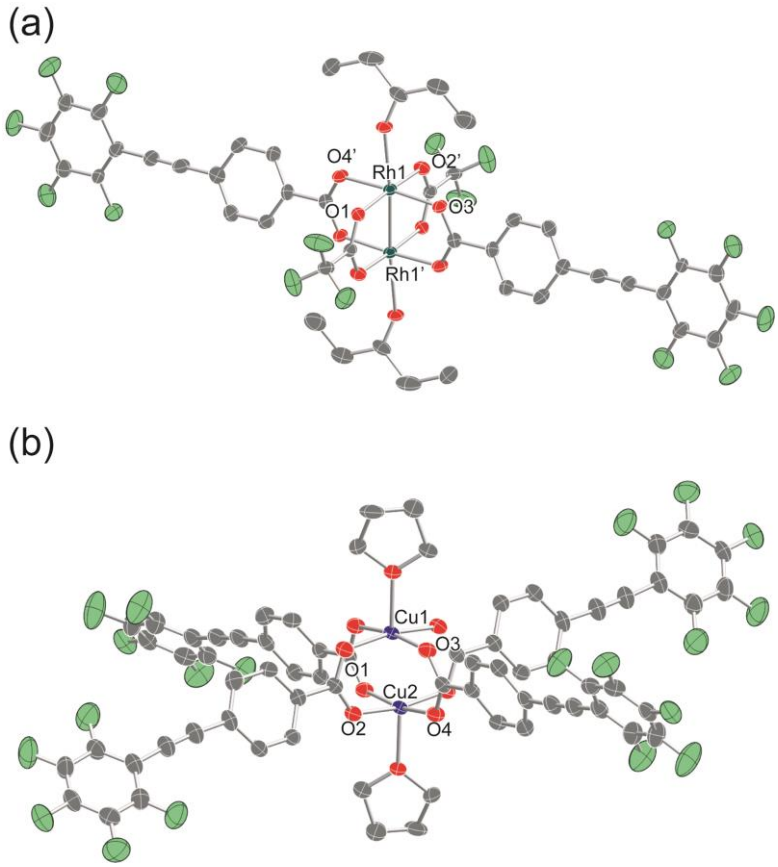

Figure 1. ORTEP drawings of (a) **1** and (b) **2** (50% probability ellipsoids). Hydrogen atoms, disordered carbon atoms of THF molecule and crystal solvent molecules are omitted for clarity. O = red, C = grey F = pale green, Rh = dark green, Cu = dark blue.

In the crystal packing structures of **1** and **2**, intermolecular multipoint arene-perfluoroarene interactions are observed. As shown in Figure 2, **1** is arranged in one-dimensional chain due to face-to-face overlap of phenylene and perfluorophenyl rings. The mean interplanar separation between phenylene and perfluorophenyl rings is 3.48 Å, which is comparable to the reported values.8 Interchain stacking are stabilized by π-π interactions between perfluorophenyl rings to form the two-dimensional sheet structure. The crystal packing structures of **2** are shown in Figure 3. An infinite two-dimensional square-grid sheet structure is formed via multipoint arene-perfluoroarene interaction between ligands. The mean interplanar separation between phenylene and perfluorophenyl rings is 3.56 Å. These two dimensional sheets are stacked though π-π interaction between ligands along the *a* axis to form columnar structure of paddle-wheel units.

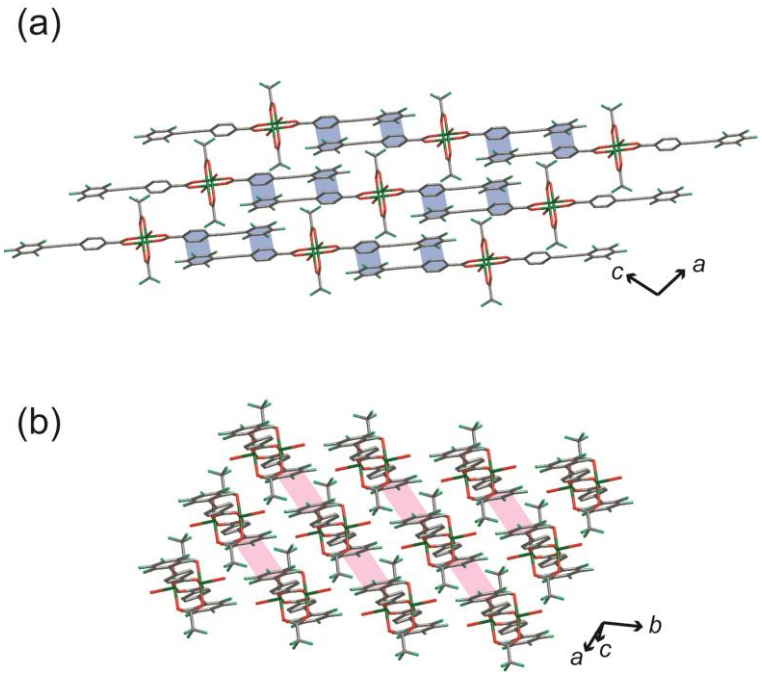

Figure 2. Crystal packing of **1** along (a) the *b* axis and (b) one-dimensional chain. One-dimensional chains formed by multipoint arene-perfluoroarene interactions (blue) are accumulated via π-π interactions between perfluoroarene rings (pink). Hydrogen atoms and carbon atoms of 3-pentanone molecules at the axial positions are omitted for clarity. O = red, C = grey, F = pale green, Rh = dark green.

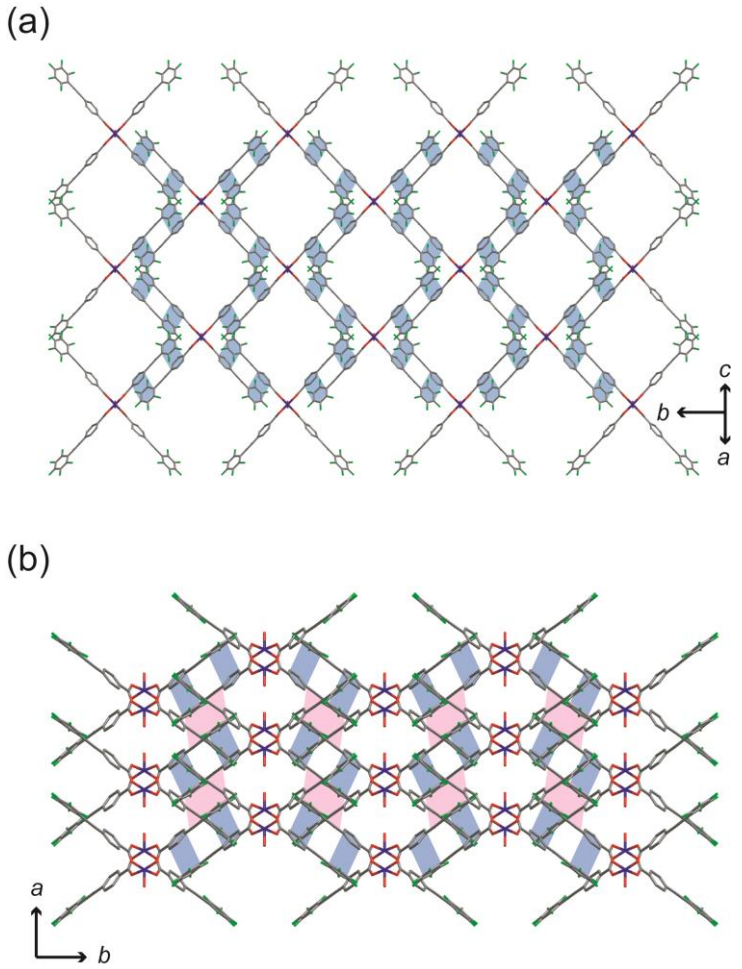

Figure 3. Crystal packing structures of **2** (a) parallel to the two-dimensional sheet and (b) along the *c* axis. Two-dimensional chains formed by multipoint arene-perfluoroarene interactions (blue) are accumulated via π-π interactions between ligands (pink). Hydrogen atoms, carbon atoms of THF at the axial positions and crystal solvent molecules are omitted for clarity. O = red, C = grey, F = pale green, Cu = dark blue.

Our approach to control the self-assembly of paddle-wheel complexes paves the way for a new field of crystal engineering. Self-assembled porous structures of paddle-wheel complexes with open axial sites are of interest for catalytic reaction or selective guest recognition. Even though several examples[15,16] based on coordination bonding network so called porous coordination polymers (PCPs) or metal-organic frameworks (MOFs) have been reported, no structures based on substitution-inert paddle-wheel dimers (e.g. $Rh_2(O_2CR)_4$) are available. This is because substitution-inert complexes require high temperature to be synthesized and often results in low yield and low crystallinity of desired products. In contrast, the utilization of arene-perfluoroarene interactions enables to assemble paddle-wheel units at low temperature, and thus can be an alternative approach. Indeed, the self-assembly of both Rh(II) and Cu(II) paddle-wheel units, was successfully achieved at room temperature and the arrangements were controlled by multipoint arene-perfluoroarene interactions as expected (Figures 2 and 3). Moreover, in the crystal packing of **2**, channel structure, in which THF molecules are accommodated as guest, was formed by the stacking of the two dimensional sheets via π-π interaction between ligands along the a axis and open axial sites are oriented to the channel (Figure 4). To the best of our knowledge, there has been only one example of supramolecular architecture composed of discrete paddle-wheel dimers where solvent accessible channel and open axial sites are coexist.[4c] Furthermore, the channel entrance size of **2** was estimated to be 13.8 × 5.8 $Å^2$ considering the van der Waals radii of constituent atoms and is much larger than that of the structure reported in the previous work (4.2 × 4.5 $Å^2$).

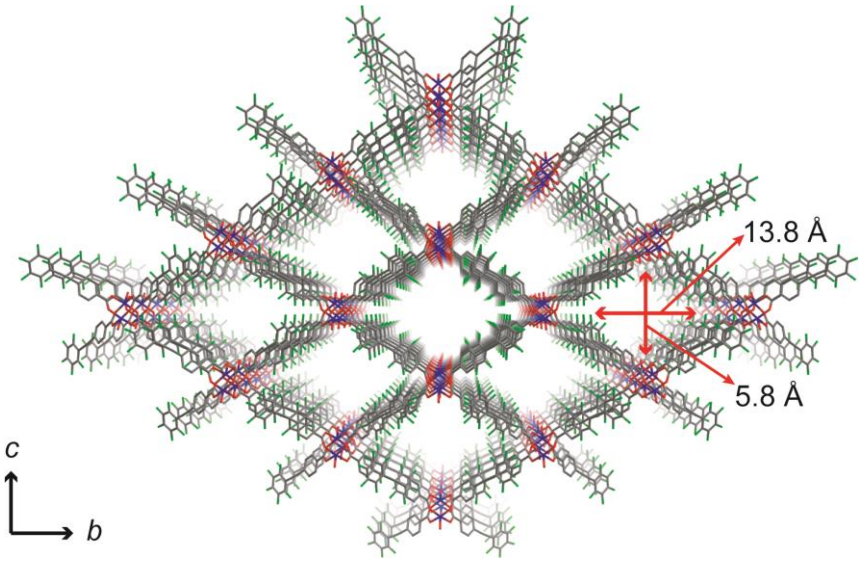

Figure 4. Crystal packing of **2** along the *a* axis. Hydrogen atoms, carbon atoms of THF at the axial positions and crystal solvent molecules observed in channels are omitted for clarity. O = red, C = grey, F = pale green, Cu = dark blue.

Estimation of stabilization energy of Ar-Ar^F interaction

As shown in Figure 2 and 3, Ar-Ar^F interactions worked dominantly for the self-assembly of paddle-wheel complexes and gave anticipated crystal packings. Therefore, I estimated the stabilization energy of this interaction by using density functional theory (DFT) calculations. For the estimation, benzene, hexafluorobenzene, co-crystal of benzene and hexafluorobenzene, pentafluorophenylethynylbenzene as a derivative of ligand H**L** and its dimer were employed. The structures of these compounds were optimized using the Gaussian 09[17] programs with the ωB97XD function[18] which is suitable for calculation of long-range interaction, and 6-31+G (d,p) as basis set.[19] As initial configurations for the calculation of optimized structures, reported crystal structures were used. The optimized structures of co-crystal of benzene and hexafluorobenzene, and dimer of pentafluorophenylethynylbenzene, and crystal structures of them[8,20] are shown in Figure 5 and 6. In the case of co-crystal of benzene and hexafluorobenzene, the parallel displaced configuration and the distance between them were well reproduced. However, in the case of dimer of pentafluorophenylethynylbenzene, the optimized structure seemed to be very different from the crystal structure. In the crystal structure, the angle between phenyl and perfluorophenyl rings is estimated to be 4.8° but in the optimized structure, the angles are 13.0° and 17.1°. Moreover, one of the pairs of arene and perfluoroarene rings interacts each other with not parallel displaced but parallel. Actually, electrostatic repulsion between arene and perfluoroarene rings is smaller than that between two arene rings because arene ring and perfluoroarene ring have negative and positive quadrupole moments, respectively.

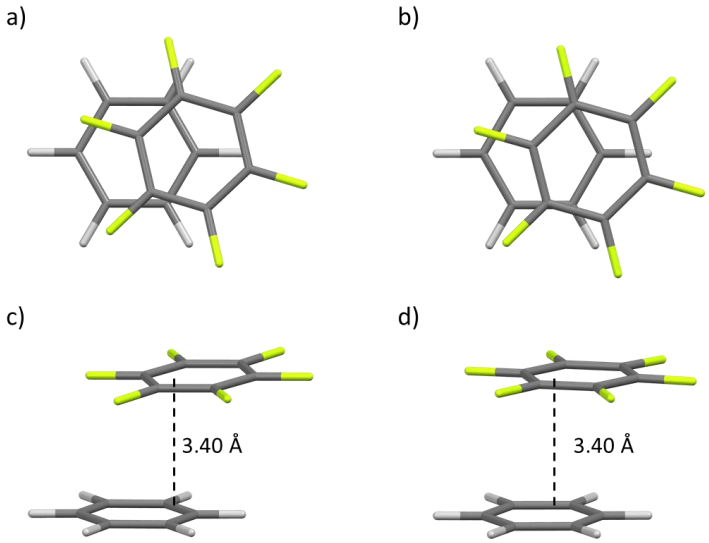

Figure 5. (a) Crystal packing of co-crystal of benzene and hexafluorobenzene (top view). (b) Optimized structure of benzene and hexafluorobenzene (top view). (c) Crystal packing of co-crystal of benzene and hexafluorobenzene (side view). (d) Optimized structure of benzene and hexafluorobenzene (side view).

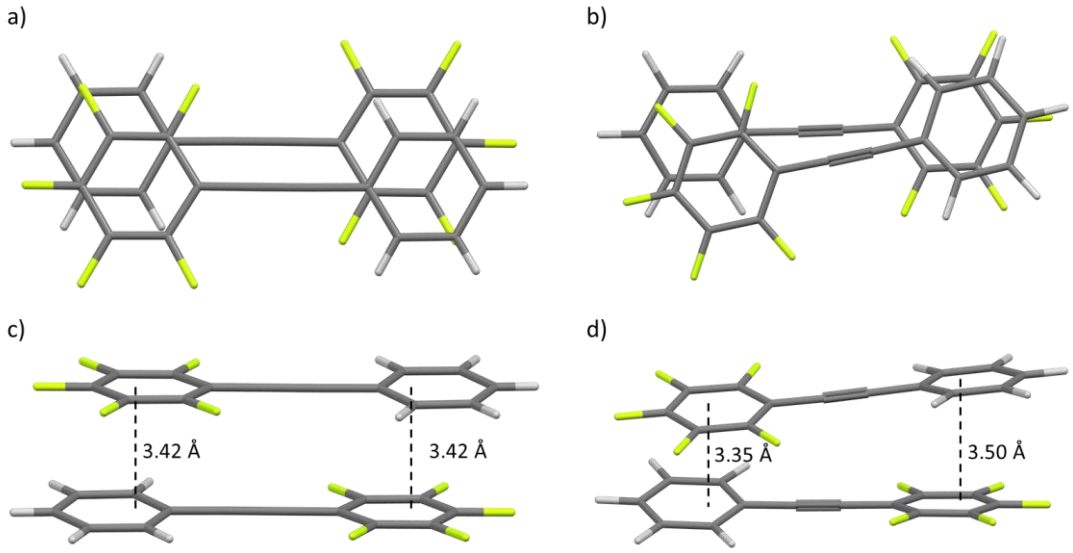

Figure 6. (a) Crystal packing of pentafluorophenylethynylbenzene (top view). (b) Optimized structure of pentafluorophenylethynylbenzene dimer (top view). (c) Crystal packing of pentafluorophenylethynylbenzene (side view). (d) Optimized structure of pentafluorophenylethynylbenzene dimer (side view).

By the comparison of total energies, co-crystal of benzene and hexafluorobenzene, and the dimer of pentafluorophenylethynylbenzene were estimated to be more stable than the single components (ΔE = -7.58 kcal mol^{-1}) and the monomer (ΔE = -16.0 kcal mol^{-1}), respectively (Table 1). Several reported theoretical studies of Ar-Ar^{F} interaction[21] have shown that the estimation of the stabilization energy is still controvertible. At least, stabilization energy increases in accordance with the increase of the interaction sites. Therefore, elongation of ligand H**L** would give more robust framework structure which can be comparable to MOFs or PCPs even non-covalent interaction is used as a tool for construction of framework.

Table 1. Comparison of the total energies and estimated stabilization energies.

Compound	Total energy (in E_h)	ΔE/kcal mol^{-1}
C_6F_6	-827.411949460	—
C_6H_6	-232.180774691	—
C_6F_6+C_6H_6	-1059.60480536	-7.58
$C_6F_5C_2Ph$ (monomer)	-1035.32515054	—
$C_6F_5C_2Ph$ (dimer)	-2070.67586021	-16.0

Conclusions

In conclusion, a new approach to construct supramolecular architecture was successfully developed by utilizing the combination of multipoint arene-perfluoroarene interaction site and paddle-wheel unit. Both I- and cross-shaped complexes with a novel ligand, H**L**, which has arene and perfluoroarene moieties bridged by ethyne linker, were synthesized by the ligand exchange reaction. In both complexes, molecular arrangements are determined by multipoint arene-perfluoroarene interaction and expected one- or two-dimensional structures are constructed at room temperature. Furthermore, the solvent accessible channel network with open axial sites, which is rarely obtained in discrete paddle-wheel units, was found in the self-assembly of the cross-shaped complex. The results presented in this contribution offer a new strategy to assemble paddle-wheel units of various metal ions with open axial sites at room temperature regardless of substitution activity. This can be a powerful tool to construct supramolecular structures applied for heterogeneous catalytic system or sensor.

Experimental section

General methods

All solvents and reagents are of the highest quality available and used as received except for diethyl amine and triethylamine. Diethyl amine and triethylamine were dried by reflux over KOH, distilled under argon, and degassed with a freeze-and-pump thaw. $Rh_2(O_2CCF_3)_4(acetone)_2$ were prepared by the literature methods. All syntheses were performed under an atmosphere of dry nitrogen or dry argon unless otherwise indicated.

Measurement apparatus

Elemental analyses were carried out on a J-SCIENCE LAB MICRO CORDER JM10 elemental analyser. ^{1}H NMR spectra were acquired on a JEOL JNM-LA500 spectrometer, where chemical shifts in $(CD_3)_2CO$ were referenced to internal tetramethylsilane. ^{19}F NMR spectra were acquired on a JEOL JNM-LA500 spectrometer, where chemical shifts in $(CD_3)_2CO$ were referenced to external trifluorotoluene.

X-ray crystallography

A crystal of **1** was mounted in a loop. Diffraction data at 123 K were measured on a Rigaku AFC8 diffractometer using a Rigaku Saturn CCD system. Graphite-monochromated Mo-Kα radiation (0.71075 Å) was used. Cell parameters were retrieved using the Crystal Clear-SM 1.4.0 software and refined using Crystal Clear-SM 1.4.0 on all observed reflections. Data reduction and empirical absorption correction using equivalent reflections and Lorentzian polarization were performed with the program Crystal Clear-SM 1.4.0. The structure was solved by direct methods using SIR-97 and refined on F^2 by the full-matrix least squares techniques with SHELXL-97.[22] All nonhydrogen atoms were refined anisotropically. A crystal of **2** was mounted in a loop. Diffraction data at 123 K were measured on a RAXIS-RAPID Imaging Plate diffractometer equipped with confocal monochromated Mo-Kα radiation and data was processed using RAPID-AUTO (Rigaku). Structures were solved by direct methods and refined by full-matrix least squares techniques on F^2 (SHELXL-97).[22] All non-hydrogen atoms were anisotropically refined, while all hydrogen atoms were placed geometrically and refined with a riding model with *U*iso constrained to be 1.2 times *U*eq of the carrier atom. For **2**, the diffused electron densities resulting from residual solvent molecules were removed from the data set using the SQUEEZE routine of PLATON and refined further using the data generated.

Syntheses

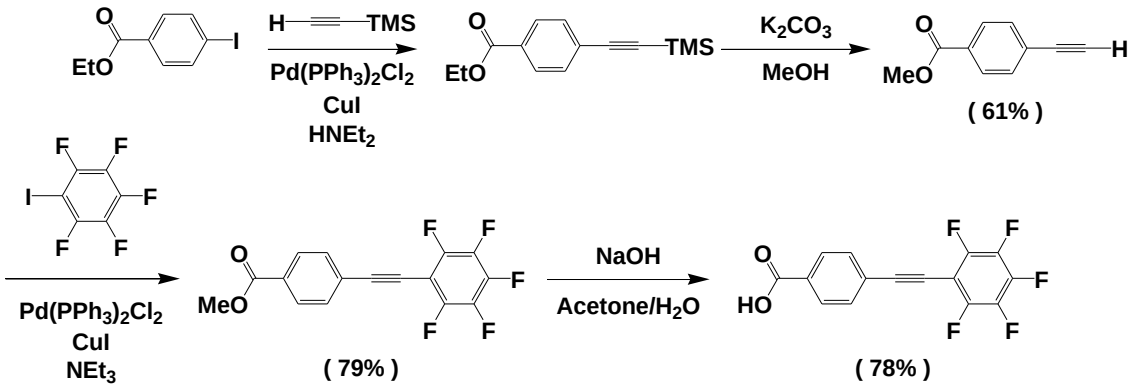

Scheme 3. Syntheses of H**L**.

Ethyl 4-(2-trimethylsilylethynyl)benzoate, ethyl 4-ethynylbenzoate, methyl 4-[(perfluorophenyl)ethynyl]benzoate which are the precursors of H**L** were prepared by the literature methods.

Synthesis of 4-[(perfluorophenyl)ethynyl]benzoic acid (HL) :

Methyl 4-[(perfluorophenyl)ethynyl]benzoate (2.15 g, 6.59 mmol) was dissolved in CH_2Cl_2 and cooled to –60°C. BBr_3 (2 eq.) was added and the solution was stirred for 30 min. under argon in the cold. Then, the cooling bath was removed and the stirring continued for another 90 min, while the solution was allowed to reach r.t. The solution was then washed twice with brine, dried over $MgSO_4$ and evaporated in vacuo to afford the yellow solid. The solid was washed with CH_2Cl_2 to obtain H**L** as a white solid. Yield 24%. ^{1}H NMR (500 MHz, $CDCl_3$) δ ppm: 7.78 (d, J = 10.0 Hz, 2H), 8.14 (d, J = 10.0, 2H); ^{19}F NMR (470.4 MHz, $(CD_3)_2CO$) δ ppm: -164.0 (dt, J = 4.7, 18.8 Hz, 2F), -154.3 (t, J = 18.8 Hz, 1F), -138. 3 (dd, J = 4.7, 18.8 Hz, 2F); Anal. Calcd. for $C_6F_5C_2C_6H_4CO_2H$: C, 57.71; H, 1.61; N, 0.00%. Found: C, 57.31; H, 1.77; N, 0.00%.

Synthesis of $Rh_2(O_2CCF_3)_2(L)_2(3\text{-pentanone})_2$ (1)

$Rh_2(O_2CCF_3)_4(acetone)_2$ (195 mg, 0.25 mmol) and H**L** (312 mg, 1.0 mmol) in 5 ml of diethyleneglycol dimethylether were stirred for 2 h at 100 ˚C. After evaporation of the solvent, the residue was purified by silica gel column chromatography (CH_2Cl_2/AcOMe 1:1). Recrystallization from Et_2O/3-pentanone gave green platelet crystals of **1**. The yield of $[Rh_2(O_2CCF_3)_2(\mathbf{L})_2]$ was 40 mg (13.3% based on $[Rh_2(O_2CCF_3)_4(acetone)_2]$). Anal. Calcd. for $Rh_2(O_2CC_6H_4C_2C_6F_5)_2(O_2CCF_3)_2$ $(Et_2O)_2 \cdot H_2O$: C, 41.33; H, 2.48; N, 0.00%. Found: C, 41.39; H, 2.27; N, 0.14%.

Synthesis of $Cu_2(L)_4(THF)_2$ (2)

H**L** (37.5 mg, 0.12 mmol) was dissolved in acetone (3.5 ml) and layered on top of a solution of Copper(II) acetate monohydrate (5.0 mg, 0.025 mmol) in THF (2.5 ml). After the solution was fully diffused, it was left to evaporate and blue platelet crystals were obtained. Anal. Calcd. for $Cu_2(O_2CC_6H_4C_2C_6F_5)_4(H_2O)_2$: C, 51.19; H, 1.43; N, 0.00%. Found: C, 51.15; H, 1.72; N, 0.00%.

Crystal data for 1: $C_{44}H_{28}F_{16}O_{10}Rh_2$, *Mr* = 1226.48, *triclinic*, space group $P\bar{1}$, (#2), a = 9.5097(53), b = 9.6296(56), c = 13.5971(75) Å, α = 103.8571(50), β = 100.5433(40), γ = 107.0596(77)°, V = 1111.9(1) $Å^3$, Z = 1, T = 123 (2) K, ρ_c = 1.832 gcm^{-3}, μ (Mo-Kα) = 0.868 cm^{-1}, $2\theta_{max}$ = 50.0°, λ(Mo-Kα) = 0.71074 Å, 7140 reflections measured, 3772 unique (R_{int} = 0.0278), 3231 ($I > 2\sigma(I)$) were used to refine 327 parameters, 0 restraints, wR_2 = 0.1576 ($I > 2\sigma(I)$), R_1 = 0.0587 ($I > 2\sigma(I)$), GOF = 1.225.

Crystal data for 2: $C_{68}H_{32}Cu_2F_{20}O_{10}$, *Mr* = 1516.02, *monoclinic*, space group $P2_1/m$, (#11), a = 9.09040(52), b = 26.70643(172), c =17.9560(84) Å, β = 101.50533(141)°, V = 4271.74(42) $Å^3$, Z = 2, T = 123 (2) K, ρ_c = 1.166 gcm^{-3}, μ(Mo-Kα) = 0.586 cm^{-1}, $2\theta_{max}$ = 50.0°, λ(Mo-Kα) = 0.71074 Å, 33173 reflections measured, 7682 unique (R_{int} = 0.071), 6213 ($I > 2\sigma(I)$) were used to refine 475 parameters, 0 restraints, wR_2 = 0.2415 ($I > 2\sigma(I)$), R_1 = 0.0758 ($I > 2\sigma(I)$), GOF = 1.143.

References

1 (a) E. Coronado, J. R. Galán-Mascarós, C. J. Gómez-García and V. Laukhin, *Nature*, **2000**, *408*, 447-449; (b) P. Cassoux, *Coord. Chem. Rev.*, **1999**, *185-186*, 213-232 ; (c) M. Ohba and H. Ōkawa, *Coord. Chem. Rev.*, **2000**, *198*, 313-328; (d) E. Pardo, R. Ruiz-García, J. Cano, X. Ottenwaelder, R. Lescouëzec, Y. Journaux, F. Lloret and M. Julve, *Dalton Trans.*, **2008**, 2780-2805; (e) M. Koberl, M. Cokoja, W. A. Herrmann and F. E. Kuhn, Dalton Trans., **2011**, *40*, 6834-6859.

2 (a) P. Ceccherelli, M. Curini, M. C. Marcotullio and O. Rosati, Tetrahedron, **1991**, *47*, 7403-7408; (b) M. P. Doyle, Acc. Chem. Res., **1986**, *19*, 348-356; (c) M. P. Doyle, K. G. High, C. L. Neslonely, T. W. Clayton Jr. and J. Lin, Organometallics, **1991**, *10*, 1225-1226; (d) S. Tanaka, S. Masaoka, K. Yamaguchi, M. Annaka and K. Sakai, Dalton Trans., **2010**, *39*, 11218-11226; (e) D. K. Kumar, A. S. Filatov, M. Napier, J. Sun, E. V. Dikarev and M. A. Petrukhina, Inorg. Chem., **2012**, *51*, 4855-4861; (f) S. A Hilderbrand, M. H. Lim and S. J. Lippard, J. Am. Chem. Soc., **2004**, *126*, 4972-4978; (g) J. Liu, Y. Wang, A. I. Benin, P. Jakubczak, R. R. Willis and M. D. LeVan, Langmuir, **2010**, *26*, 14301-14307; (h) S. Bordiga, L. Regli, F. Bonino, E. Groppo, C. Lamberti, B. Xiao, P. S. Wheatley, R. E. Morris and A. Zecchina, Phys. Chem. Chem. Phys., **2007**, *9*, 2676-2685.

3 (a) D. L. Reger, A. Debreczeni and M. D. Smith, Inorg. Chem. **2011**, *50*, 11754-11764; (b) D. L. Reger, A. Debreczeni and M. D. Smith, Inorg. chim. Acta, **2011**, *378*, 42-48; (c) G. S. Papaefstathiou, B. G. Darrow and L. R. MacGillivray, Journal of Chemical Crystallography, **2002**, *32*, 191-195.

4 (a) P. Smart, Á. Bejarano-Villafuerte and L. Brammer, CrystEngComm, **2013**, 15, 3151-3159; (b) P. Smart, G. M. Espallargas and L. Brammer, CrystEngComm, **2008**, 10, 1335-1344; (c) D. Maspoch, D. Ruiz-Molina, K. Wurst, C. Rovira and J. Veciana, Chem. Commun., **2002**, 2958-2959.

5 J. H. Williams, *Acc. Chem. Res.*, **1993**, *26*, 593-598.

6 C. R. Patrick and G. S. Prosser, *Nature*, **1960**, 187, 1021.

7 (a) J. Hernández-Trujillo, F. Colmenares, G. Cuevas and M. Coatas, *Chem. Phys. Lett.*, **1997**, *265*, 503-507; (b) A. P. West, Jr., S. Mecozzi and D. A. Dougherty, *J. Phys. Org. Chem.*, **1997**, *10*, 347-350.

8 C. E. Smith, P. S. Smith, R. LI. Thomas, E. G. Robins, J. C. Collings, C. Dai, A. J. Scott, S. Borwick, A. S. Batsanov, S. W. Watt, S. J. Clark, C. Viney, J. A. K. Howard, W. Clegg and T. B. Marder, *J. Mater. Chem.*, **2004**, *14*, 413-420.

9 (a) K. Sonogashira, Compr. Org. Synth., **1991**, *3*, 521-549; (b) J. Tsuji, *Palladium Reagents and Catalysts: Innovations in Organic Synthesis*, Wiley, Chichester, **1995**; (c) R. F. Heck, *Palladium Reagents in Organic Synthesis*, Academic Press, London, **1985**.

10 A. Schaate, P. Roy, T. Preuße, S. J. Lohmeier, A. Godt and P. Behrens, *Chem. Eur. J.*, **2011**, *17*, 9320 – 9325.

11 Y. Zhang and J. Wen, *Journal of Fluorine Chemistry*, **1990**, *47*, 533-535.

12 J. L. Bear, J. Kitchens and M. R. Willcott, *J. inorg. nucl. Chem.*, **1971**, *33*, 3479-3486.

13 (a) F. A. Cotton, C. A. Murillo, and R.A Walton,"*Multiple Bonds Between Metal Atoms*", 3rd ed., Springer Science and Business Media, New York, **2005**; (b) E. B. Royar and S. D. Robinson, *Platinum Metals Rev.*, **1982**, *26*, 65-69.

14 (a) M. M. Borel and A. Leclare, *Acta Crystallogr. Sect. B*, **1976**, *32*, 1275-1278; (b) J. A. Moreland and R. J. Doedens, *J. Am. Chem. Soc.*, **1975**, *97*, 508-513.

15 (a) S. S.-Y. Chui, S. M.-F. Lo, J. P. H. Charmant, A. G. Orpen, I. D. Williams, *Science*, **1999**, *283*, 1148 – 1150; (b) Z. Guo, H. Wu, G. Srinivas, Y. Zhou, S. Xiang, Z. Chen, Y. Yang, W. Zhou, M. O'Keeffe and B. Chen, *Angew. Chem. Int. Ed.*, **2011**, *50*, 3178-3181; (c) B. Zheng, Z. Yang, J. Bai, Y. Li and S. Li, *Chem. Commun.*, **2012**, *48*, 7025-7027.

16 (a) S. A. Bourne, J. Lu, A. Mondal, B. Moulton and M. J. Zaworotko, Angew. Chem. Int. Ed., **2001**, *40*, 2111-2113; (b) A. D. Burrows, C. G. Frost, M. F. Mahon, M. Winsper, C. Richardson, J. P. Attfield and J. A. Rodgers, Dalton Trans., **2008**, 6788-6795; (c) R.-Q. Zhong, R.-Q. Zou and Q. Xu, *CrystEngComm*, **2011**, *13*, 577-584.

17 M. J. Frisch, G. W. Trucks, H. B. Schlegel, G. E. Scuseria, M. A. Robb, J. R. Cheeseman, G. Scalmani, V. Barone, B. Mennucci, G. A. Petersson, H. Nakatsuji, M. Caricato, X. Li, H. P. Hratchian, A. F. Izmaylov, J. Bloino, G. Zheng, J. L. Sonnenberg, M. Hada, M. Ehara, K. Toyota, R. Fukuda, J. Hasegawa, M. Ishida, T. Nakajima, Y. Honda, O. Kitao, H. Nakai, T. Vreven, J. A. Montgomery, Jr. J. E. Peralta, F. Ogliaro, M. Bearpark, J. J. Heyd, E. Brothers, K. N. Kudin, V. N. Staroverov, T. Keith, R. Kobayashi, J. Normand, K. Raghavachari, A. Rendell, J. C. Burant, S. S. Iyengar, J. Tomasi, M. Cossi, N. Rega, J. M. Millam, M. Klene, J. E. Knox, J. B. Cross, V. Bakken, C. Adamo, J. Jaramillo, R. Gomperts, R. E. Stratmann, O. Yazyev, A. J. Austin, R. Cammi, C. Pomelli, J. W. Ochterski, R. L. Martin, K. Morokuma, V. G. Zakrzewski, G. A. Voth, P. Salvador, J. J. Dannenberg, S. Dapprich, A. D. Daniels, O. Farkas, J. B. Foresman, J. V. Ortiz, J. Cioslowski, D. J. Fox, Gaussian 09 (Revision C.01), Gaussian, Inc. Wallingford CT, **2010**.

18 J.-D. Chai and M. Head-Gordon, *Phys. Chem. Chem. Phys.*, **2008**, *10*, 6615.

19 W. J. Hehre, L. Radom, P. V. R. Schleyer, J. A. Pople, "*Ab Initio MolecularOrbital Theory"*, Wiley, New York, **1986**.

20 J. H. Williams, J. K. Cockcroft and A. N. Fitch, *Angew. Chem. Int. Ed.*, **1992**, *31*, 1655–1657.

21 (a) A. P. West, S. Mecozzi and D. A. Dougherty, *J. Phys. Org. Chem.*, **1997**, *10*, 347–350; (b) O. R. Lozman, R. J. Bushby and J. G. Vinter, *J. Chem. Soc., Perkin Trans. 2*, **2001**, 1446–1452; (c) S. Tsuzuki, T. Uchimaru and M. Mikami, The *J. Phys. Chem. A*, **2006**, *110*, 2027–2033; (d) B.

Landeros-Rivera, R. Moreno-Esparza and J. Hernández-Trujillo, *RSC Adv.*, **2016**, *6*, 77301–77309.

22 G. M. Sheldrick, *Program for Crystal Structure Refinement*, University of Göttingen, Germany, **1997**.

Chapter 2

Flexible structural transformation of porous frameworks

*Dalton Transactions, **2015**, 44, 15334–15342.*

Introduction

Metal–organic frameworks (MOFs) or porous coordination polymers (PCPs)[1,2] are crystalline materials composed of inorganic building units and organic linkers and have attracted considerable attention as new types of porous materials. In particular, MOFs or PCPs with open metal sites are of interest because these sites can strongly interact with adsorbed molecules to afford specific functionalisation of the pore surfaces for adsorption/separation,[3] heterogeneous catalysis,[4] and sensing.[5] One of the most straightforward strategies to construct such materials is to embed open metal sites on secondary building units (SBUs) of the framework.[6] The Rh(II) paddlewheel complex, which is composed of four substitution-inert carboxylate ligands and two substitution-labile axial ligands, would be an attractive SBU with D4h symmetry because the porous frameworks constructed are expected to show high stability arising from the substitution-inert carboxylate ligands and the high reactivity of the substitution-labile axial sites known as active centres for many catalytic reactions.[7] However, it is hard to construct MOFs or PCPs by linking substitution-inert metal-based SBUs via covalent linkers (Scheme 1a) because the covalent linking of these SBUs often prevents the formation of single crystalline materials.[8] Although there are many reports on single crystal structures of MOFs and PCPs consisting of substitution- labile SBUs with active sites (e.g., HKUST-1,[6a] MOF-74,[6b] and so on[9]), to the best of our knowledge, no single crystal structures of MOFs or PCPs constructed by substitution-inert SBUs with those sites have been reported so far.

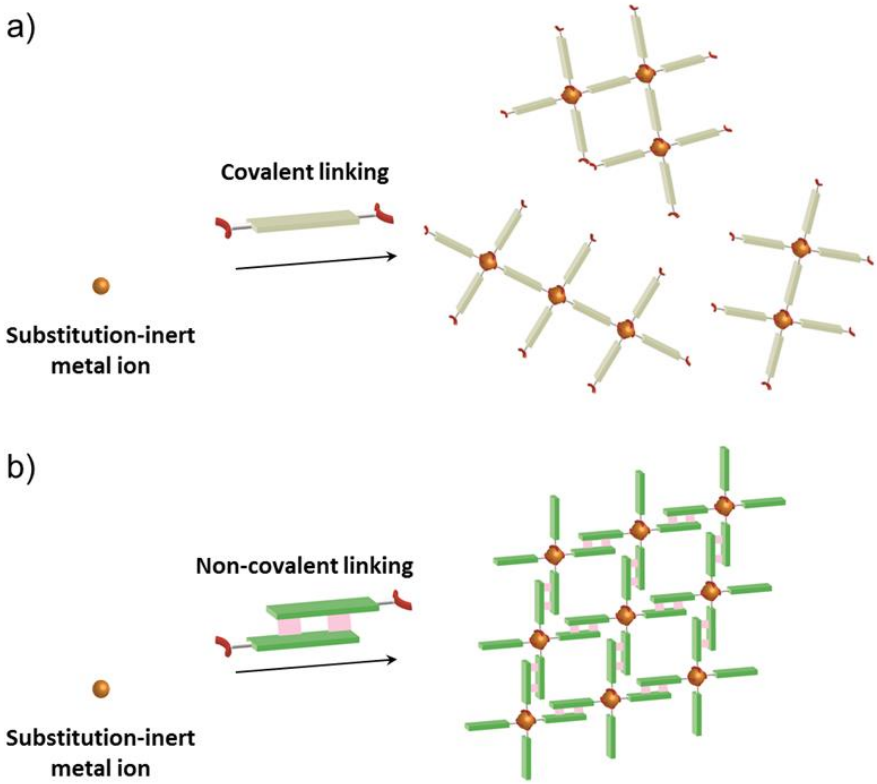

Scheme. 1 Schematic illustration of the self-assembly of substitutioninert SBUs via (a) covalent linking and (b) non-covalent linking.

Here, we show an effective approach to construct a porous framework based on substitution-inert SBUs with active sites. Recently, many reports have proved that non-covalent interactions (e.g., hydrogen bonds,[10] π-π interactions,[11] combination of hydrogen bonds and π-π interactions,[12] and van der Waals interaction6[3]) can be promising tools for construction of porous materials. In comparison to covalent linking, these interactions can work in ambient condition to afford comparable well-defined framework. A key to our success is the usage of this ‘‘non-covalent’’ interaction (Scheme 1b) for the self-assembly of Rh(II) paddle-wheel dimers (Scheme 2a). As a module for non-covalent linking, a monocarboxylate ligand with multipoint arene-perfluoroarene[14] (Ar-Ar^F) interaction sites was designed (Scheme 2b). As we previously reported that this interaction enabled the unidirectional face-to-face interaction mode of aromatic rings to work dominantly, and the controlled self-assembly of molecules can be achieved.[15]

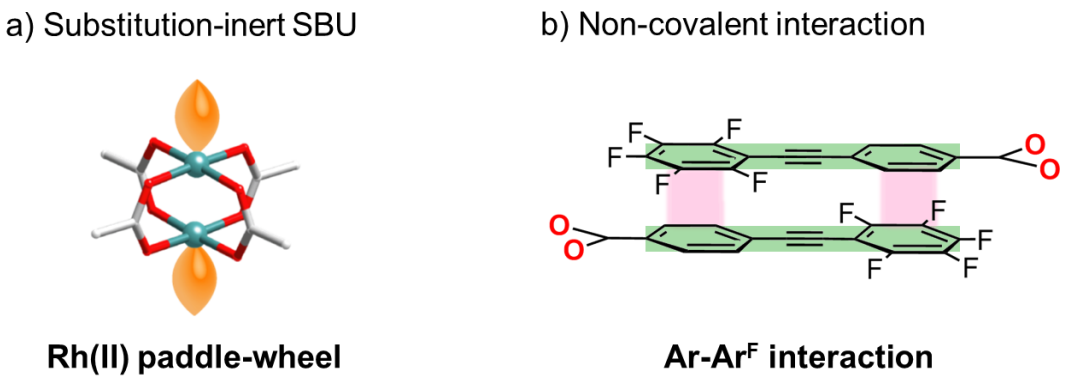

Scheme 2. Schematic illustration of (a) substitution inert SBU and (b) non-covalent interaction employed in this study.

Results and discussion

Syntheses of paddle-wheel complexes

Synthesis of the Rh(II) complex was performed by the reaction of $Na_4[Rh_2(CO_3)_4]\cdot 3H_2O$ with 8 eq. of Hppeb at 100 °C in dimethylacetamide/H_2O (3:1) for 8 h. A four substituted complex, $Rh_2(ppeb)_4(Et_2O)_2$, was obtained in 27% yield by subsequent column chromatography using neutral alumina (Et2O as the eluent). Note that the use of $Na_4[Rh_2(CO_3)_4]\cdot 3H_2O$ was crucial, and the reaction of Hppeb with carboxylate precursors, Rh(II) acetate or Rh(II) trifluoroacetate, did not afford the desired complex possibly due to the slow reaction rate of the di-substituted carboxylate complex.[15] The slow evaporation of the THF/Et_2O mixed solution of $Rh_2(ppeb)_4(Et_2O)_2$ afforded single crystals of $Rh_2(ppeb)_4(THF)_2$ (**3-THF**) suitable for X-ray crystallography. **3-PN** and **3-AD** were also obtained by recrystallization of $Rh_2(ppeb)_4(Et_2O)_2$. The recrystallisation of $Rh_2(ppeb)_4(Et_2O)_2$ from slow evaporation of the mixed solution of Et_2O/3-pentanone afforded $Rh_2(ppeb)_4$(3-pentanone)$_2$ (**3-PN**). To obtain $Rh_2(ppeb)_4$(1-amantylamine)$_2$ (**3-AD**), recrystallisation was performed by layering Et_2O solution of 1-adamantylamine on Et_2O solution of $Rh_2(ppeb)_4(Et_2O)_2$. These three compounds were characterised by single-crystal X-ray diffraction (Table 1) and IR spectroscopy.

Table 1. Crystallographic data and structural refinements for **3-THF**, **3-PN** and **3-AD**

Compound	**3-THF**	**3-PN**	**3-AD**
Formula	$C_{68}H_{32}F_{20}O_{10}Rh_2$	$C_{170}H_{132}F_{40}O_{26}Rh_4$	$C_{92}H_{70}F_{20}N_2O_{11}Rh_2$
Formura weight	1594.76	3762.40	1965.32
Temperature (°C)	-150	-150	-150
Crystal system	Monoclinic	Triclinic	Triclinic
Space group	*C*2/*m* (#12)	*P*-1 (#2)	*P*-1 (#2)
a (Å)	18.6449(7)	15.1526(7)	10.8625(8)
b (Å)	27.2267(14)	15.3844(4)	13.8827(10)
c (Å)	8.8932(4)	19.5087(4)	14.9217(11)
α (deg)	90	99.0550(7)	103.6458(15)
β (deg)	107.4822(12)	96.0045(7)	93.1519(15)
γ (deg)	90	112.8590(4)	94.0312(16)
V (Å^3)	4306.0(3)	4069.14(17)	2175.3(3)
Z	2	1	1
D_c (g cm^{-3})	1.230	1.535	1.500
μ (mm^{-1})	0.471	0.514	0.483
F(000)	1580	1900	994
R_1 [a]	0.0660	0.0554	0.0511
wR_2 [b]	0.1742	0.1875	0.1511
Goodness-of-fit on F^2	1.135	1.111	1.089

[a] $R_1 = \Sigma||F_o| - |F_c||/ \Sigma|F_o|$. [b] $wR_2 = [\Sigma(w(F_o^2-F_c^2)^2) / \Sigma w(F_o^2)^2]^{1/2}$.

Crystal structures

The crystal structure of **3-THF** is comprised of a Rh(II) paddle-wheel with THF molecules coordinated at the axial sites (Figure 1a). Four ppeb- ligands occupied the positions in the equatorial plane of each rhodium atom. The Rh1-Rh1' distance was 2.3875(13) Å, which is in the range found for previously reported Rh(II) paddle-wheel dimers (2.316 to 2.486 Å).18 The angle between the phenylene and perfluorophenyl rings was estimated to be 18.4°.

In the crystal packing structure of **3-THF**, aforementioned multipoint Ar-Ar^F interaction played a key role in stabilising the molecular assembly. As shown in Figure 1b, an infinite two-dimensional (2-D) square-grid sheet structure was formed via multipoint Ar-Ar^F interactions between the ligands. The mean interplanar separation between the phenylene and perfluorophenyl rings was 3.56(16) Å. These 2-D sheets were stacked through π-π interactions (denoted as blue line in Figure 1b) to form a columnar structure of paddle-wheel units along the c axis. As a result, a porous structure with the channel entrance size[19] of 13.8 × 12.1 $Å^2$ was formed (Figure 1c), and THF molecules were contained in the pores as guests.

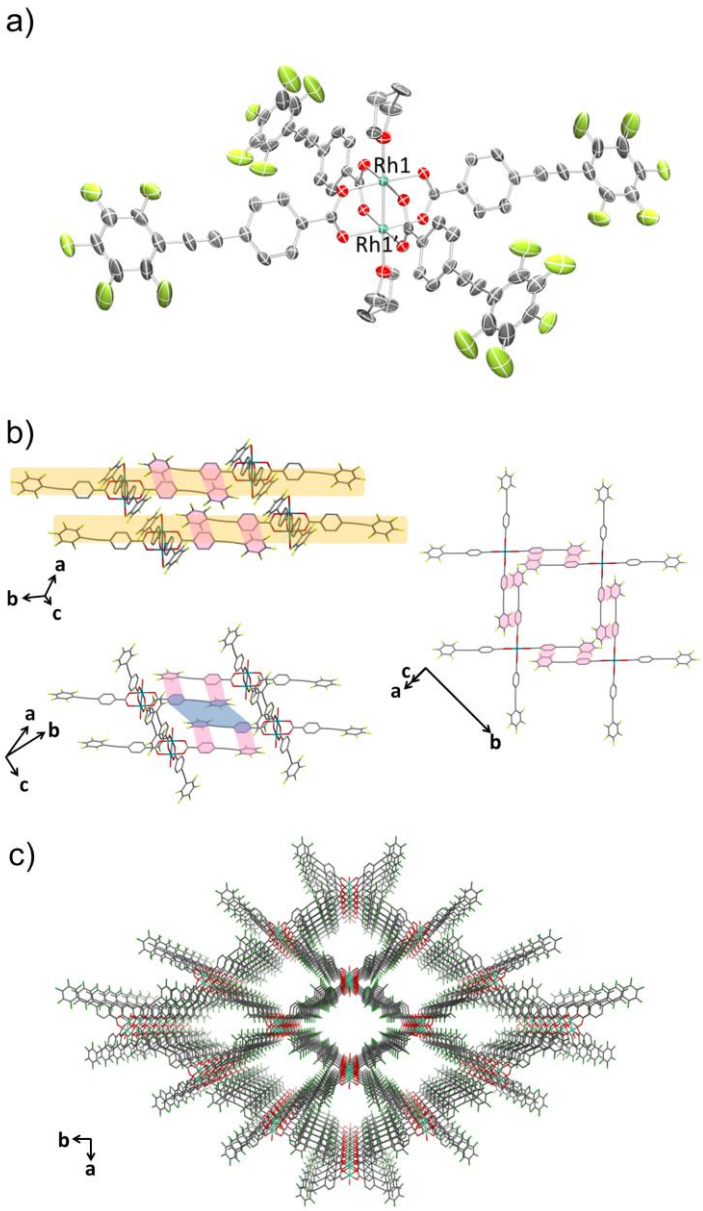

Figure 1. (a) An ORTEP drawing of **3-THF** (50% probability ellipsoids). Hydrogen atoms are omitted for clarity. (b) 2-D sheet structure of **3-THF**. Ar–Ar^{F} interactions and π–π interactions are shown in red and blue lines respectively. Hydrogen atoms and carbon atoms of THF at the axial positions are omitted for clarity. (c) Crystal packing of **3-THF** along the c axis. Hydrogen atoms, and carbon atoms of THF at the axial positions are omitted for clarity. O = red, C = grey, F = pale green, Rh = sea green.

The recrystallisation of $Rh_2(ppeb)_4(Et_2O)_2$ from Et_2O/3-pentanone afforded a similar crystal structure composed of a Rh(II) paddle-wheel complex bearing 3-pentanone at the axial sites, $Rh_2(ppeb)_4(3\text{-pentanone})_2$ (**3-PN**) (Figure 2). In the crystal structure of **3-PN**, the mean interplanar separation between phenylene and perfluorophenyl rings was 3.49(12) Å, and the channel entrance size was estimated to be 12.9 × 10.5 $Å^2$. It should be noted that the active sites of these complexes were exposed to the pores in both structures.

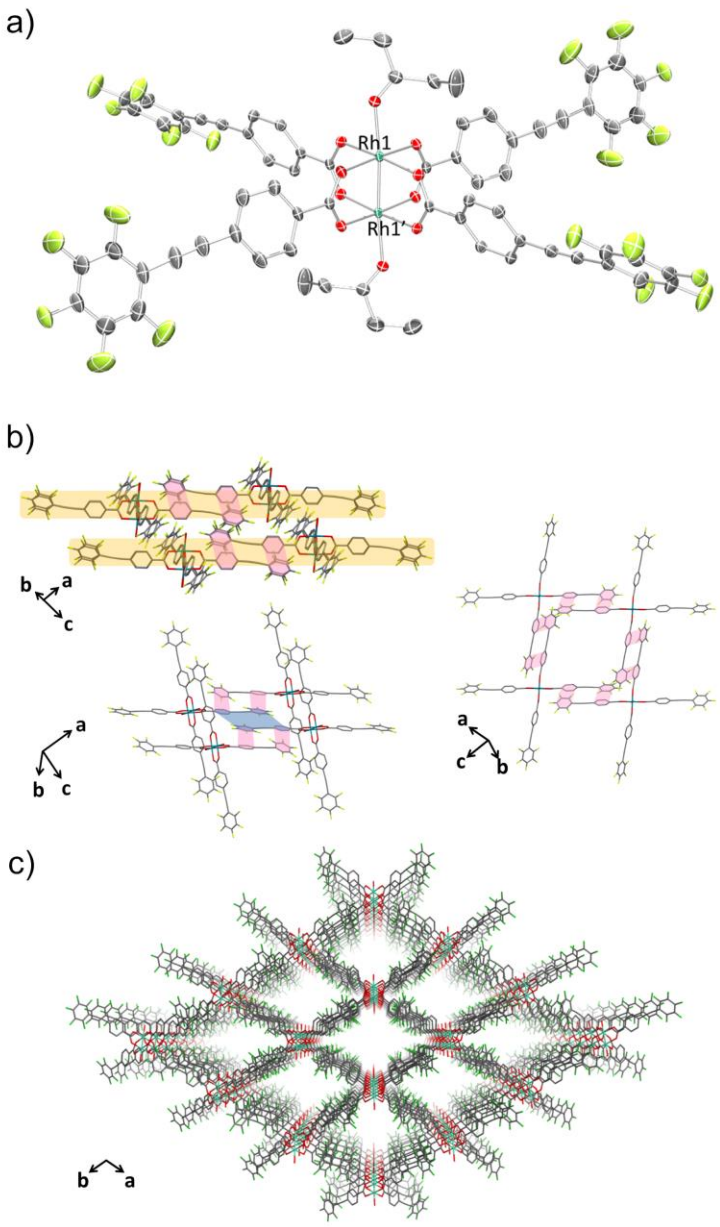

Figure 2. An ORTEP drawing of **3-PN** (50% probability ellipsoids). Hydrogen atoms and crystal solvent molecules are omitted for clarity. (b) 2-D sheet structure of **3-PN**. Ar–Ar^{F} interactions and π–π interactions are shown in red and blue lines respectively. Hydrogen atoms, carbon atoms of 3-pentanone at the axial positions and crystal solvent molecules observed in the channels are omitted for clarity. (c) Crystal packing of **3-PN** along the *c* axis. Hydrogen atoms, and carbon atoms of 3-pentanone at the axial positions and crystal solvent molecules observed in the channels are omitted for clarity. O = red, C = grey, F = pale green, Rh = sea green.

The reaction of $Rh_2(ppeb)_4(Et_2O)_2$ with 1-adamantylamine was subsequently performed to examine the adjustability of the framework to bulky molecules, and the targeted axial ligand substituted complex, $Rh_2(ppeb)_4$(1-adamantylamine)$_2$ (**3-AD**, Figure 3a), was obtained. The distance between two rhodium atoms in **3-AD** was 2.4140(7) Å, which is comparable to that of **3-THF** or **3-PN**. For **3-AD**, the angles between the phenylene and perfluorophenyl rings were 16.3° and 5.9°. In the crystal structure of **3-AD**, a 2-D sheet structure stabilised by multipoint Ar-Ar^F interactions was also obtained (Figure 3b). However, π-π interactions between the 2-D sheets were not observed because the bulkiness of the axial ligands prevented close contact between sheets. Alternatively, the ppeb- ligands exhibited a conformation almost perpendicular to the 2-D sheets, and CF-π interaction[20] between the ppeb- ligands formed inter-sheet stacking. As a result, a 1-D channel structure with an entrance size of 10.1 × 8.2 Å^2 was obtained (Figure. 3c). The mean interplanar separation between the phenylene and perfluorophenyl rings was 3.50(16) Å. The axial ligands were also exposed to the pores despite the different stacking mode from **3-THF** and **3-PN**. The comparison between the assembling-patterns between these structures is shown in Figure 4. The horizontal distances between the Rh dimeric nodes in neighbouring 2-D sheets (denoted as $d1$ and d_2) were found to be $d_1 = d_2 = 4.96$ Å for **3-THF**, $d_1 = 6.08$ Å, $d_2 = 5.82$ Å for **3-PN** and $d_1 = 10.70$ Å, $d_2 = 6.11$ Å for **3-AD** and were mainly different between the three structures, reflecting the bulkiness of the axial ligands. These crystallographic observations indicate that the 2-D sheet structures in these porous frameworks are well defined by the multipoint Ar-Ar^F interactions and that the interlayer stacking structures are controllable in response to the size and shape of the axial ligands.

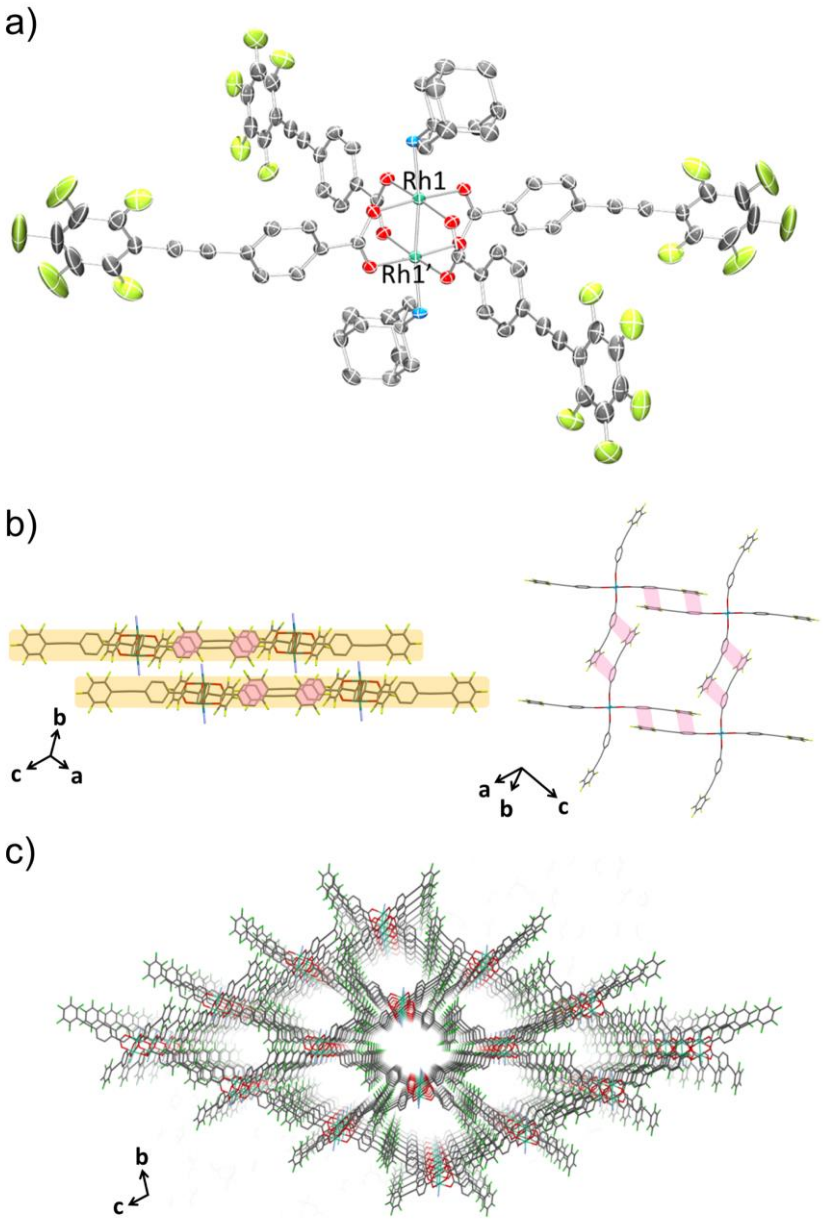

Figure 3. (a) An ORTEP drawing of **3-AD** (50% probability ellipsoids). Hydrogen atoms and crystal solvent molecules are omitted for clarity. (b) 2-D sheet structure of **3-AD**. Ar–Ar^{F} interactions are shown in red lines. Hydrogen atoms, and carbon atoms of **3-AD**amantylamine at the axial positions and crystal solvent molecules observed in the channels are omitted for clarity. (c) Crystal packing of **3-AD** along the *a* axis. Hydrogen atoms, and carbon atoms of 1-adamantylamine at the axial positions and crystal solvent molecules observed in the channels are omitted for clarity. O = red, C = grey, F = pale green, N = blue, Rh = sea green.

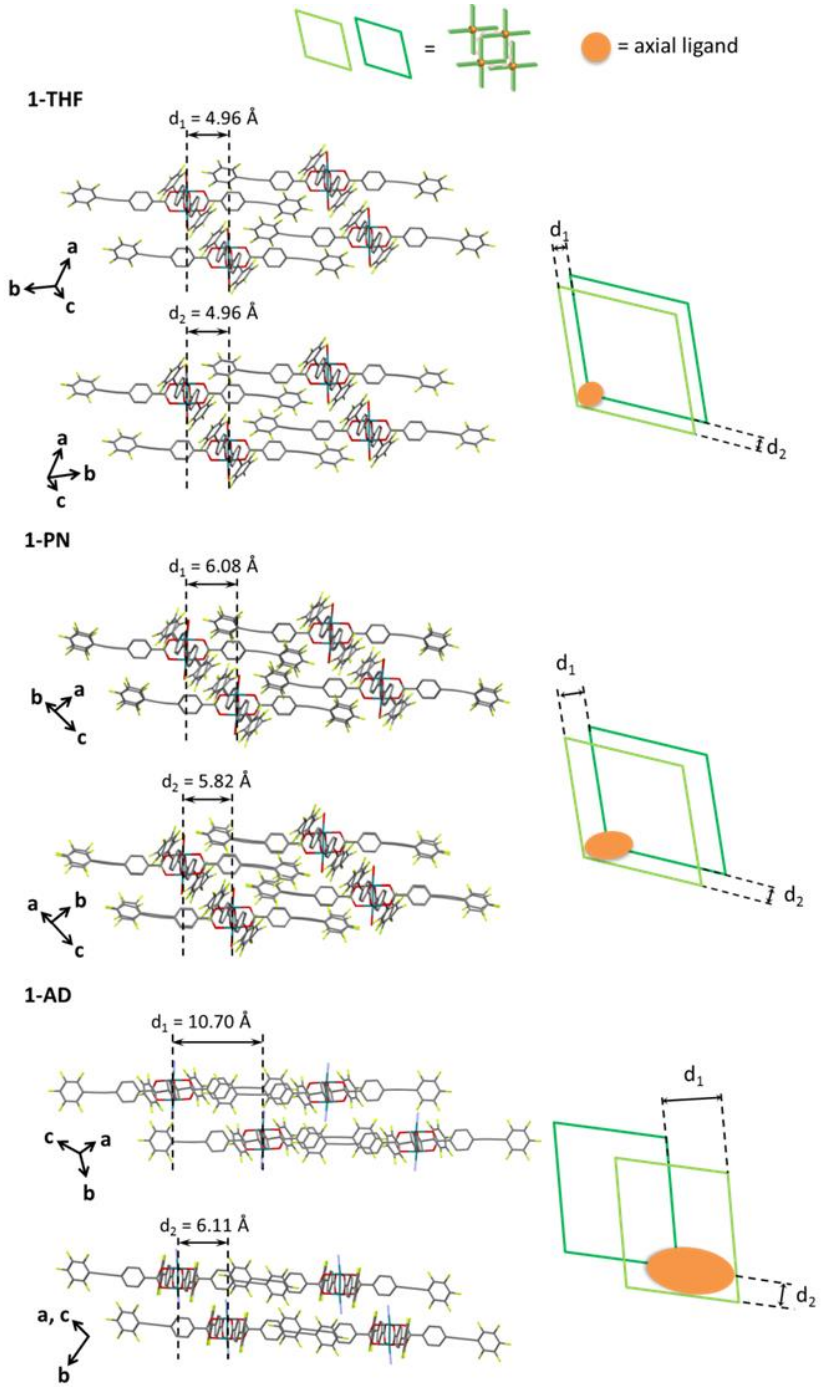

Figure. 4 Side view of the crystal packing (left) and the schematic illustration of the top view of the interlayer stacking structure (right) for **3-THF** (top), **3-PN** (middle) and **3-AD** (bottom). In the schematic illustration, the axial ligands are represented as orange circles.

The effect of the axial ligands on the porous properties

The effect of the axial ligands on the porous properties of the frameworks was also investigated by several measurements. A TG curve of **3-AD** exhibited no weight loss upon heating up to 284 °C (Figure 5c), which indicated the strong coordination ability of the axial ligands to the metal centres. Upon further heating up to 600 °C, the degradation of the complex was observed. It should be noted that the removal of the guest molecules (Et_2O) was not observed due to their highly volatile nature. The removal of the axial ligand was also not observed due to their strong coordination ability. Furthermore, the CO_2 adsorption isotherms for **3-AD** evacuated at 40 ˚C (Figure 5f) and 120 ˚C (Fig 6c) exhibited almost identical sorption profiles, suggesting the retention of the porous structure due to the "capping" of active sites with strongly coordinated axial ligands. In contrast, the TG curves of **3-THF** and **3-PN** indicated the release of axial ligands in the temperature range of 100–170 °C with a weight loss of 5.30% (**3-THF**) and 5.82% (**3-PN**), respectively (Figure 5a-b). The degradation of the complexes was observed in the temperature range of 327–600 °C. In the CO_2 adsorption isotherms of **3-THF** and **3-PN** evacuated at 40 ˚C and 120 ˚C, the amount of adsorbed CO_2 gradually increased as the pressure increased and showed hysteresis during the desorption process (Figure 5d-e and Figure 6a-b) and the adsorption amount are dependent to the temperature of pre-treatment, which may be attributed to the transformation of the interlayer stacking structure arising from the exchange or the loss of the axial ligands. These results clearly indicate the difference in the lability of the axial ligands between **3-AD** and other two structures, **3-THF** and **3-PN**. Additionally, N_2 adsorption measurements at 77 and 195 K were performed and almost no adsorption of N_2 was observed for **3-THF** and **3-PN** (Figure 7a-b and Figure 8a-b), suggesting the selective CO_2 adsorption over N_2 in these frameworks. In contrast to **3-THF** and **3-PN**, N_2 was slightly adsorbed to **3-AD** at 77 K (Figure 7c), although no adsorption of N_2 was observed at 195 K (Figure 8c).

PXRD measurements of the samples after the removal of guest and the dissociation of the axial ligands were performed to investigate the structural change in these processes. The experiments were performed for **3-AD** and **3-PN**, which have the unremovable axial ligands and the removable ligands, respectively. Note that the PXRD patterns for as-synthesized compounds were measured under the vapour of guest molecules to prevent the loss of guest molecules. In the case of **3-AD**, PXRD pattern changed after the evacuation at 40 ˚C (from A to B in Figure 9), suggesting the structural change attributed to the removal of guest molecules. Subsequent evacuation of the sample at 120 ˚C gave the almost identical PXRD pattern (Figure 9 C), which

indicates the strong coordination of axial ligands. These results are fully consistent with the result of TGA and CO_2 adsorption measurements. In the case of **3-PN**, PXRD pattern changed after evacuation at 40 ˚C (from D to E in Figure 10) and the structural transformation accompanied by the removal of guest was observed. In contrast to **3-AD**, the subsequent evacuation at 120 ˚C caused the significant change of the PXRD pattern (from E to F in Figure 10) and the structural transformation due to the dissociation of the axial ligands was indicated. At this stage, we could not determine the structure after the removal of the guest molecules or the axial ligands, and thus, the detailed discussion on the CO_2 adsorption profiles was not allowed. However, the results of CO_2 adsorption and PXRD measurements revealed that the crystallinity and porosity of the sample were maintained throughout the removal of guest molecules and the dissociation of the axial ligands, and the framework structures transformed flexibly accompanied by these processes.

Additionally, PXRD patterns before and after the CO_2 adsorption were also examined. As shown in Figure 11-14, the samples of **3-PN** and **3-AD** did not show significant change in PXRD pattern after the CO_2 adsorption measurements regardless of the pre-treatment temperature. These results indicate that our frameworks recover their initial structures after the CO_2 adsorption/desorption processes.

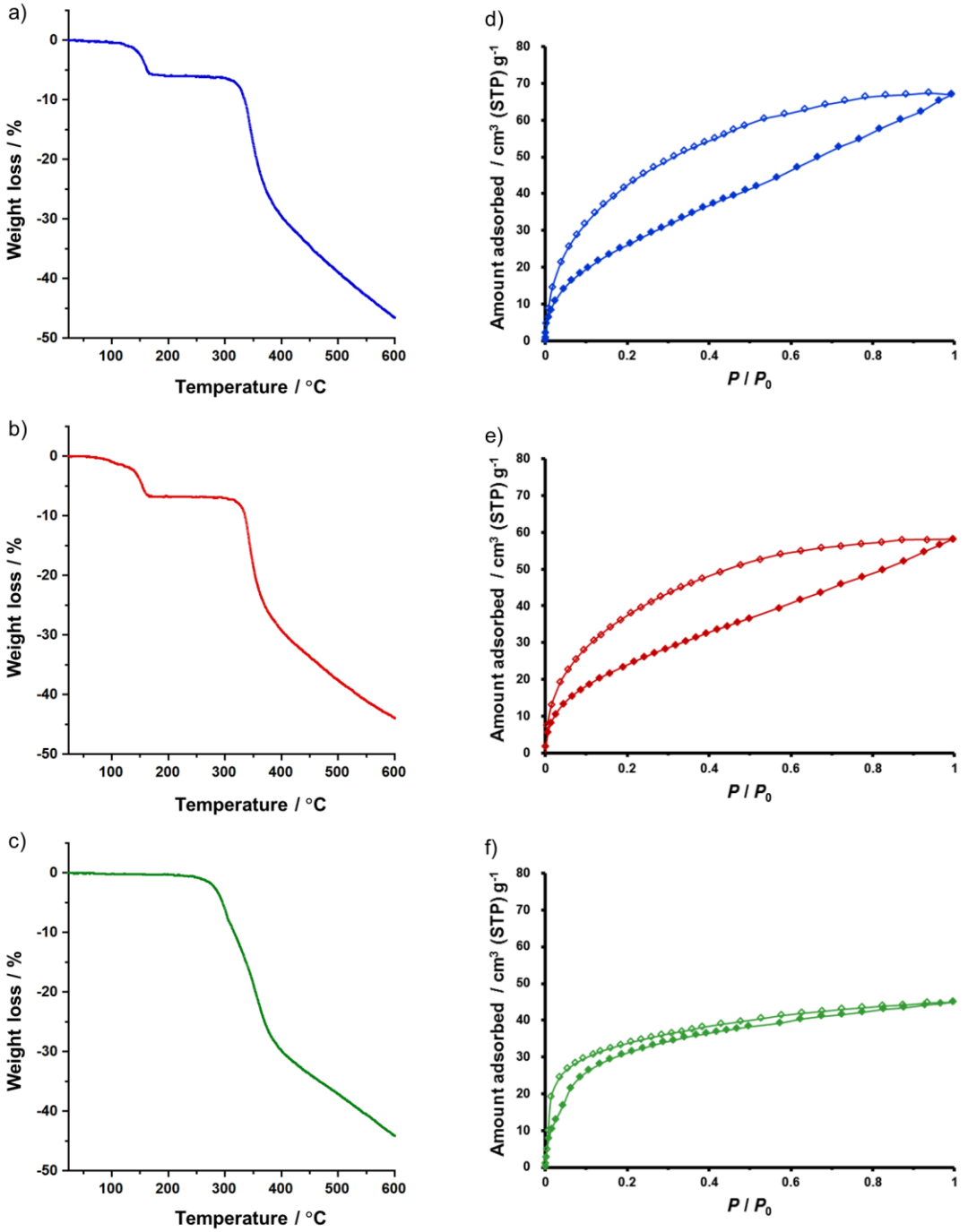

Figure 5. TGA profiles of (a) **3-THF**, (b) **3-PN** and (c) **3-AD** with a heating rate of 20 K min^{-1}. CO_2 sorption isotherms of (d) **3-THF**, (e) **3-PN** and (f) **3-AD** at 195 K. Filled shapes: adsorption. Open shapes: desorption. The samples of **3-THF**, **3-PN** and **3-AD** for the CO_2 adsorption were evacuated at 40 ˚C before the measurements.

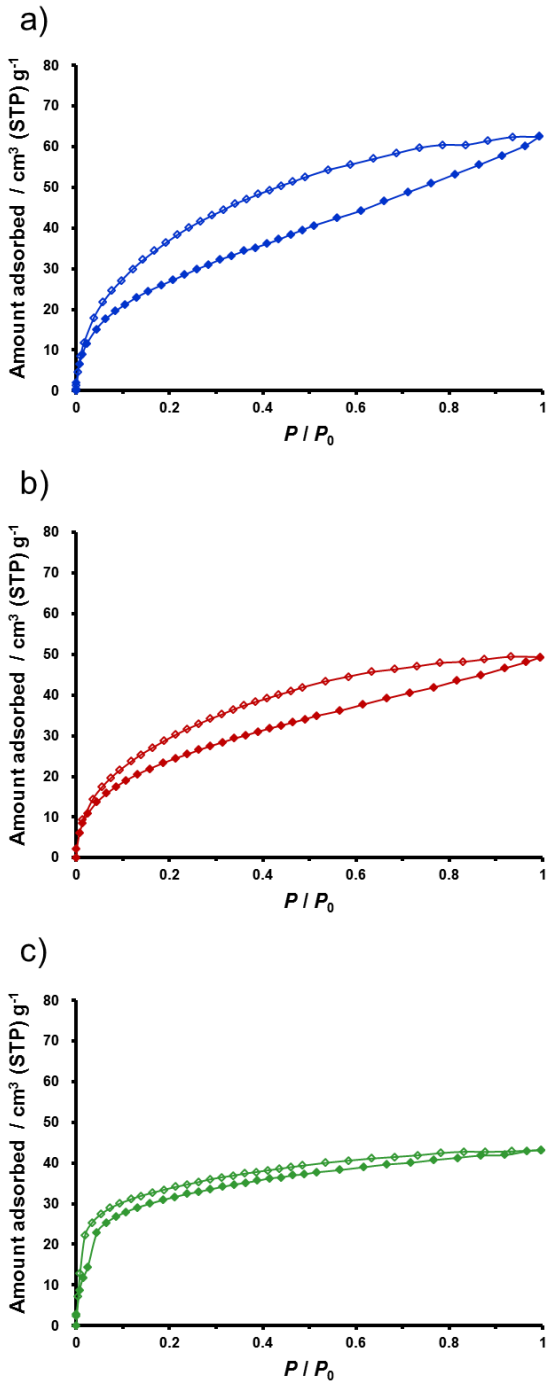

Figure 6. CO_2 sorption isotherms of (a) **3-THF**, (b) **3-PN**, and (c) **3-AD** at 195 K. Filled shapes: adsorption. Open shapes: desorption. The samples of **3-THF**, **3-PN** and **3-AD** for the CO_2 adsorption were evacuated at 120 ˚C before the measurements.

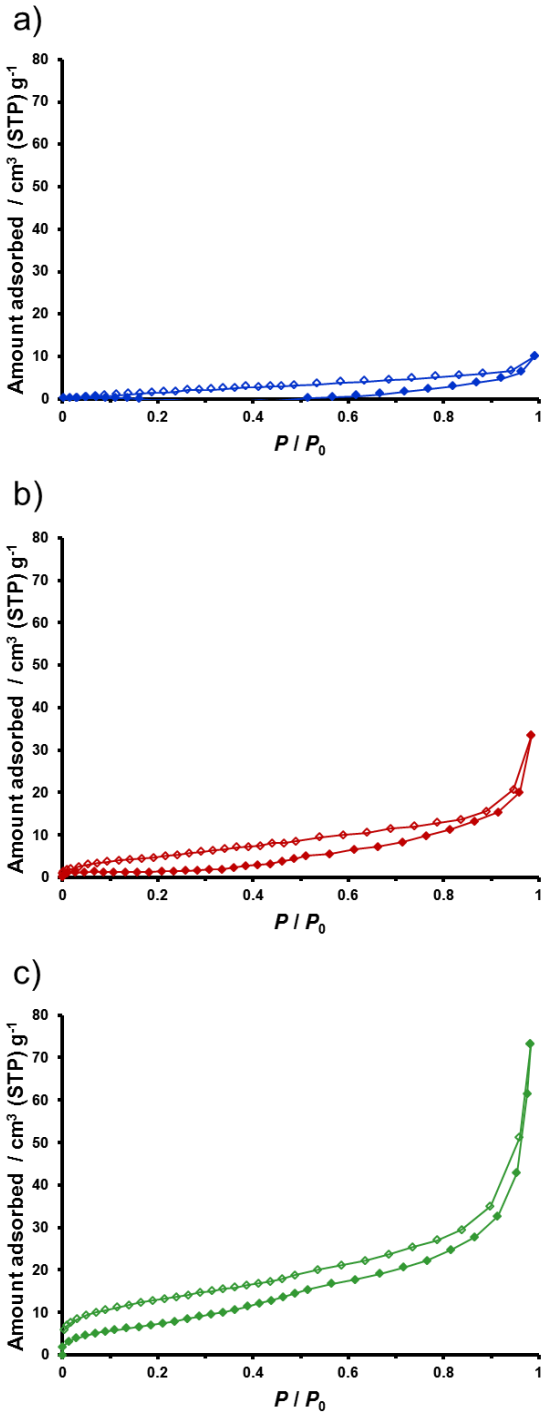

Figure 7. N_2 sorption isotherms of (a) **3-THF**, (b) **3-PN**, and (c) **3-AD** at 77 K. Filled shapes: adsorption. Open shapes: desorption. The samples of **3-THF**, **3-PN** and **3-AD** for the N2 adsorption were evacuated at 40 ˚C before the measurements.

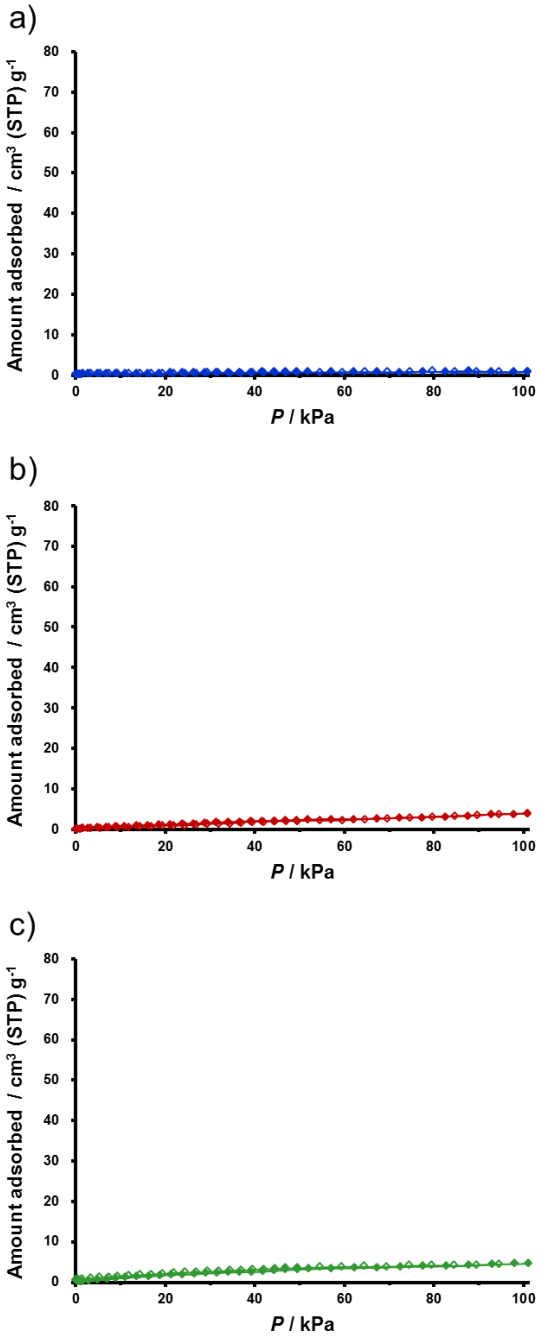

Figure 8. N_2 sorption isotherms of (a) **3-THF**, (b) **3-PN**, and (c) **3-AD** at 195 K. Filled shapes: adsorption. Open shapes: desorption. The samples of **3-THF**, **3-PN** and **3-AD** for the N_2 adsorption were evacuated at 40 ˚C before the measurements.

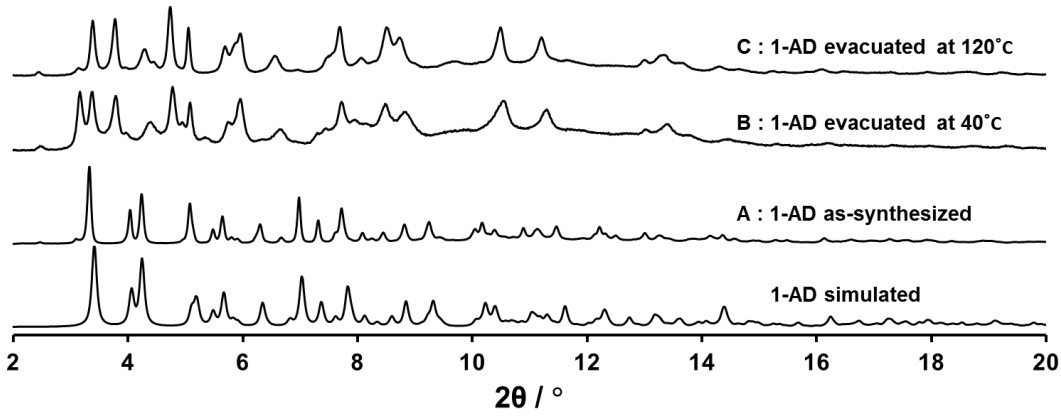

Figure 9. PXRD patterns of (A) **3-AD** as-synthesized, (B) **3-AD** evacuated at 40°C, and (C) **3-AD** evacuated at 120°C.

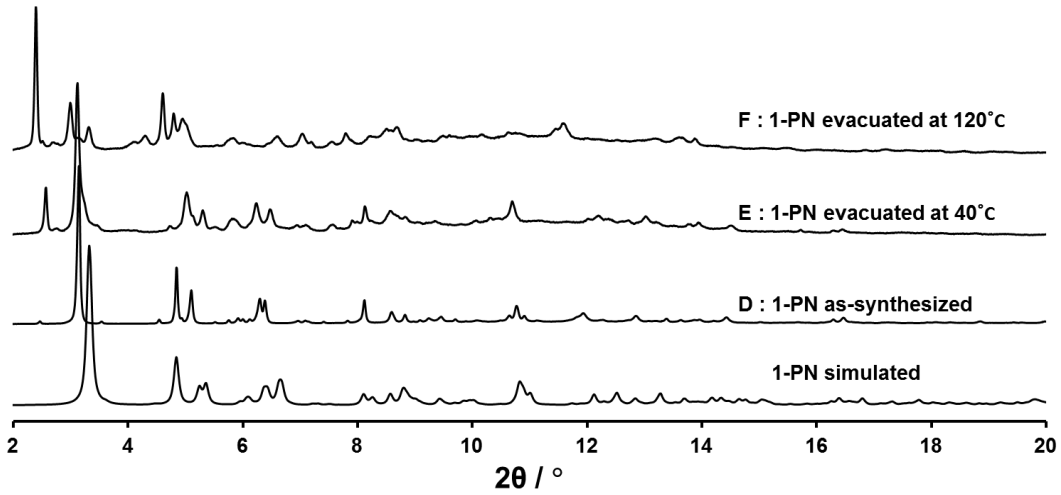

Figure 10. PXRD patterns of (D) **3-PN** as-synthesized, (E) **3-PN** evacuated at 40°C, and (F) **3-PN** evacuated at 120°C.

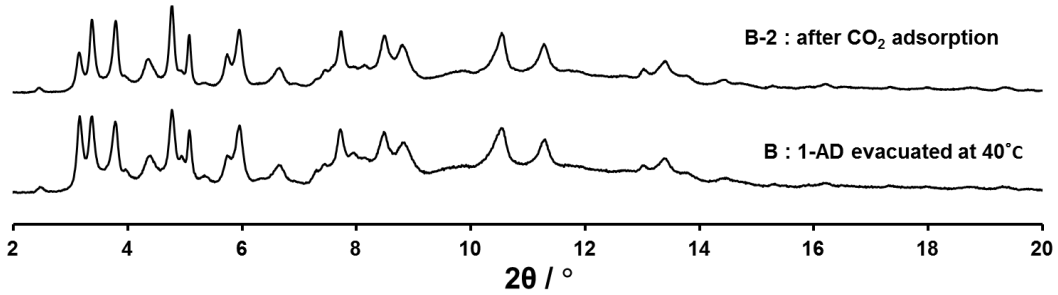

Figure 11. PXRD patterns of (B) **3-AD** evacuated at 40°C and (B-2) **3-AD** after the CO2 adsorption measurement.

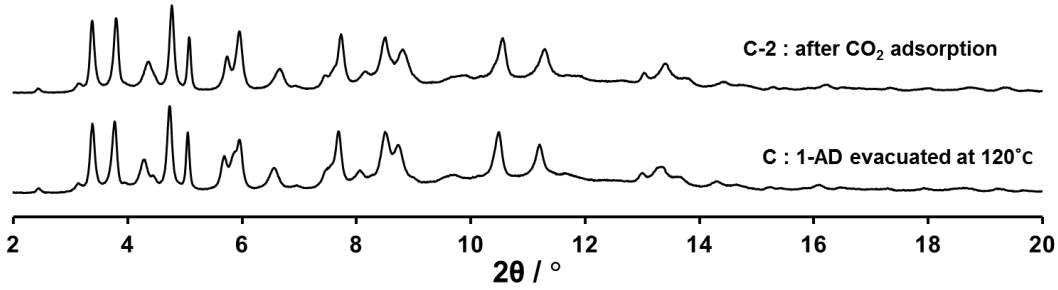

Figure 12. PXRD patterns of (C) **3-AD** evacuated at 120°C and (C-2) **3-AD** after the CO2 adsorption measurement.

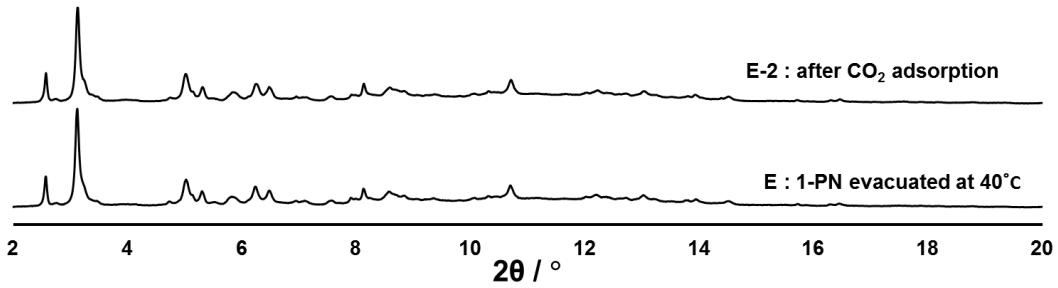

Figure 13. PXRD patterns of (E) **3-PN** evacuated at 40°C and (E-2) **3-PN** after the CO_2 adsorption measurement.

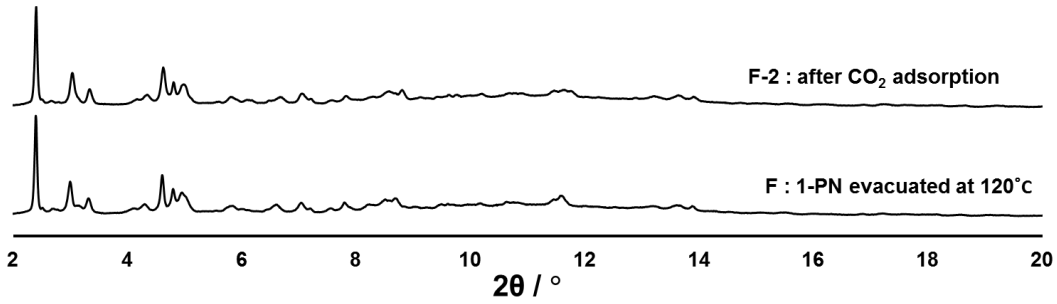

Figure 14. PXRD patterns of (F) **3-PN** evacuated at 120°C and (F-2) **3-PN** after the CO_2 adsorption measurement.

Flexible Structural Transformation during the Ligand Exchange Reaction of the Frameworks

The structural flexibility of **3-THF** and **3-PN** and the reactivity of the open axial sites in these frameworks were examined by PXRD measurements. Initially, crystalline sample of **3-THF** was evacuated at room temperature for 1 h and exposed to 3-pentanone vapour for 1 h. PXRD patterns of before and after the treatment suggested the complete structural transformation from **3-THF** to **3-PN** (Figure 15c-d, blue and red lines). Subsequently, obtained powder sample of **3-PN** was evacuated at room temperature for 1 h and exposed to THF vapour for 1 h. PXRD pattern of the sample treated with THF revealed the regeneration of **3-THF** (Figure 15e). These results indicated that the active sites of the SBUs in our framework effectively worked to control the structural flexibility of each phase.

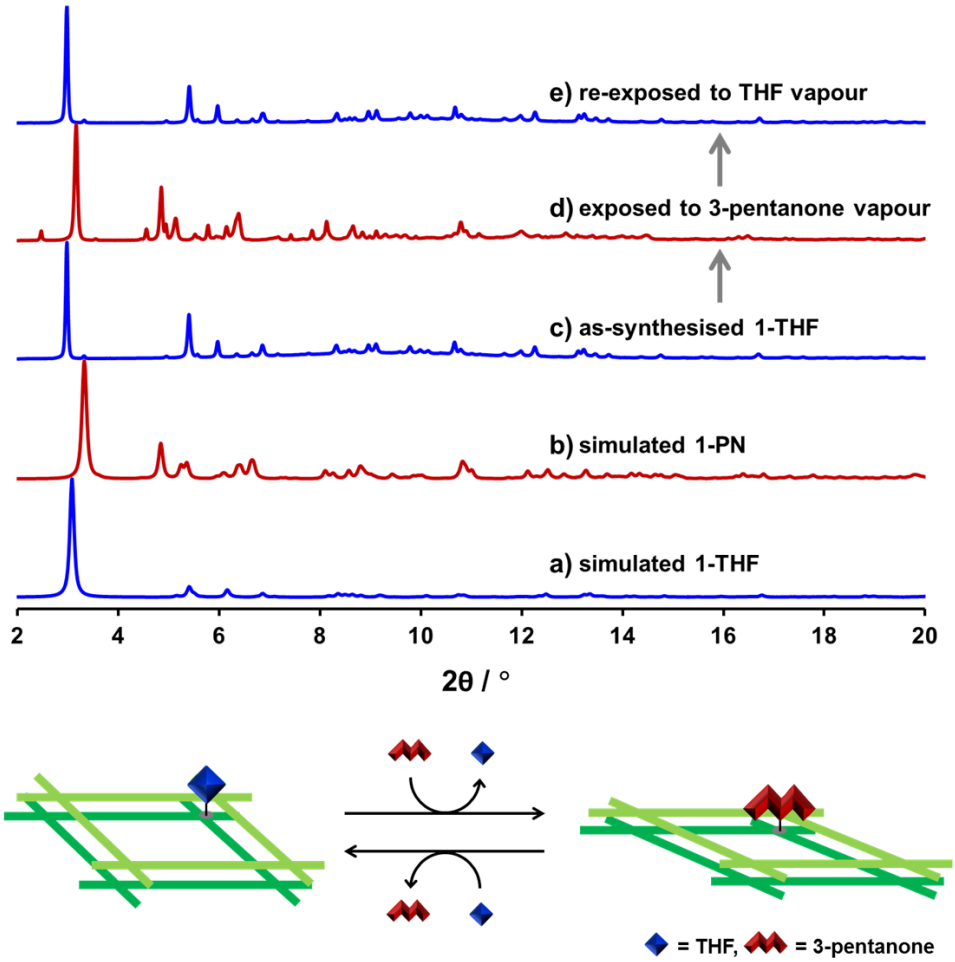

Figure 15. Simulated XRD patterns of (a) **3-THF** and (b) **3-PN** and PXRD patterns of as-synthesised (c) **3-THF**, (d) the sample of **3-THF** exposed to 3-pentanone vapour, and (e) the sample re-exposed to THF vapour. Schematic illustration of the structural transformation between **3-THF** and **3-PN** induced by the reversible ligand substitution reaction (bottom) (λ = 0.79978 Å).

Conclusions

In conclusion, we demonstrated the construction and structural determination of porous frameworks composed of a substitution-inert complex with active sites. Three novel Rh(II) paddle-wheel complexes, $Rh_2(ppeb)_4(X)_2$ (X = THF (**3-THF**), 3-pentanone (**3-PN**), and 1-adamantylamine (**3-AD**)), were successfully assembled to form porous frameworks with a solvent accessible columnar channel by utilizing multipoint Ar-Ar^F interaction. The obtained supramolecular structures possessed active sites exposed to the channel, and the comparison of crystal packing of the three complexes revealed the structural difference induced by the size and the structure of the axial ligands. Furthermore, the porous properties of these frameworks were also examined by several experiments. Although the axial ligands of **3-AD** did not dissociate upon heating and during the sorption process, the axial ligands of **3-THF** and **3-PN** were labile to the axial ligand substitution reaction, and the induced-fit structural transformation in response to the ligand substitution was observed in the crystalline state. We believe that our results presented here should be a key example to construct porous materials based on substitution-inert metal ions with active sites that can be applied for catalytic reactions and chemical sensors.

Experimental

General Methods

All solvents and reagents are of the highest quality available and used as received except for diethylamine and triethylamine. Diethylamine and triethylamine were dried by reflux over KOH, distilled under argon, and degassed with a freeze-and-pump thaw. 4-[(perfluorophenyl)ethynyl]benzoic acid (Hppeb) and $Na_4[Rh_2(CO_3)_4]$ were prepared by the literature methods.[15,16] All syntheses were performed under an atmosphere of dry nitrogen or dry argon unless otherwise indicated. Elemental analysis was carried out on a J-SCIENCE LAB MICRO CORDER JM10 elemental analyser. ^{1}H NMR spectrum was acquired on a JEOL JNM-LA500 spectrometer, where chemical shifts in DMF-d_7 were referenced to internal tetramethylsilane. ^{19}F NMR spectrum was acquired on a JEOL JNM-LA500 spectrometer, where chemical shifts in DMF-d_7 were referenced to external trifluorotoluene. Thermogravimetric analyses (TGA) were carried out with a SHIMADZU DTG-60 under a nitrogen atmosphere. TGA profiles of **3-THF**, **3-PN** and **3-AD** were measured with a heating rate of 20 K min^{-1}. Fourier transformed infrared spectra were measured on a Perkin-Elmer Spectrum 100 FT-IR spectrometer equipped with an ATR (Attenuated Total Reflectance) accessory.

Synthetic Procedures

Synthesis of $Rh_2(ppeb)_4(Et_2O)_2$:

$Na_4[Rh_2(CO_3)_4]\cdot{}_3H_2O$ (59 mg, 0.10 mmol) and Hppeb (250 mg, 0.80 mmol) in 40 ml of DMA/H2O mixed solvents were stirred for 8 h at 100 ˚C. After evaporation of the solvent, the residue was washed with water and dissolved in Et_2O and subsequently purified by column chromatography using neutral alumina (Et_2O as eluent). The yield of $[Rh_2(ppeb)_4]$ was 44 mg (27% based on $Na_4[Rh_2(CO_3)_4]\cdot 3H_2O$). ^{1}H NMR (500 MHz, DMF-d_7) δ ppm: 7.64 (d, J = 10.0 Hz, 2H), 7.98 (d, J = 10.0, 2H); ^{19}F NMR (470.4 MHz, DMF-d_7) δ ppm: -164.3 (dt, J = 4.7, 18.8 Hz, 2F), -154.5 (t, J = 18.8 Hz, 1F), -138.9 (dd, J = 4.7, 18.8 Hz, 2F); Anal. Calcd. for $Rh_2(O_2CC_6H_4C_2C_6F_5)_4(Et_2O)_2\cdot 2H_2O$: C, 49.96; H, 2.60; N, 0.00%. Found: C, 49.79; H, 2.60; N, 0.13%.

Syntheses of 3-THF, 3-PN, 3-AD :

The three kinds of axial ligand substituted complexes were synthesised by the recrystallization of $Rh_2(ppeb)_4(Et_2O)_2$. $Rh_2(ppeb)_4(THF)_2$ (**3-THF**), $Rh_2(ppeb)_4(_3$-pentanone$)_2$ (**3-PN**) were obtained by the slow evaporation of the mixed solution of Et_2O/THF and Et_2O/3-pentanone containing $Rh_2(ppeb)_4(Et_2O)_2$, respectively.

For $Rh_2(ppeb)_4$(1-adamantylamine)$_2$ (**3-AD**), the recrystallisation was performed by layering the Et2O solution of 1-adamantylamine on the Et_2O solution of $Rh_2(ppeb)_4(Et_2O)_2$. FTIR-ATR (cm‑1): 441w, 466s, 522s, 583w, 646m, 699m, 761s, 774s, 850m, 861m, 884m, 965s, 988s, 1018w, 1042w, 1113m, 1141w, 1176w, 1286w, 1389s, 1496s, 1523m, 1549w, 1597m (COO-), 2227w (C≡C), 2876w, 2978w (**3-THF**). FTIR-ATR (cm‑1): 411m, 465s, 522s, 582w, 645m, 699m, 725w, 761s, 774s, 813w, 859m, 964s, 989s, 1020m, 1113m, 1143w, 1178m, 1250w, 1288m, 1305m, 1391s, 1483m, 1496s, 1523m, 1548m, 1596m (COO-), 1677m, 1718w, 2227w (C≡C), 2980w (**3-PN**). FTIR-ATR (cm‑1): 403w, 428w, 463s, 520s, 644m, 698m, 717w, 762s, 773s, 849m, 860m, 924m, 965s, 988s, 1017m, 1061w, 1094w, 1115m, 1141w, 1178w, 1290w, 1311w, 1385s, 1450w, 1496s, 1523m, 1547w, 1600m (COO-), 2228w (C≡C), 3275w (NH2), 3333w(NH2) (**3-AD**).

X-ray crystallography

Crystals of **3-THF**, **3-PN** and **3-AD** were mounted in a loop. Diffraction data at 123 K were measured on a RAXIS-RAPID Imaging Plate diffractometer equipped with confocal monochromated Mo-Kα radiation and data was processed using RAPID-AUTO (Rigaku). Structures were solved by direct methods and refined by full-matrix least squares techniques on F^2 (SHELXL-97).[17] All of the non-hydrogen atoms were anisotropically refined, while all of the hydrogen atoms (except for amine hydrogen atoms of 1-adamantylamine in **3-AD**, which were found on a difference Fourier map and refined isotropically) were placed geometrically and refined with a riding model with *U*iso constrained to be 1.2 times the *U*eq of the carrier atom. For **3-THF**, the diffused electron densities resulting from residual solvent molecules were removed from the data set using the SQUEEZE routine of PLATON and refined further using the data generated. CCDC reference numbers 1049445–1049447 (**3-THF**, **3-PN** and **3-AD**).

Crystal data for $Rh_2(ppeb)_4(THF)_2$ (3-THF): $C_{68}H_{32}F_{20}O_{10}Rh_2$, *Mr* = 1594.76, *monoclinic*, space group *C*2/*m*, (#12), *a* = 18.6449(7), *b* = 27.2267(14), *c* = 8.8932(4) Å, β = 107.4822(12)°, *V* = 4306.0(3) Å^3, *Z* = 2, *T* = 123(2) K, ρ_c = 1.230 g cm^{-3}, μ(Mo-Kα) = 0.471 cm^{-1}, $2\theta_{max}$ = 50.0°, λ(Mo-Kα) = 0.710747 Å, 16 842 reflections measured, 3892 unique (R_{int} = 0.0312), 3549 ($I > 2\sigma(I)$) were used to refine 238 parameters, 6 restraints, wR_2 = 0.1742 ($I > 2\sigma(I)$), R_1 = 0.0660 ($I > 2\sigma(I)$), GOF = 1.135.

Crystal data for $Rh_2(ppeb)_4$(3-pentanone)$_2$ (3-PN):. $C_{170}H_{132}F_{40}O_{26}Rh_4$, *Mr* = 3762.40, *triclinic*, space group $P\bar{1}$, (#2), *a* = 15.1526(7), *b* = 15.3844(4), *c* = 19.5087(4) Å, α = 99.0550(7)°, β = 96.0045(7)°, γ = 112.8590(7)°, *V* = 4069.14(17) Å^3, *Z* = 1, *T* = 123 (2) K, ρ_c = 1.535 g cm^{-3}, μ(Mo-Kα) = 0.514 cm^{-1}, $2\theta_{max}$ = 54.96°, λ(Mo-Kα) = 0.710747 Å, 40 282 reflections measured, 18 528 unique (R_{int} = 0.0223), 13 311 ($I > 2\sigma(I)$) were used to refine 1081 parameters, 0 restraints, wR_2 = 0.1875 ($I > 2\sigma(I)$), R_1 = 0.0554 ($I > 2\sigma(I)$), GOF = 1.111.

Crystal data for $Rh_2(ppeb)_4$(1-adamantylamine)$_2$ (3-AD): $C_{92}H_{70}F_{20}N_2O_8Rh_2$, *Mr* = 1965.32, triclinic, space group $P\bar{1}$, (#2), *a* = 10.8625(8), *b* = 13.8827(10), *c* = 14.9217(11) Å, α = 103.6458(15)°, β = 93.1519(15)°, γ = 94.0312(16)°, *V* = 2175.3(3) Å^3, *Z* = 1, *T* = 123 (2) K, ρ_c = 1.500 g cm^{-3}, μ(Mo-Kα) = 0.483 cm^{-1}, $2\theta_{max}$ = 54.94°, λ(Mo-Kα) = 0.710747 Å, 21 333 reflections measured, 9889 unique (R_{int} = 0.031), 8336 ($I > 2\sigma(I)$) were used to refine 602 parameters, 6 restraints, wR_2 = 0.1511 ($I > 2\sigma(I)$), R_1 = 0.0511 ($I > 2\sigma(I)$), GOF = 1.089.

References

1 (a) B. Moulton, M. J. Zaworotko, *Chem. Rev.*, **2001**, *101*, 1629-1658; (b) S. Kitagawa, R. Kitaura, S. Noro, *Angew. Chem. Int. Ed.*, **2004**, *43*, 2334-2375; (c) G. Férey, C. Serre, *Chem. Soc. Rev.*, **2009**, *38*, 1380-1399; (d) J. Lee, O. K. Farha, J. Roberts, K. A. Scheidt, S. T. Nguyen, J. T. Hupp, *Chem. Soc. Rev.*, **2009**, *38*, 1450-1459; (e) M. D. Allendorf, C. A. Bauer, R. K. Bhakta, R. J. T. Houk, *Chem. Soc. Rev.*, **2009**, *38*, 1330-1352; (f) D. Zacher, O. Shekhah, C. Wöll, R. A. Fischer, *Chem. Soc. Rev.*, **2009**, *38*, 1418-1429; (g) K. Sumida, D. L. Rogow, J. A. Mason, T. M. McDonald, E. D. Bloch, Z. R. Herm, T.-H. Bae, J. R. Long, *Chem. Rev.*, **2012**, *112*, 724-781; (h) M. Yoon, R. Srirambalaji, K. Kim, *Chem. Rev.*, **2012**, *112*, 1196-1231; (i) J.-R. Li, J. Sculley, H.-C. Zhou, *Chem. Rev.*, **2012**, *112*, 869-932; (j) C. Wang, T. Zhang, W. Lin, *Chem. Rev.*, **2012**, *112*, 1084-1104; (k) H. Furukawa, K. E. Cordova, M. O'Keeffe, O. M. Yaghi, *Science*, **2013**, *341*, 974-986.

2 (a) Y. Inokuma, S. Yoshioka, J. Ariyoshi, T. Arai, Y. Hitora, K. Takada, S. Matsunaga, K. Rissanen, M. Fujita, *Nature*, **2013**, *495*, 461-466; (b) B. D. Chandler, G. D. Enright, K. A. Udachin, S. Pawsey, J. A. Ripmeester, D. T. Cramb, G. K. H. Shimizu, *Nat. Mater.*, **2008**, *7*, 229-235; (c) W. M. Bloch, A. Burgun, C. J. Coghlan, R. Lee, M. L. Coote, C. J. Doonan, C. J. Sumby, *Nat. Chem.*, **2014**, *6*, 906-912; (d) J. Rabone, Y.-F. Yue, S. Y. Chong, K. C. Stylianou, J. Bacsa, D. Bradshaw, G. R. Darling, N. G. Berry, Y. Z. Khimyak, A. Y. Ganin, P. Wiper, J. B. Claridge, M. J. Rosseinsky, *Science*, **2010**, *329*, 1053-1057; (e) G. K. H. Shimizu, J. M. Taylor, S. Kim, *Science*, **2013**, *341*, 354-355; (f) H. Deng, S. Grunder, K. E. Cordova, C. Valente, H. Furukawa, M. Hmadeh, F. Gándara, A. C. Whalley, Z. Liu, S. Asahina, H. Kazumori, M. O'Keeffe, O. Terasaki, J. F. Stoddart, O. M. Yaghi, *Science*, **2012**, *336*, 1018-1023.

3 (a) E. D. Bloch, W. L. Queen, R. Krishna, J. M. Zadrozny, C. M. Brown, J. R. Long, *Science*, **2012**, *335*, 1606-1610; (b) S. Xiang, Z. Zhang, C. Zhao, K. Hong, X. Zhao, D. Ding, M. Xie, C. Wu, M. C. Das, R. Gill, K. M. Thomas, B. Chen, *Nat. Commun.*, **2011**, *2*, 204; (c) E. D. Bloch, M. R. Hudson, J. A. Mason, S. Chavan, V. Crocellà, J. D. Howe, K. Lee, A. L. Dzubak, W. L. Queen, J. M. Zadrozny, S. J. Geier, L.-C. Lin, L. Gagliardi, B. Smit, J. B. Neaton, S. Bordiga, C. M. Brown, J. R. Long, *J. Am. Chem. Soc.*, **2014**, *136*, 10752-10761; (d) Y.-S. Bae, C. Y. Lee, K. C. Kim, O. K. Farha, P. Nickias, J. T. Hupp, S. T. Nguyen, R. Q. Snurr, *Angew. Chem. Int. Ed.*, **2012**, *51*, 1857-1860; (e) Z. Guo, H. Wu, G. Srinivas, Y. Zhou, S. Xiang, Z. Chen, Y. Yang, W. Zhou, M. O'Keeffe, B. Chen, *Angew. Chem. Int. Ed.*, **2011**, *50*, 3178-3181.

4 (a) C.-D. Wu, A. Hu, L. Zhang W. Lin, *J. Am. Chem. Soc.*, **2005**, *127*, 8940-8941; (b) Z. Zhang, Y. Chen, S. He, J. Zhang, X. Xu, Y. Yang, F. Nosheen, F. Saleem, W. He, X. Wang, *Angew. Chem. Int. Ed.*, **2014**, ***53***, 12517-12521; (c) W. Xuan, C. Ye, M. Zhang, Z. Chen, Y. Cui, *Chem. Sci.*, **2013**, ***4***, 3154-3159.

5 (a) B. Chen, Y. Yang, F. Zapata, G. Lin, G. Qian, E. B. Lobkovsky, *Adv. Mater.*, 2007, ***19***,

1693-1696; (b) N. B. Shustova, A. F. Cozzolino, S. Reineke, M. Baldo, M. Dincă, *J. Am. Chem. Soc.*, **2013**, *133*, 13326-13329.

6 (a) S. S.-Y. Chui, S. M.-F. Lo, J. P. H. Charmant, A. G. Orpen, I. D. Williams, *Science*, **1999**, 283, 1148-1150; (b) N. L. Rosi, J. Kim, M. Eddaoudi, B. Chen, M. O'Keeffe, O. M. Yaghi, *J. Am. Chem. Soc.*, **2005**, *127*, 1504-1518.

7 (a) P. Ceccherelli, M. Curini, M. C. Marcotullio, O. Rosati, Tetrahedron, **1991**, *47*, 7403-7408; (b) M. P. Doyle, *Acc. Chem. Res.*, **1986**, *19*, 348-356; (c) M. P. Doyle, K. G. High, C. L. Neslonely, T. W. Clayton Jr., J. Lin, *Organometallics*, **1991**, *10*, 1225-1226; (d) S. Tanaka, S. Masaoka, K. Yamauchi, M. Annaka, K. Sakai, *Dalton Trans.*, **2010**, *39*, 11218-11226; (e) D. K. Kumar, A. S. Filatov, M. Napier, J. Sun, E. V. Dikarev, M. A. Petrukhina, *Inorg. Chem.*, **2012**, *51*, 4855-4861; (f) J. Hansen, H. M. L. Davies, Coord. Chem. Rev., **2008**, *252*, 545-555; (g) K. P. Kornecki, J. F. Briones, V. Boyarskikh, F. Fullilove, J. Autschbach, K. E. Schrote, K. M. Lancaster, H. M. L. Davies, J. F. Berry, *Science*, **2013**, *342*, 351-354.

8 (a) G. Férey, C. Serre, C. Mellot-Draznieks, F. Millange, S. Surblé, J. Dutour, I. Margiolaki, *Angew. Chem. Int. Ed.*, **2004**, *43*, 6296-6301; (b) G. Férey, C. Mellot-Draznieks, C. Serre, F. Millange, S. Surblé, J. Dutour, I. Margiolaki, Science, **2005**, *309*, 2040-2042.

9 (a) P. D. C. Dietzel, Y. Morita, R. Blom and H. Fjellvåg, *Angew. Chem. Int. Ed.*, **2005**, *44*, 6354-6358; (b) B. Chen, N. W. Ockwig, A. R. Millward, D. S. Contreras and O. M. Yaghi, *Angew. Chem. Int. Ed.*, **2005**, *44*, 4745-4749; (c) X.-S. Wang, S. Ma, P. M. Forster, D. Yuan, J. Eckert, J. J. López, B. J. Murphy, J. B. Parise and H.-C. Zhou, *Angew. Chem. Int. Ed.*, **2008**, *47*, 7263-7266; (d) D. Yuan, D. Zhao, D. Sun, and H.-C. Zhou, *Angew. Chem. Int. Ed.*, **2010**, *49*, 5357-5361; (e) M. Dincă , A. Dailly, Y. Liu, C. M. Brown, D. A. Neumann and J. R. Long, *J. Am. Chem. Soc.*, **2006**, *128*, 16876-16883; (f) T. M. McDonald, D. M. D'Alessandro, R. Krishnac and J. R. Long, *Chem. Sci.*, **2011**, *2*, 2022–2028; (g) Y. Liu, J. F. Eubank, A. J. Cairns, J. Eckert, V. C. Kravtsov, R. Luebke and M. Eddaoudi, *Angew. Chem. Int. Ed.*, 2007, *46*, 3278-3283; (h) M. Pang, A. J. Cairns, Y. Liu, Y. Belmabkhout, H. C. Zeng and Mohamed Eddaoudi, *J. Am. Chem. Soc.*, **2012**, *134*, 13176-13179.

10 (a) P. Li, Y. He, J. Guang, L. Weng, J. C.-G. Zhao, S. Xiang and B. Chen, *J. Am. Chem. Soc.*, **2014**, *136*, 547-549; (b) W. Yang, A. Greenaway, X. Lin, R. Matsuda, A. J. Blake, C. Wilson, W. Lewis, P. Hubberstey, S. Kitagawa, N. R. Champness and M. Schröder, *J. Am. Chem. Soc.*, **2010**, *132*, 14457-14469; (c) M. Mastalerz and I. M. Oppel, *Angew. Chem. Int. Ed.*, **2012**, *51*, 5252-5255; (d) S. A. Dalrymple and G. K. H. Shimizu, *J. Am. Chem. Soc.*, **2007**, *129*, 12114-12116; (e) P. S. Nugent, V. Lou Rhodus, T. Pham, K. Forrest, L. Wojtas, B. Space and Michael J. Zaworotko, *J. Am. Chem. Soc.*, **2013**, *135*, 10950-10953; (f) P. Li, Y. He, Y. Zhao, L. Weng, H. Wang, R. Krishna, H. Wu, W. Zhou, M. O'Keeffe, Y. Han and B. Chen, *J. Am. Chem. Soc.*, **2015**, *54*, 574-577.

11 (a) M. J. Bojdys, M. E. Briggs, J. T. A. Jones, D. J. Adams, S. Y. Chong, M. Schmidtmann and A. I. Cooper, *J. Am. Chem. Soc.*, **2013**, *135*, 16566-16571; (b) T. Kaczorowski, I. Justyniak, T. Lipińska, J. Lipkowski and J. Lewiński, *J. Am. Chem. Soc.*, **2009**, *131*, 5393-5395; (c) M. Mastalerz, M. W. Schneider, I. M. Oppel and O. Presly, *Angew. Chem. Int. Ed.*, **2011**, *50*, 1046-1051; (d) K. Sokołowski, W. Bury, I. Justyniak, D. Fairen-Jimenez, K. Sołtys, D. Prochowicz, S. Yang, M. Schröder and Janusz Lewiński, *Angew. Chem. Int. Ed.*, **2013**, *52*, 13414-13418; (e) G. Zhang, O. Presly, F. White, I. M. Oppel and M. Mastalerz, *Angew. Chem. Int. Ed.*, **2014**, *53*, 1516-1520; (f) C. Redshaw, S. Jana, C. Shang, M. R. J. Elsegood, X. Lu and Z. X. Guo, *Organometallics*, **2010**, 29, 6129-6132.

12 (a) J. Lü, C. Perez-Krap, M. Suyetin, N. H. Alsmail, Y. Yan, S Yang, W. Lewis, E. Bichoutskaia, C, C. Tang, A. J. Blake, R. Cao and M. Schröder, *J. Am. Chem. Soc.*, **2014**, *136*, 12828-12831; (b) W. Bury, I. Justyniak, D. Prochowicz, A. Rola-Noworyta and Janusz Lewiński, *Inorg. Chem.*, **2012**, *51*, 7410-7414; (c) J. Lewiński, T. Kaczorowski, D. Prochowicz, T. Lipińska, I. Justyniak, Z. Kaszkur and J. Lipkowski, *Angew. Chem. Int. Ed.*, **2010**, *49*, 7035-7039.

13 (a) H. Kim, Y. Kim, M. Yoon, S. Lim, S. M. Park, G. Seo and K. Kim, *J. Am. Chem. Soc.*, **2010**, *132*, 12200-12202; (b) T. Tozawa, J. T. A. Jones, S. I. Swamy, S. Jiang, D. J. Adams, S. Shakespeare, R. Clowes, D. Bradshaw, T. Hasell, S. Y. Chong, C. Tang, S. Thompson, J. Parker, A. Trewin, J. Bacsa, A. M. Z. Slawin, A. Steiner and A. I. Cooper, *Nature Mat.*, **2009**, *8*, 973-978; (c) J. T. A. Jones, T. Hasell, X. Wu, J. Bacsa, K. E. Jelfs, M. Schmidtmann, S. Y. Chong, D. J. Adams, A. Trewin, F. Schiffman, F. Cora, B. Slater, A. Steiner, G. M. Day and A. I. Cooper, *Nature*, **2011**, *474*, 367-361; (d) C. G. Bezzu, M. Helliwell, J. E. Warren, D. R. Allan, N. B. McKeown, Science, **2010**, *327*, 1627-1630; (e) T. Hasell, S. Y. Chong, M. Schmidtmann, D. J. Adams and A. I. Cooper, *Angew. Chem. Int. Ed.*, **2012**, *51*, 7154-7157; (f) M. W. Schneider, I. M. Oppel, A. Griffin and M. Mastalerz, *Angew. Chem. Int. Ed.*, **2013**, *52*, 3611-3615.

14 (a) J. H. Williams, Acc. Chem. Res., **1993**, *26*, 593-598; (b) C. R. Patrick, G. S. Prosser, *Nature*, **1960**, *187*, 1021.

15 T. Itoh, M. Kondo, M. Kanaike, S. Masaoka, *CrystEngComm*, **2013**, *15*, 6122-6126.

16 C. R. Willson, H. Taube, *Inorg. Chem.*, **1975**, *47*, 533-535.

17 G. M. Sheldrick, Program for Crystal Structure Refinement, University of Göttingen, Germany, **1997**.

18 (a) F. A. Cotton, C. A. Murillo, R.A Walton, "Multiple Bonds Between Metal Atoms", 3rd ed., Springer Science and Business Media, New York, **2005**; (b) E. B. Royar, S. D. Robinson, Platinum Metals Rev., **1982**, *26*, 65-69.

19 The channel entrance size was estimated by considering the wan der waals radii of constituent atoms, and the atoms at axial ligands are omitted for the calculation.

20 (a) N. Hayashi, T. Mori, K. Matsumoto, *Chem. Commun.*, **1998**, 1905-1906; (b) K. Reichenbächer, H. I. Süss, J. Hulliger, *Chem. Soc. Rev.*, **2005**, *34*, 22-30; (c) X. Xu, B. Pooi, H. Hirao, S. H. Hong, *Angew. Chem. Int. Ed.*, **2014**, *53*, 1283-1287.

Chapter 3

Attempt to construct porous frameworks by utilization of Ar-Ar^F interaction and photodimerization

Introduction

Metal–organic frameworks (MOFs) or porous coordination polymers (PCPs) appeared as a new class of porous materials about two decades ago and have developed dramatically to be applied in many research areas.[1] Especially, open metal sites-incorporated MOFs or PCPs are interesting due to the direct interaction between substrate and metal center.[1f-r] To explore open metal sites-incorporated MOFs or PCPs with enhanced or advanced activity, synthetic methods have also been developed,[2] but there is still one remaining challenge. Since these materials are constructed by coordination-driven self-assembly, substitution-inert metal based building unit with open metal sites is difficult to be incorporated. In our group, previously we have succeeded in construction of porous framework by non-covalent linking of Rh_2 paddle-wheel units.[3] However, non-covalently linked framework can be affected by the guest molecules which sometimes disturb the interaction for self-assembly. For instance, aprotic solvent can interfere in hydrogen bonding and aromatic solvent can interfere in π-π interaction. One of the strategies to avoid such kind of problem is linking discrete molecule or low dimensional coordination polymer by photodimerization reaction. In the research field of MOFs or PCPs, [2+2] photodimerization of stilbene moiety is one of the most widely used reactions.[4-7] As previously reported, it is proved that photodimerization enables us to construct coordination polymer with higher dimension.[4] Moreover, conversion accompanied with single crystal to single crystal (SC-SC) manner[4b, 4c, 4e, 5] and tuning of pore surface[5j, 5p, 6] are also expected.

Here in we show an attempt to construct substitution-inert Rh_2 paddle-wheel units based MOF by the utilization of self-assembly via non-covalent interaction and [2+2] photo dimerization reaction. A new Rh(II) paddle-wheel dimer with non-covalent interaction sites and photo chemically reactive site was synthesized to examine the crystal packing and photodimerization reaction.

To achieve [2+2] photodimerization reaction, Schmidt criteria (i.e., two C=C bonds aligned parallel and distance between them less than 4.2 Å)[8] should be satisfied at solid state. Several strategies have been developed to control the molecular

arrangements of stilbene moiety (Scheme 1).[9] Among the four strategies, arene-perfulorarene interaction is simplest way because in other cases, we have to consider some problems such as bulkiness of ligand or couter ion which can obstruct pores, incorporation of more than one component, and competition between coordination and intermolecular interaction. Considering strategies mentioned above, a novel ligand, 4-[(*E*)-2-(perfluorophenyl)vinyl]benzoic acid ((*E*)-Hppvb, Chart 1) was designed. Arene and perfluoroarene moieties of (*E*)-Hppvb are bridged by C=C bond which is expected to photo dimerize in the crystalline state.[9b]

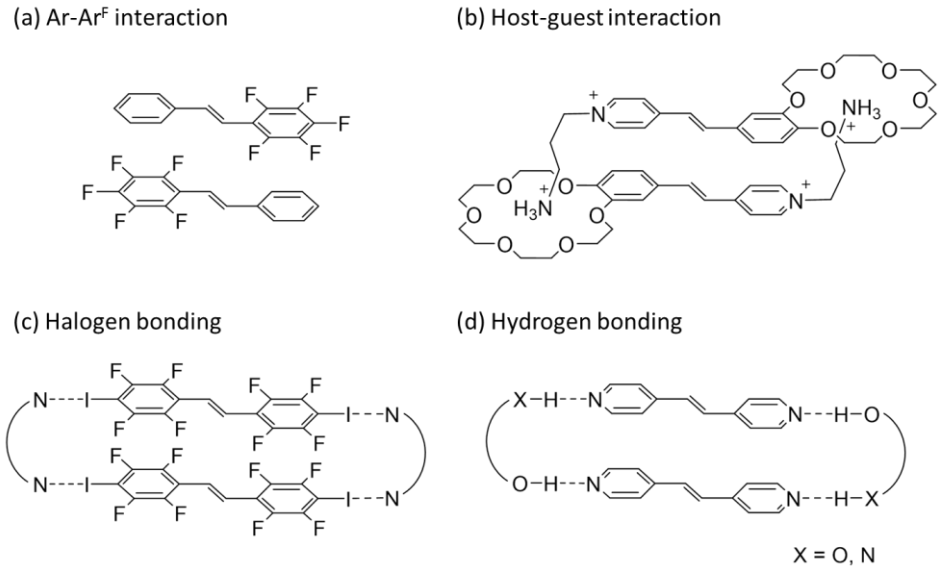

Scheme. 1 Schematic illustration of intermolecular interactions. Multipoint arene-perfluoroarene interaction exhibits *unidirectional* arrangement, whereas other interactions show multidirectional arrangements.

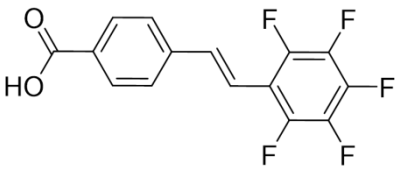

Chart 1. Chemical structure of (*E*)-Hppvb.

Synthesis and crystal structures of ligand (*E*)-Hppvb

The synthesis of (*E*)-Hppvb is summarized in Scheme 2. Firstly, [4-(Methoxycarbonyl)benzyl](triphenyl)phosphonium bromide was synthesized from the reaction of methyl4-(bromomethyl)benzoate with PPh_3.[10] Then, Methyl 4-[(*E*)-2-(perfluorophenyl)vinyl]benzoate as an ester precursor was synthesized via Wittig reaction.[11] Finally, the ester precursor was hydrolyxed by NaOH to give (*E*)-Hppvb, which was characterized by ^{1}H NMR, ^{19}F NMR, elemental analysis and single-crystal X-ray diffraction. The total synthetic yield was 38%.

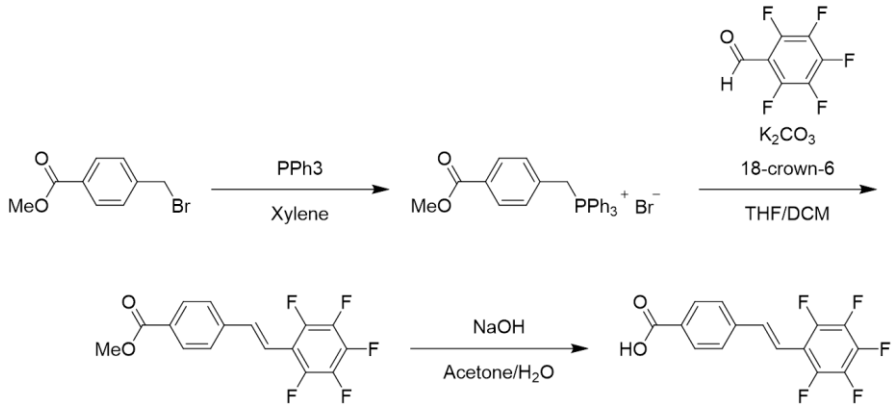

Scheme 2. Synthesis of (*E*)-Hppvb.

Crystal structures of (*E*)-Hppvb

From the recrystallization of (*E*)-Hppvb with several solvents, we obtained two types of crystal packing. One of them was obtained from THF and the crystal structure and packing are shown in Figure 1. In this case, (*E*)-Hppvb packed in a head-to-head fashion and two carboxylic acids form a dimer via OH···O hydrogen bond (O1···H2 distance: 1.83 Å at -20 ˚C). The dimers stacked through not Ar-Ar^F interaction but π-π interaction (Figure 1). The C=C bonds separation is 5.01 Å at -20 ˚C (longer than 4.2 Å), so photodimerization is not expected to proceed. It should be noted that this crystal showed structural transformation with temperature decrease and SC-XRD of the sample at -150 ˚C was successfully analysed. While the crystal at -20 ˚C showed a monoclinic *P* $2_1/c$ space group, the crystal at -150 ˚C exhibited *P* $2_1/n$ space group and the *b* axis of the unit cell drastically changed from 5.97671(19) Å to 29.9942(7) Å (Table 1). The crystal packing at lower temperature was similar to that of the crystal at -20 ˚C, but at -150 ˚C, five (*E*)-Hppvb ligands was observed independently to show disarray crystal packing in some direction compared to the crystal at higher temperature as shown in Figure 2. Hydrogen bond between carboxylic acid was 1.82 Å at -150 ˚C. The structural change caused a sliding of π- π stacking between carboxylic acids dimer and C=C bonds separation became shorter to be 4.94 Å (Figure 1). However, the separation is still too far to proceed [2+2] photodimerization (< 4.2 Å).

Table 1. Crystallographic data and structural refinements for (*E*)-Hppvb recrystallized from THF measured at -20 ˚C (left) and -150 ˚C (right).

Formula	$C_{15}H_7F_5O_2$
Fw	314.21
Color, habit	Colorless, stick
Crystal system	Monoclinic
Space group	*P* $2_1/c$
a (Å)	5.0074(2)
b (Å)	5.97671(19)
c (Å)	41.8405(14)
α (deg)	90
β (deg)	92.255(7)
γ (deg)	90
V, A^3	1251.23(8)
Z	4
T (K)	253
R_1	0.0440
wR_2	0.1397
GOF	1.057

Formula	$C_{15}H_7F_5O_2$
Fw	314.21
Color, habit	Colorless, stick
Crystal system	Monoclinic
Space group	*P* $2_1/n$
a (Å)	4.93490(10)
b (Å)	29.9942(7)
c (Å)	41.3917(10)
α (deg)	90
β (deg)	93.255(7)
γ (deg)	90
V, A^3	6116.85
Z	20
T (K)	123
R_1	0.0587
wR_2	0.1579
GOF	1.009

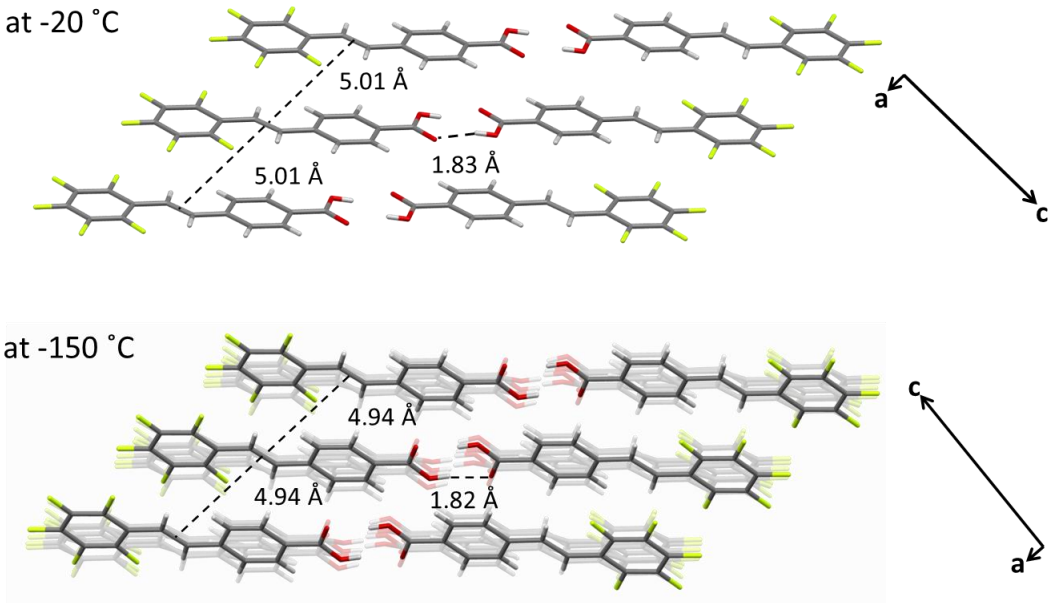

Figure 1. Crystal packings of (*E*)-Hppvb recrystallized from THF measured at -20 ˚C along the b axis (top) and -150 ˚C along the b axis (bottom).

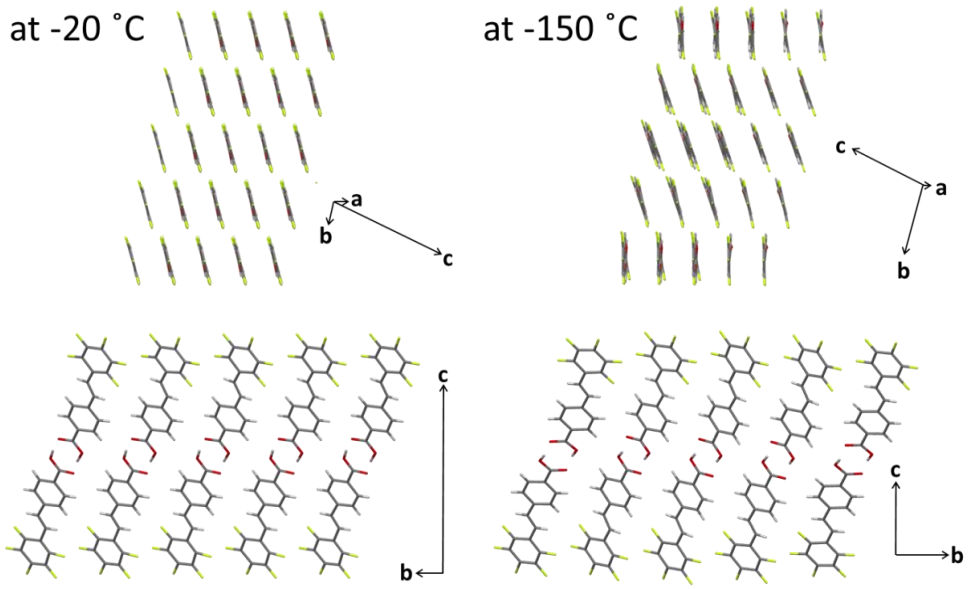

Figure 2. Crystal packings of (*E*)-Hppvb recrystallized from THF measured at -20 ˚C (left) and -150 ˚C (right).

Another one was obtained from DMF and the crystal structure and packing are shown in figure X. In this case, in contrast to that crystallized from THF, (*E*)-Hppvb stacked in a head-to-tail fashion and proton of carboxylic acid is hydrogen bonded to oxygen atom of DMF (O3···H1 distance: 1.75 Å) (Figure 3). That's why dimerization of carboxylic acid was not observed and Ar-Ar^{F} interaction could work dominantly for the stacking of (*E*)-Hppvb. In addition, C=C bonds lie parallel and separated by 3.68 and 3.79 Å, which are suitable distance for photodimerization.

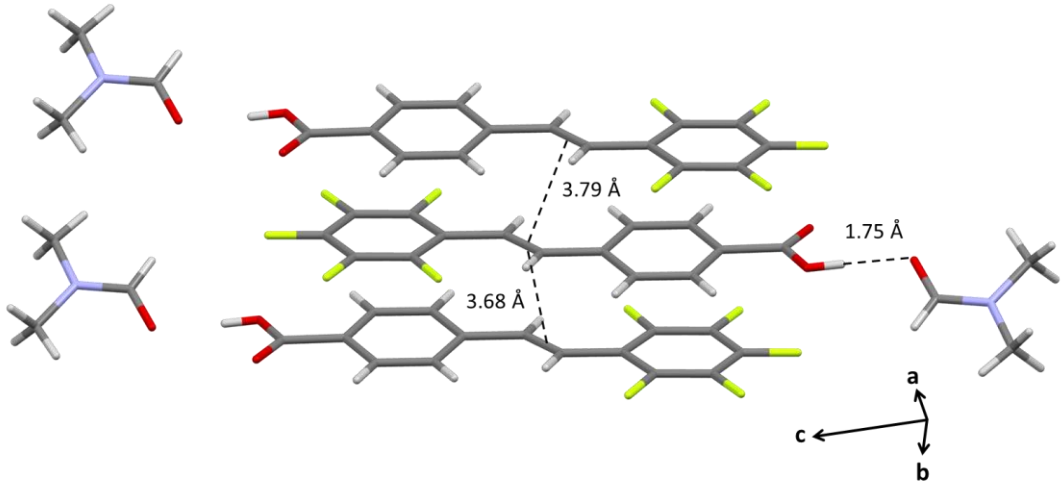

Figure 3. Crystal packing of (*E*)-Hppvb recrystallized from DMF.

Photodimerization of (*E*)-Hppvb

Next, we examined photodimerization reaction of the crystalline samples. Firstly, to confirm the maximal absorption wavelength, a UV-Vis absorption spectrum of (*E*)-Hppvb was measured. In 30 μM DMF solution, the spectra shows π-π* transition in UV-region with λ_{max} at 315 nm and molar absorptivity of ca. 32500 (Figure 4). For the irradiation of exact wavelength near the λ_{max}, a Hg lamp manufactured by Asahibunko, REX-250 was initially used. The lamp enables us to irradiate emission line with spectral distribution of 315 nm ± 5nm.

By the irradiation of UV-light to crystalline sample obtained from DMF solution which is likely to photodimerize, photodimerized product was partially obtained (Scheme 3) and an isomerized product of (*E*)-Hppvb, (*Z*)-Hppvb and unidentified product were also observed in ^{1}H NMR spectra. We also tried photo irradiation with a different Hg lamp which has wide spectral distribution, C-HGFI manufactured by Nikon. Interestingly, photo irradiation for 24 hours gave only photo dimerized product without any side product (Figure 5).

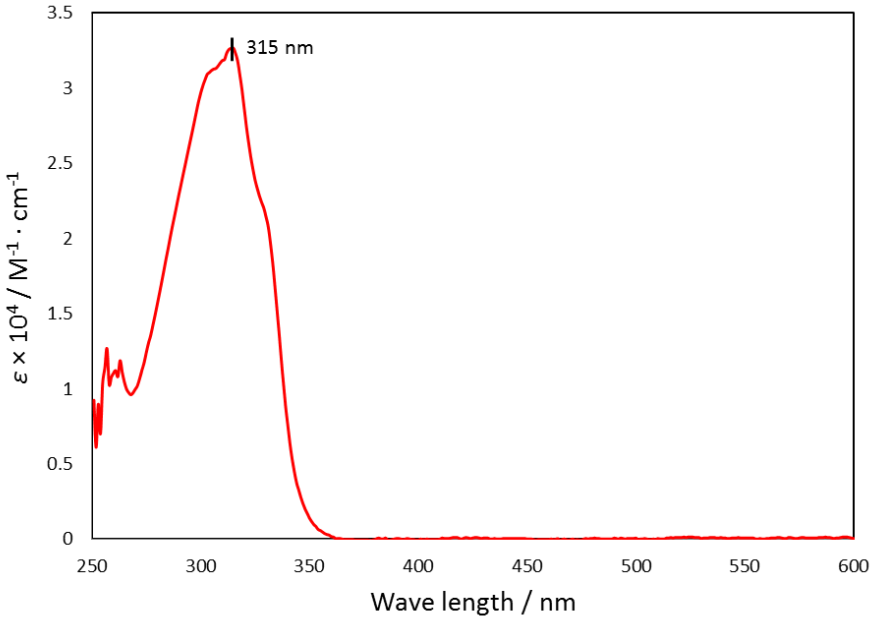

Figure 4. A UV-Vis absorption spectrum of (*E*)-Hppvb in DMF at room temperature.

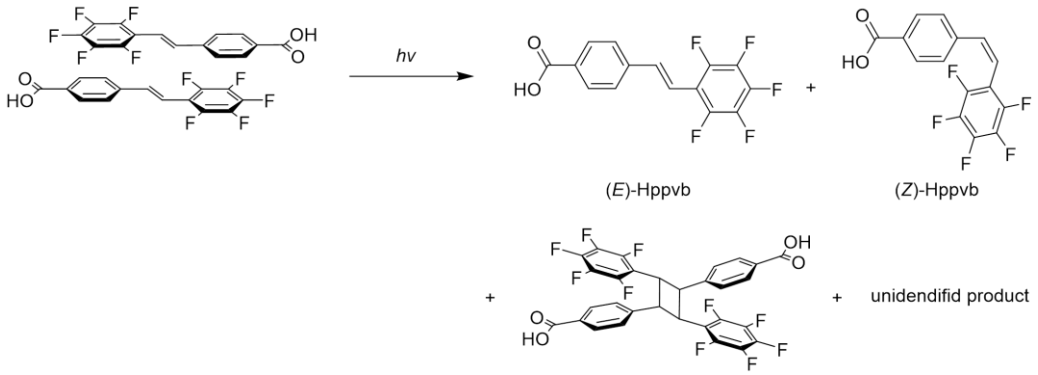

Scheme 3. Photo irradiation to crystalline powder of (*E*)-Hppvb obtained from DMF solution by a REX-250 Hg lamp.

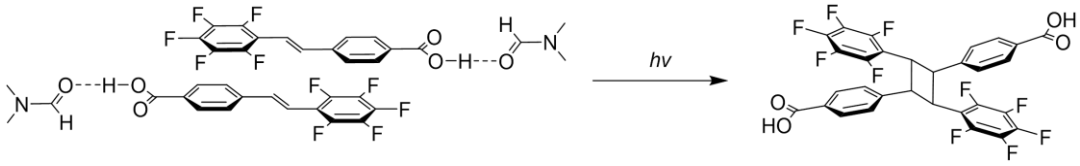

Scheme 4. Photo irradiation to crystalline powder of (*E*)-Hppvb obtained from DMF solution by a C-HGFI Hg lamp.

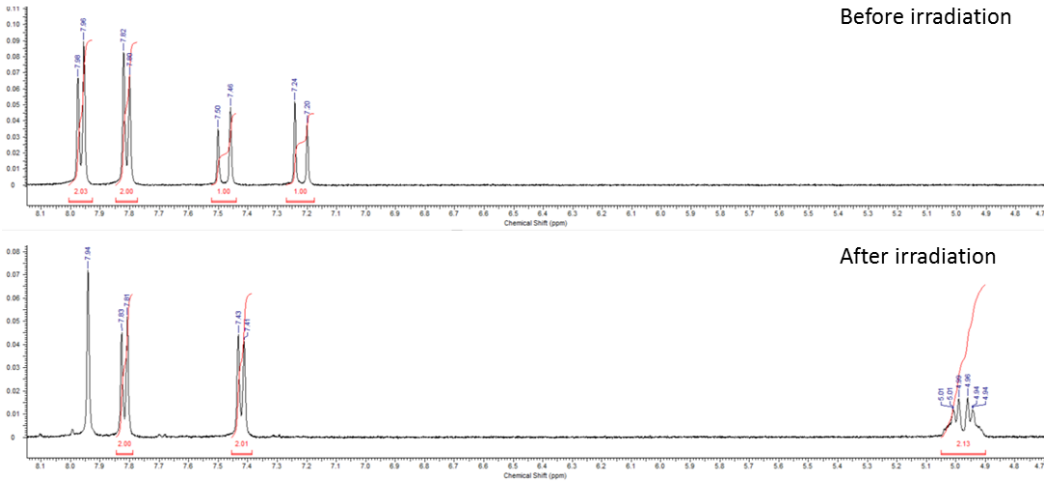

Figure 5. ^{1}H NMR spectra of crystalline powder of (*E*)-Hppvb obtained from DMF solution in DMSO-d_6 before irradiation (top) and after irradiation (bottom). A singlet peak observed at 7.94 is derived from DMF.

SC-SC transformation during photodimerization was also examined. At -150ºC, C-HGFI Hg lamp was irradiated to the single crystal obtained from DMF solution for 1 hour or 24 hours, but in both cases, single crystallinity of the sample has lost (Scheme 5).

In contrast with the crystalline sample obtained from DMF solution, photo irradiation toward the crystalline sample given by THF solution, led to no change (Scheme 6) possibly due to the long separation between two C=C bond (5.01 Å, see Figure 1). As previously reported, C=C bond separation at solid state is crucial for photo dimerization reaction.

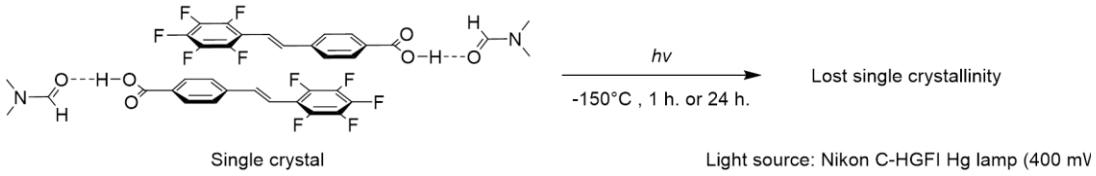

Scheme 5. Photo irradiation to single crystal of (*E*)-Hppvb obtained from DMF solution.

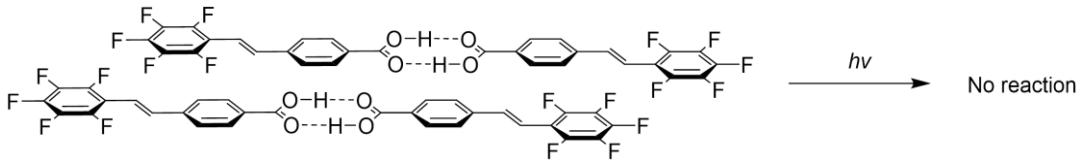

Scheme 6. Photo irradiation to single crystal of (*E*)-Hppvb obtained from THF solution.

Syntheses of Rh paddle-wheel complexes

Synthesis of the Rh(II) complex was performed by the reaction of $Na_4[Rh_2(CO_3)_4]$ with 8 eq. of Hppeb at 100 °C in DMF/H_2O (3:1) for 10 h. A four substituted complex, $Rh_2((E)\text{-ppvb})_4(DMF)_2$, was obtained in 70% yield by subsequent column chromatography using neutral alumina (Et_2O/DMF as the eluent). (*Z*)-ppvb$^-$ which can be formed by isomerization of the ligand was not observed in ^{1}H NMR. The slow evaporation of the THF/Et_2O solution of $Rh_2((E)\text{-ppvb})_4$ (**4**) afforded two types of single crystals of $Rh_2((E)\text{-ppvb})_4(THF)_2$ (**4-THF** with space group of *C*2/*m* and $P\bar{1}$) suitable for X-ray crystallography. $Rh_2((E)\text{-ppvb})_4(2\text{-butanoe})_2$ **4-BN** was also obtained by recrystallization of **4** from slow evaporation of the mixed solution of Et_2O/2-butanone. By the slow evaporation of the saturated DMF solution of **4** with few drops of pyridine, $Rh_2((E)\text{-ppvb})_4(pyridine)_2$ (**4-PY**) was grown.

Crystal structures of Rh complexes

The crystal structure of **4-THF** with space group of *C*2/*m* (**4-THF-1**) is comprised of a Rh(II) paddle-wheel with THF molecules coordinated at the axial sites (Figure 6). Four (*E*)-ppvb$^-$ ligands occupied the positions in the equatorial plane of each rhodium atom. The Rh1-Rh1' distance was 2.3848(8) Å, which is in the range found for previously reported Rh(II) paddle-wheel dimers (2.316 to 2.486 Å). The angle between the phenylene and perfluorophenyl rings was estimated to be 16.0°.

In the crystal packing structure of **4-THF-1**, as reflected in cell parameters, similar crystal packing structure compared to **3-THF** was obtained. multipoint Ar-Ar^F interactions played a key role in stabilizing the molecular assembly. As shown in Figure 6b, an infinite two-dimensional (2-D) square-grid sheet structure was formed via multipoint Ar-Ar^F interactions between the ligands. The mean interplanar separation between the phenylene and perfluorophenyl rings was 3.5(2) Å. These 2-D sheets were stacked through π-π interactions (denoted as blue line in Fig. 6b) to form a columnar structure of paddle-wheel units along the c axis. As a result, a porous structure with the channel entrance size of 15.3 × 12.0 Å^2 was formed (Fig. 6c),[13] and THF molecules were contained in the pores as guests.

Another crystal structure of **4-THF** with space group of $P\bar{1}$ (**4-THF-2**) of which Rh1-Rh1' distance was 2.3811(9) Å also shows an infinite two-dimensional (2-D) square-grid sheet structure stabilized with multipoint Ar-Ar^F interactions, but stacking pattern of the 2-D sheets was different (Figure 7). The channel shape was not rhomboidal but parallelogram and the channel entrance size was 14.7 × 14.1 Å^2. The differences are arising from coordination mode of THF molecules at axial sites. While in **4-THF-1**, THF coordinates with staggered configuration and the five-membered ring is totally parallel to Rh-Rh bond, THF coordinates with eclipsed-like configuration and the five-membered ring is not parallel to Rh-Rh bond in **4-THF-2** (Figure 8).

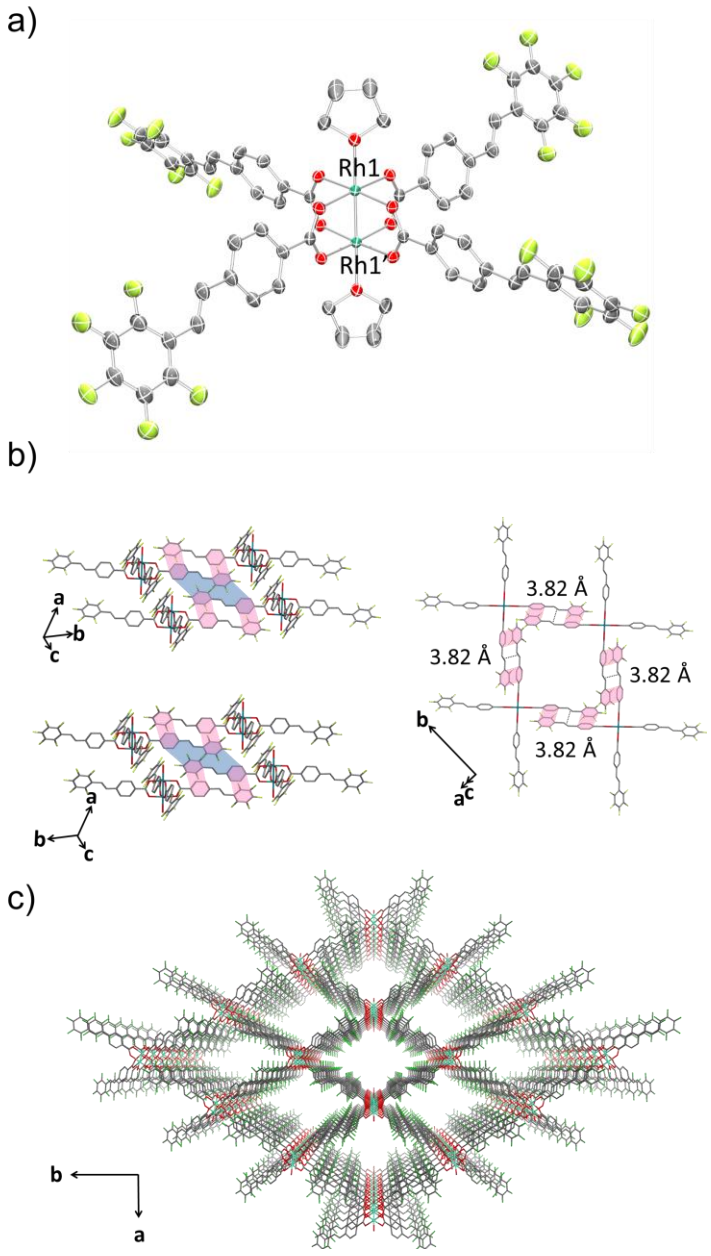

Figure 6. (a) An ORTEP drawing of **4-THF-1** (50% probability ellipsoids). Hydrogen atoms are omitted for clarity. (b) 2-D sheet structure of **4-THF-1**. Ar–Ar^{F} interactions and π–π interactions are shown in red and blue lines respectively. Hydrogen atoms and carbon atoms of THF at the axial positions are omitted for clarity. (c) Crystal packing of **4-THF-1** along the c axis. Hydrogen atoms, and carbon atoms of THF at the axial positions are omitted for clarity. O = red, C = grey, F = pale green, Rh = sea green.

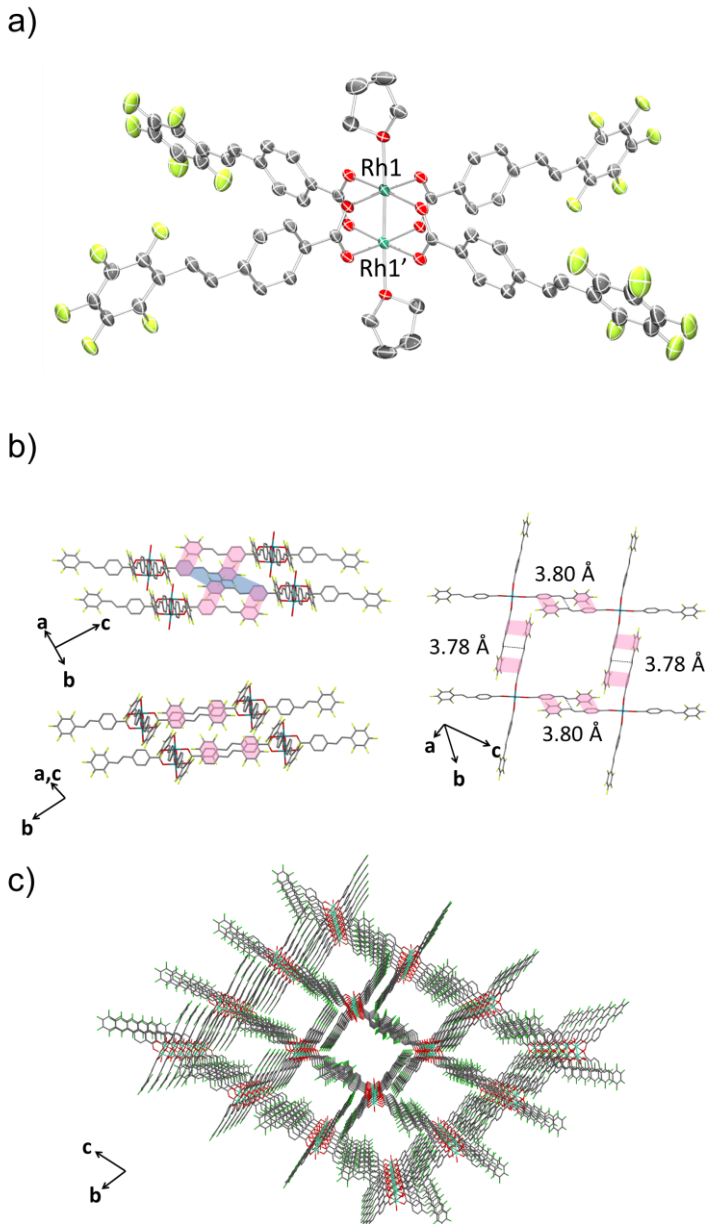

Figure 7. (a) An ORTEP drawing of **4-THF-2** (50% probability ellipsoids). Hydrogen atoms are omitted for clarity. (b) 2-D sheet structure of **4-THF-2**. Ar–Ar^F interactions and π–π interactions are shown in red and blue lines respectively. Hydrogen atoms and carbon atoms of THF at the axial positions are omitted for clarity. (c) Crystal packing of **4-THF-2** along the *c* axis. Hydrogen atoms, and carbon atoms of THF at the axial positions are omitted for clarity. O = red, C = grey, F = pale green, Rh = sea green.

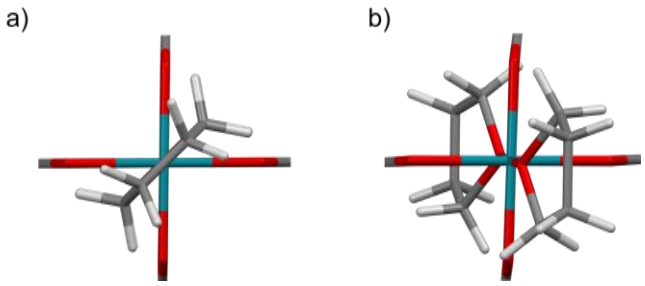

Figure 8. Top view of (a) **4-THF-1** and (b) **4-THF-2**.

The recrystallisation of $Rh_2(ppeb)_4$ from Et_2O/2-butanone afforded a crystal structure of Rh(II) paddle-wheel complex bearing 2-butanone at the axial sites, $Rh_2((E)\text{-ppvb})_4(2\text{-butanone})_2$ (**4-BN**) which is analogous to **4-THF-1** (Figure 9). In the crystal structure of **4-BN**, the mean interplanar separation between phenylene and perfluorophenyl rings was 3.34(15) Å, and the channel entrance size was estimated to be 15.0 × 10.8 $Å^2$. It should be noted that the active sites of these complexes were exposed to the pores in these structures.

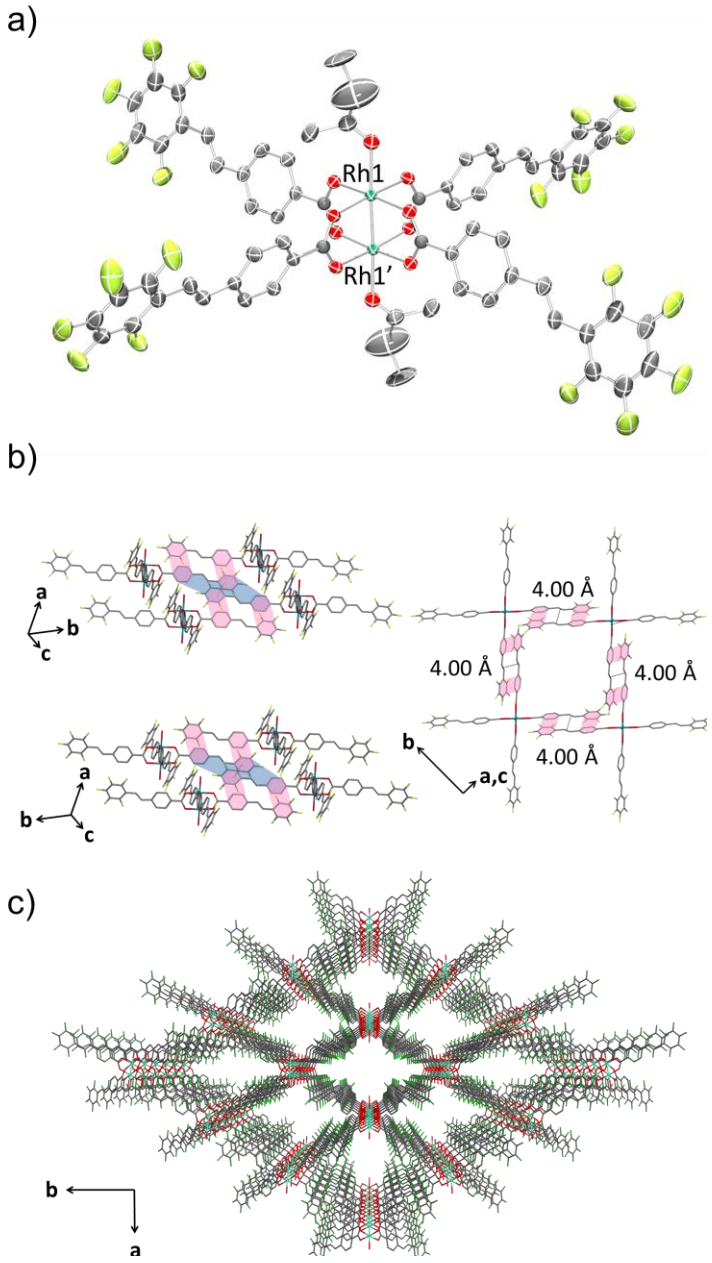

Figure 9. (a) An ORTEP drawing of **4-BN** (50% probability ellipsoids). Hydrogen atoms and crystal solvent molecules are omitted for clarity. (b) 2-D sheet structure of **4-BN**. Ar–Ar^{F} interactions and π–π interactions are shown in red and blue lines respectively. Hydrogen atoms, carbon atoms of 2-butanone at the axial positions and crystal solvent molecules observed in the channels are omitted for clarity. (c) Crystal packing of **4-BN** along the *c* axis. Hydrogen atoms, and carbon atoms of 2-butanone at the axial positions and crystal solvent molecules observed in the channels are omitted for clarity. O = red, C = grey, F = pale green, Rh = sea green.

In the crystal structure of **4-PY**, rhodium atoms have an octahedral coordination environment with pyridine at axial position. The equatorial positions are well occupied by the oxygen atoms of (*E*)-ppvb$^-$ ligand. The length of Rh-Rh bond is 2.40203(11) Å which is in the common range of rhodium paddle-wheel dimers (2.316 to 2.486 Å).[12] The angle between arene and perfluoroarene is estimated to be 12,6°. Crystal packing showed no 2-D sheets as observed in **4-THF** or **4-BN** and instead, intermolecular Ar-Ar^F interaction and π-π interaction between perfluorophenyl rings leading to a 0-dimensional porous framework as shown in Figure 10. As regards C=C bond separation, the distance is less than 4.2 Å (3.45 Å), but the C=C bonds are in a criss-cross arrangement and satisfies only one of the Schmidt criteria.

In our lab, we have found that use of high polar solvent for recrystallization, such as DMF or DMSO prevents the overlap of two ligands to interact each other. It could be due to the dipole-dipole interaction caused by high polarity of these solvent which intervene in the process for self-assembly.

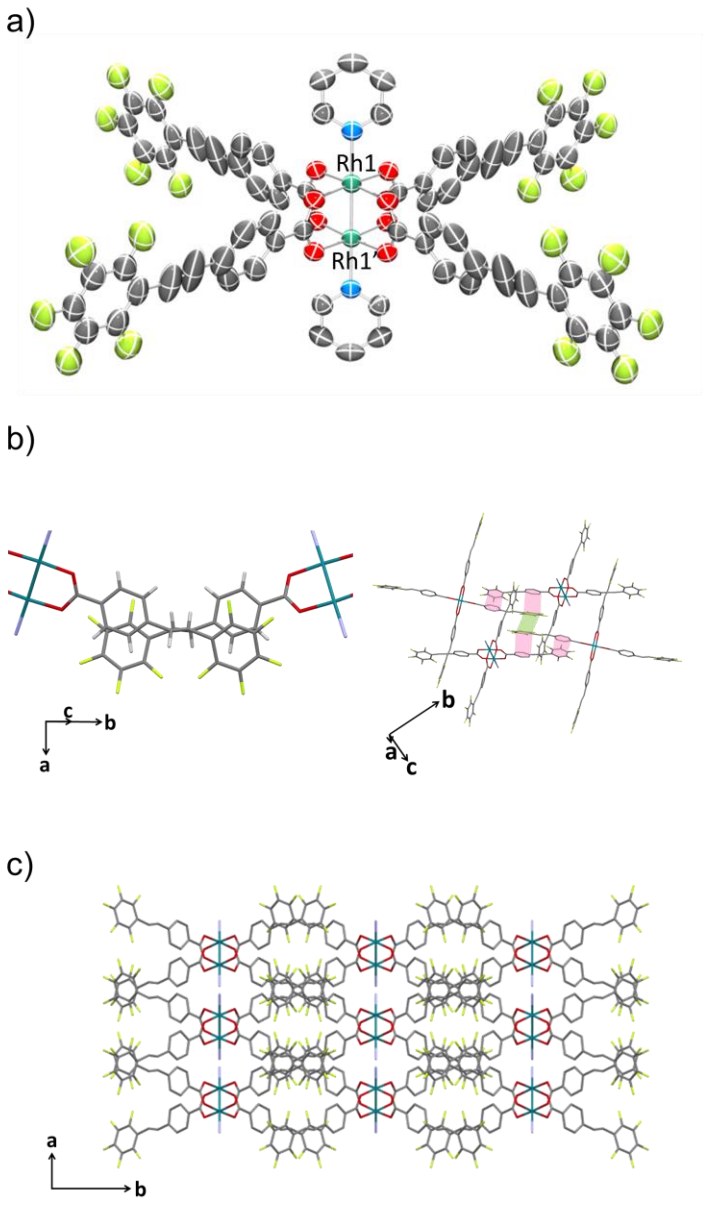

Figure 10. An ORTEP drawing of **4-PY** (50% probability ellipsoids). Hydrogen atoms and crystal solvent molecules are omitted for clarity. (b) Right: criss cross arrangement of C=C bonds. The axial ligands are partially omotted for clarity. Left: Ar–Ar^F interactions and π–π interactions between Ar^F rings are shown in red and greenish yellow lines respectively. Hydrogen atoms, carbon atoms of pyridine at the axial positions and crystal solvent molecules observed are omitted for clarity. (c) Crystal packing of **4-PY** along the *c* axis. Hydrogen atoms, and carbon atoms of 2-butanone at the axial positions and crystal solvent molecules observed are omitted for clarity. O = red, C = grey, F = pale green, N = blue, Rh = sea green.

Trial for photo polymerization of Rh complexes

For examination of the photodimerization reaction of $Rh_2((E)\text{-ppvb})_4$, absorption spectrum of $Rh_2((E)\text{-ppvb})_4$ were measured. $Rh_2((E)\text{-ppvb})_4$ in Et_2O solution showed π-π^* transition in UV-region with λ_{max} at 321 nm and molar absorptivity of ca. 20000 and *d-d* transition with λ_{max} at 607 nm and molar absorptivity of ca. 400 which is as well as reported Rh paddle-wheel complexes (Figure 11). Although, complex **4** has four (*E*)-ppvb$^-$ ligands per one molecule, absorbance in UV region is much lower than (*E*)-Hppvb.

To perform the photodimerization reaction at solid state, **4-THF** and **4-BN** were employed because C=C bond orientation seemed to be appropriate for [2+2] photodimerization reaction (two C=C bonds lie parallel and the separation of < 4.2 Å).

Firstly, photo irradiation at single crystal state was performed (Scheme 7). After the irradiation with the Hg lamp (C-HGFI) at -150°C for 24 hours to **4-THF-1** and for 48 hours to **4-BN**, both of them exhibited no change in those cell parameters. The crystal structures of them after the irradiation were analyzed, but any electron density peak which is corresponding to photo dimerized product, cyclobutane ring, was not observed in the Fourier maps.

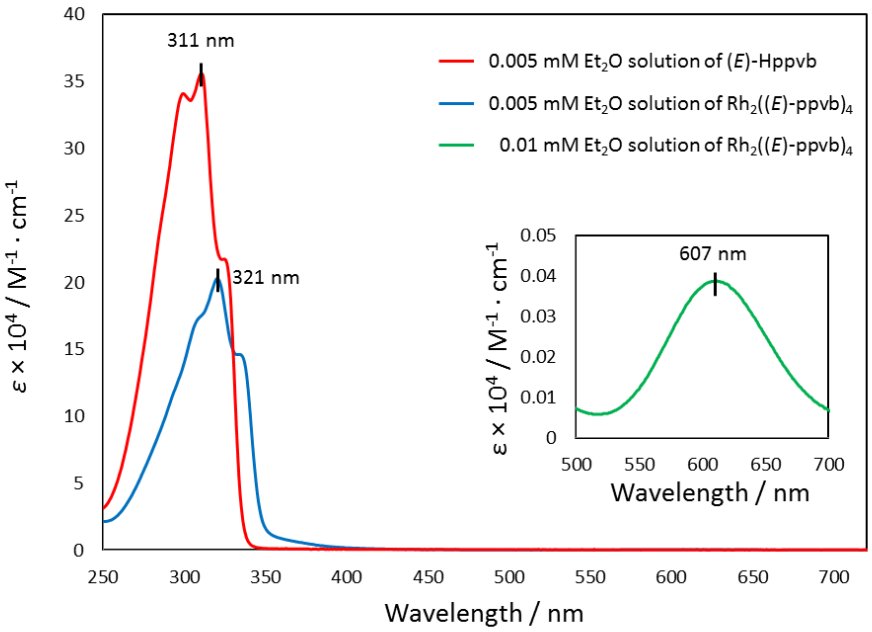

Figure 11. UV-Vis absorption spectra of (*E*)-Hppvb and Rh_2((*E*)-ppvb)$_4$ in Et_2O at room temperature.

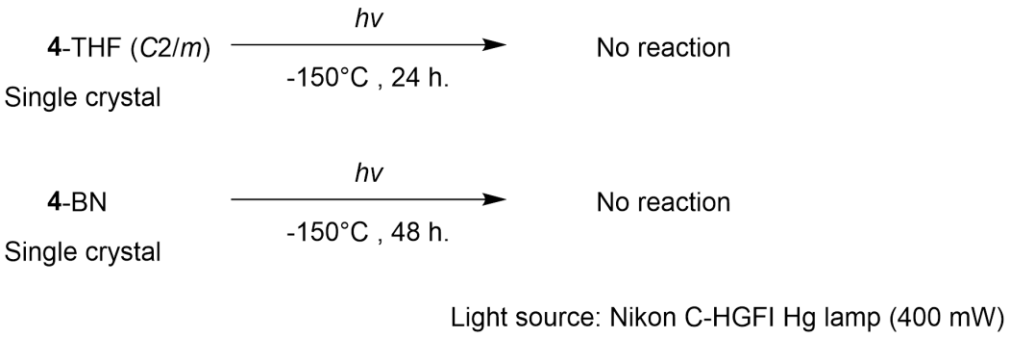

Scheme 7. UV-light irradiation to single crystal of **4-THF** and **4-BN**.

The photodimerization reaction with crystalline powder of **4-BN** was also performed (Scheme 8). After the irradiation of Hg lamp (C-HGFI) for 84 hours at room temperature, the sample was dissolved in DMF-d_7 and ^{1}H NMR was measured but NMR spectra suggested only small change campared to that before irradiation (Figure 12).

These results indicate that excited state of the ligand might be quenched by Rh center. Quenching by *d-d* transition makes it difficult to react photo chemically compared to Zn(II) or Cd(II) complex which has completely ocuupied *d* orbitals.

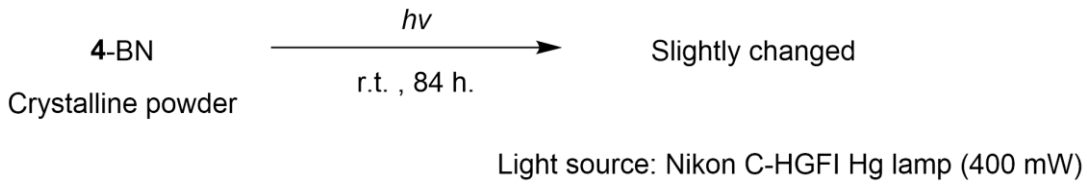

Scheme 8. UV-light irradiation to single crystal of **4-BN**.

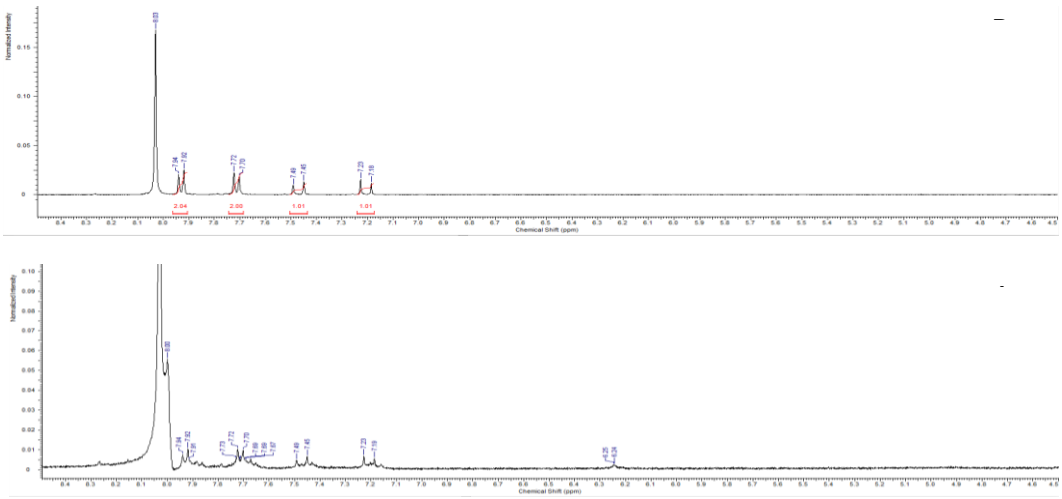

Figure 12. ^{1}H NMR spectra of **4-BN** in DMSO-d_6 before irradiation (top) and after irradiation (bottom). A singlet peak observed at 7.94 is derived from DMF.

Conclusions

In conclusion, we performed a new attempt to construct porous framework based on a substitution-inert Rh(II) paddle-wheel complexes. A novel ligand, (*E*)-Hppvb, which has arene and perfluoroarene ring bridged by photochemically active ethene linker, was synthesized for self-assembly and photo polymerization of the complexes. In the crystal packing of (*E*)-Hppvb crystallized from DMF, molecular arrangements were well-defined by Ar-Ar^F interaction and Schmidt criteria were successfully satisfied. Thus, photo dimerization reaction proceeded quantitatively by irradiation of Hg lamp. By using of the ligand, three novel Rh(II) paddle-wheel complexes, $Rh_2((E)\text{-ppvb})_4(X)_2$ (X = THF (**4-THF**), 2-butanone (**4-BN**), and pyridine (**4-PY**)), were synthesized. In the case of **4-THF** and **4-BN**, as expected, Rh dimers were successfully assembled to form porous frameworks with a 1-D channel via multipoint Ar-Ar^F interaction. However, UV-light irradiation by Hg lamp didn't give photo polymerized products of Rh dimers although C=C bond separation and direction of two C=C bonds were suitable to cause [2+2] photodimerization of the ligands. The reason seemed to be quenching of excited state of the ligand by Rh center, so some strategies such as co-crystallizing of Rh dimer with Zn(II) complex are needed to overcome this problem.

Experimental section

General methods

All solvents and reagents are of the highest quality available and used as received. {[4-(methoxycarbonyl)phenyl]methyl}triphenylphosphonium bromide was prepared by the literature methods.[10] All syntheses were performed under an atmosphere of dry nitrogen or dry argon unless otherwise indicated.

Measurement apparatus

Elemental analyses were carried out on a J-SCIENCE LAB MICRO CORDER JM10 elemental analyser. ^{1}H NMR spectra were acquired on a JEOL JNM-ECS400 spectrometer, where chemical shifts in $CDCl_3$ or DMSO-d_6 or DMF-d_7 were referenced to internal tetramethylsilane.

Syntheses

Synthesis of (*E*)-Meppvb.

(*E*)-Meppvb was synthesized *via* Wittig reaction according to the procedure by C. Richert and co-workers.[11] To a suspension of {[4-(methoxycarbonyl)phenyl]methyl}triphenylphosphonium bromide (8.29 g, 16.8 mmol) in a mixture of dry THF (250 ml) and dry CH_2Cl_2 (150 mL) were added K_2CO_3 (11.6 g, 83.9 mmol) and 18-crown-6 (165.8 mg, 627 μmol) inside the glove box. Yellow mixture was formed and the mixture stirred for 10 minutes. Addition of 2,3,4,5,6-Pentafluorobenzaldehyde (2.4 ml, 19.4 mmol) led to disappearance of the yellow color. The mixture was refluxed under stirring for 10h. Then, water was added and extracted with EtOAc (500 × 2 mL). Organic layer was washed twice with brine and dried over $MgSO_4$. After evaporation of the solvent under vacuum, the crude product was purified by column chromatography on silica gel (Hexane/EtOAc, step gradient 1:19 to 1:1). To obtained solid after evaporation of the fractions was added EtOAc and the solid was dissolved partially. Interestingly, the remaining powder was analyzed as pure (*E*)-Meppvb. It means that (*E*)-Meppvb has lower solubility than (*Z*)-Meppvb.

^{1}H NMR (400 MHz, $CDCl_3$) δ ppm: 3.94 (s, 3H), 7.09 (d, J = 16 Hz, 1H), 7.47 (d, J = 16Hz, 1H), 7.59 (d, J = 8Hz, 2H), 8.06 (d, J = 8Hz, 2H).

Note: This compound is thermally unstable (*cis-trans* isomerization occurs at room temperature). It should be stored in the refrigerator. In the case of (*E*)-Hppvb, such a

phenomenon was not observed. As soon as (*E*)-Meppvb is obtained, saponify it quickly. Since separation of *E*/*Z* mixture of Meppvb is sometimes difficult, the Pd-catalyzed isomerization reaction[14] can be utilized to give only (*E*)-Meppvb as shown in Scheme 9.

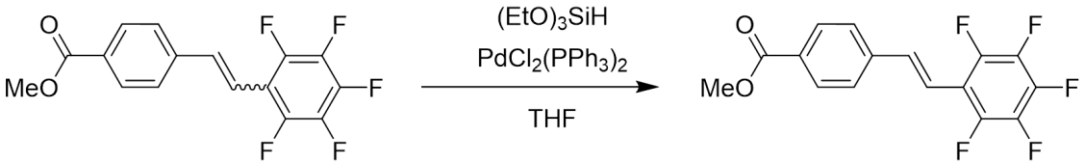

Scheme 9. Pd-catalyzed isomerization of Meppvb.

Reaction condition: In a dried 25 mL Schlenk flask, the *E*/*Z* mixture of Meppvb (1.0 g, 3.0 mmol) and a magnet bar were introduced. The flask was brought in a glove box and then $PdCl_2(PPh_3)_2$ was added (21 mg, 0.03 mmol, 1 mol%). After 7 mL of anhydrous THF was injected, 1 eq of $(EtO)_3SiH$ (548 µL, 3.0 mmol, 1eq) was added. The flask was immersed in a 65 °C oil bath until the complete reaction, around 10 hours. The orange resulting mixture was quenched with 3 mL of water and extracted by EtOAc (15 × 3 mL). Then organic layers were reassembled and washed with a brine solution (15 × 2 mL), dried over $MgSO_4$ and concentrated under pressure through an evaporator (35 °C, 150 hPa). The residue was purified by column chromatography on silica gel (Hexane/AcOEt, 19:1) to give the desired product, (*E*)-Meppvb (404 mg, 40% yield).

Synthesis of (*E*)-Hppvb.

(*E*)-Meppvb (100.7 mg, 0.307 mmol) was added in a 50mL round bottom flask as well as 23 ml of acetone and 5mL of water. After stirring until dissolution of the starting material, 1eq. of NaOH aq. (91.9 mg of NaOH was dissolved in 10 ml of water, and the 1.33 ml, 0,06 mmol of the solution was taken) was added dropwise. The mixture was stirred over night at room .temperature. Then, water was added to the solution and the acetone is removed by evaporator (40°C, 150 hPa). The solution was filtered and acidified with HCl (10%) at pH = 2. Precipitationof solid was observed. It is collected by filtration and dried under vacuum (80.9 mg, 84% yield). ^{1}H NMR (400 MHz, DMSO-d_6) δ ppm: 7.22 (d, J = 16 Hz, 1H), 7.48 (d, J = 16Hz, 1H), 7.81 (d, J = 8Hz, 2H); 7.97 (d, J = 8Hz, 2H); Anal. Calcd. for $C_6F_5C_2H_2C_6H_4CO_2H$: C, 57.34; H, 2.25; N, 0.00%. Found: C, 56.98; H, 2.39; N, 0.00%.

Synthesis of Rh_2((*E*)-ppvb)$_4$.

A 200mL flask was charged with $Na_4[Rh_2(CO_3)_4]\cdot 3H_2O$ (90 mg, 0.15 mmol, 1 eq.) and

(*E*)-Hppvb (375 mg, 1.2 mmol, 8 eq.) previously grounded together for 5 minutes in a mortar. The flask was connected to a Schlenk line and under argon a mixture of water/DMF (15 mL of water and 45 mL of DMF) was introduced with needle. The blue mixture resulting was refluxed for 10 hours to give green suspension. The solvent was evaporated under vacuum, and then the obtained green solid was washed with water and air-dried. The obtained solid was then purified by column chromatography (neutral alumina, Et_2O:DMF = 1:1) and the green fraction was evaporated by heating under vacuum to obtain 176 mg of green solid. 70% yield based on $Na_4[Rh_2(CO_3)_4]\cdot 3H_2O$. ^1H NMR (400 MHz, DMF-d_7) δ ppm: 7.21 (d, J = 16 Hz, 1H), 7.47 (d, J = 16Hz, 1H), 7.71 (d, J = 8Hz, 2H); 7.93 (d, J = 8Hz, 2H); Anal. Calcd. for $Rh_2(O_2CC_6H_4C_2H_2C_6F_5)_2(HCONC_2H_6)_2$: C, 49.40; H, 2.39; N, 1.75%. Found: C, 49.77; H, 2.71; N, 1.64%.
Note: Instead of evaporation of DMF and water after the reaction, extraction of the reaction mixture with Et_2O is also possible because the complex is soluble in Et_2O. Starting Rh source also can be removed through this process. Solubility of this complex is lower than $Rh_2(ppeb)_4$.[3]

Syntheses of 4-THF-1, 4-THF-2, 4-BN and 4-PY: The three kinds of axial ligand substituted complexes were synthesised by the recrystallization of $Rh_2((E)\text{-ppvb})_4(Et_2O)_2$. $Rh_2((E)\text{-ppvb})_4(THF)_2$ (**4-THF-1, 4-THF-2**) and $Rh_2((E)\text{-ppvb})_4(2\text{-butanone})_2$ (1-PN) were obtained by the slow evaporation of the mixed solution of Et_2O/THF and Et_2O/2-butanone containing $Rh_2((E)\text{-ppvb})_4(Et_2O)_2$, respectively. For $Rh_2((E)\text{-ppvb})_4(pyridine)_2$ (**4-PY**), the recrystallization was performed by slow evaporation of a saturated DMF solution of $Rh_2((E)\text{-ppvb})_4$ with few drops of pyridine.

X-ray crystallography

All crystals were mounted in a loop. Diffraction data at 123 K except for crystal for (*E*)-Hppvb recrystallized from THF were measured on a RAXIS-RAPID Imaging Plate diffractometer equipped with confocal monochromated Mo-Kα radiation and data was processed using RAPID-AUTO (Rigaku). Structures were solved by direct methods and refined by full-matrix least squares techniques on F^2 (*SHELXL-97*).[15] All non-hydrogen atoms were anisotropically refined, while all hydrogen atoms were placed geometrically and refined with a riding model with U_{iso} constrained to be 1.2 times U_{eq} of the carrier atom. For **4-THF-1**, **4-THF-2** and **4-BN**, the diffused electron densities resulting from residual solvent molecules were removed from the data set using the SQUEEZE routine of PLATON and refined further using the data generated.

Crystal data for (*E*)-Hppvb recrystallized from DMF: $C_{18}H_{14}F_5NO_3$, *Mr* = 387.3, triclinic, space group $P\bar{1}$, (#2), *a* = 6.1337(2) Å, *b* = 7.2926(3) Å, *c* = 18.9653(9) Å, α = 99.183(2)°, β = 97.2556(13)°, γ = 92.5150(10)°, *V* = 828.97(6) Å^3, *Z* = 2, *T* = 123 (2) K, ρ_c = 1.552 gcm^{-3}, μ(Mo-Kα) = 0.142 cm^{-1}, $2\theta_{max}$ = 54.92, λ(Mo-Kα) = 0.710747 Å, 8231 reflections measured, 3762 unique (R_{int} = 0.0226), 2967 ($I > 2\sigma(I)$) were used to refine 251 parameters, 0 restraints, wR_2 = 0.1813 ($I > 2\sigma(I)$), R_1 = 0.0554 ($I > 2\sigma(I)$), GOF = 1.176.

Crystal data for (*E*)-Hppvb recrystallized from THF: See main text.

Crystal data for 4-THF-1: $C_{68}H_{20}F_{10}O_5Rh$, *Mr* = 801.41, *monoclinic*, space group *C*2/*m*, (#12), *a* = 19.059(5) Å, *b* = 27.720(5) Å, *c* = 8.753(2) Å, β = 113.044(8)°, *V* = 4255.3(17) Å^3, *Z* = 4, *T* = 123 (2) K, ρ_c = 1.251 gcm^{-3}, μ(Mo-Kα) = 0.0477 cm^{-1}, $2\theta_{max}$ = 54.96, λ(Mo-Kα) = 0.710747 Å, 19721 reflections measured, 4974 unique (R_{int} = 0.0349), 4313 ($I > 2\sigma(I)$) were used to refine 235 parameters, 0 restraints, wR_2 = 0.1086 ($I > 2\sigma(I)$), R_1 = 0.0388 ($I > 2\sigma(I)$), GOF = 1.075.

Crystal data for 4-THF-2: $C_{68}H_{20}F_{10}O_5Rh$, *Mr* = 801.41, *triclinic*, space group $P\bar{1}$, (#2), *a* = 8.1305(6), *b* = 15.0984(9), *c* = 18.8876(12) Å, α = 69.737(5)°, β = 80.387(5)°, γ = 85.807(6)°, *V* = 2144.3(3) Å^3, *Z* = 2, *T* = 123 (2) K, ρ_c = 1.241 gcm^{-3}, μ(Mo-Kα) = 0.473 cm^{-1}, $2\theta_{max}$ = 54.92, λ(Mo-Kα) = 0.710747 Å, 20 111 reflections measured, 9715 unique (R_{int} = 0.0226), 8136 ($I > 2\sigma(I)$) were used to refine 461 parameters, 0 restraints, wR_2 = 0.1679 ($I > 2\sigma(I)$), R_1 = 0.0559 ($I > 2\sigma(I)$), GOF = 1.179.

Crystal data for 4-BN: $C_{40}H_{15}F_{10}O_6Rh$, *Mr* = 884.43, *monoclinic*, space group *C*2/*m*, (#12), *a* = 17.3423(8) Å, *b* = 25.9712(14) Å, *c* = 9.4516(5) Å, β = 106.120(8)°, *V* = 4089.6(4) Å^3, *Z* = 4, *T* = 123 (2) K, ρ_c = 1.436 gcm^{-3}, μ(Mo-Kα) = 0.506 cm^{-1}, $2\theta_{max}$ = 54.96, λ(Mo-Kα) = 0.710747 Å, 19 008 reflections measured, 4737 unique (R_{int} = 0.0341), 4297 ($I > 2\sigma(I)$) were used to refine 238 parameters, 0 restraints, wR_2 = 0.1509 ($I > 2\sigma(I)$), R_1 = 0.0586 ($I > 2\sigma(I)$), GOF = 1.043.

Crystal data for 4-PY: $C_{40}H_{17}F_{10}N_3O_6Rh$, *Mr* = 928.48, *orthorhombic*, space group *Ccmb*, (#64), *a* = 13.8159(5) Å, *b* = 29.5065(11) Å, *c* = 17.0354(6) Å, *V* = 6944.6(5) Å^3, *Z* = 8, *T* = 123 (2) K, ρ_c = 1.776 gcm^{-3}, μ(Mo-Kα) = 0.602 cm^{-1}, $2\theta_{max}$ = 54.92, λ(Mo-Kα) = 0.710747 Å, 33 164 reflections measured, 4045 unique (R_{int} = 0.0226), 2382 ($I > 2\sigma(I)$) were used to refine 254 parameters, 0 restraints, wR_2 = 0.2290 ($I >$

$2\sigma(I)$), R_1 = 0.0697 ($I > 2\sigma(I)$), GOF = 1.004.

References

1 (a) S. Kitagawa, R. Kitaura, S. Noro, *Angew. Chem. Int. Ed.*, **2004**, *43*, 2334-2375; (b) M. D. Allendorf, C. A. Bauer, R. K. Bhakta, R. J. T. Houk, *Chem. Soc. Rev.*, **2009**, *38*, 1330-1352; (c) C. Wang, T. Zhang, W. Lin, *Chem. Rev.*, **2012**, *112*, 1084-1104; (d) A. Dhakshinamoorthy, A. M. Asiri and H. García, *Angew. Chem. Int. Ed.*, **2016**, *55*, 5414–5445. (e) M. C. So, G. P. Wiederrecht, J. E. Mondloch, J. T. Hupp and O. K. Farha, *Chem. Commun.*, **2015**, *51*, 3501–3510. (f) J. Lee, O. K. Farha, J. Roberts, K. A. Scheidt, S. T. Nguyen, J. T. Hupp, *Chem. Soc. Rev.*, **2009**, *38*, 1450-1459; (g) K. Sumida, D. L. Rogow, J. A. Mason, T. M. McDonald, E. D. Bloch, Z. R. Herm, T.-H. Bae, J. R. Long, *Chem. Rev.*, **2012**, *112*, 724-781; (h) M. Yoon, R. Srirambalaji, K. Kim, *Chem. Rev.*, **2012**, *112*, 1196-1231; (i) J.-R. Li, J. Sculley, H.-C. Zhou, *Chem. Rev.*, **2012**, *112*, 869-932; (j) C. Wang, T. Zhang, W. Lin, *Chem. Rev.*, **2012**, *112*, 1084-1104; (k) H. Furukawa, K. E. Cordova, M. O'Keeffe, O. M. Yaghi, *Science*, **2013**, *341*, 974-986. (l) P. Kumar, A. Deep and K.-H. Kim, *Trend. Anal. Chem.*, **2015**, *73*, 39–53. (m) L. Sun, M. G. Campbell and M. Dincă, *Angew. Chem. Int. Ed.*, **2016**, *55*, 3566–3579; (n) P. C. A. D. Silva, S. M. F. Vilela, J. P. C. Tomé and F. A. A. Paz, *Chem. Soc. Rev.*, **2015**, *44*, 6774–6803; (o) A. H. Chughtai, N. Ahmad, H. A. Younus, A. Laypkov and F. Verpoort, *Chem. Soc. Rev.*, **2015**, *44*, 6804–6849; (p) X. Zhang, W. Wang, Z. Hu, G. Wang and K. Uvdal, *Coord. Chem. Rev.*, **2015**, *284*, 206–235; (q) M. I. Nandasiri, S. R. Jambovane, B. P. Mcgrail, H. T. Schaef and S. K. Nune, *Coord. Chem. Rev.*, **2016**, *311*, 38–52; (r) Y. Cui, B. Li, H. He, W. Zhou, B. Chen and G. Qian, *Acc. Chem. Res.*, **2016**, *49*, 483–493.

2 (a) S. S.-Y. Chui, S. M.-F. Lo, J. P. H. Charmant, A. G. Orpen and I. D. Williams, *Science*, **1999**, *283*, 1148–1150; (b) N. L. Rosi, J. Kim, M. Eddaoudi, B. Chen, M. O'keeffe and O. M. Yaghi, *J. Am. Chem. Soc.*, **2005**, *127*, 1504–1518; (c) N. Klein, I. Senkovska, I. A. Baburin, R. Grünker, U. Stoeck, M. Schlichtenmayer, B. Streppel, U. Mueller, S. Leoni, M. Hirscher and S. Kaskel, *Chem.-Eur. J.*, **2011**, *17*, 13007–13016; (d) B. Chen, X. Zhao, A. Putkham, K. Hong, E. B. Lobkovsky, E. J. Hurtado, A. J. Fletcher and K. M. Thomas, *J. Am. Chem. Soc.*, **2008**, *130*, 6411–6423; (e) K. K. Tanabe and S. M. Cohen, *Chem. Soc. Rev.*, **2011**, *40*, 498–519; (f Z. Wang and S. M. Cohen, *Chem. Soc. Rev.*, **2009**, *38*, 1315; (g) J. D. Evans, C. J. Sumby and C. J. Doonan, *Chem. Soc. Rev.*, **2014**, *43*, 5933–5951; (h) P. Deria, J. E. Mondloch, O. Karagiaridi, W. Bury, J. T. Hupp and O. K. Farha, *Chem. Soc. Rev.*, **2014**, *43*, 5896–5912.

3 T. Itoh, M. Kondo, H. Sakamoto, K. Wakabayashi, M. Kanaike, K. Itami and S. Masaoka, *Dalton Trans.*, **2015**, 44, 15334–15342.

4 (a) R. Medishetty, R. Tandiana and J. J. Vittal, *Cryst. Growth Des.*, **2014**, *14*, 3186–3190.; (b) Y.-C. Ou, D.-S. Zhi, W.-T. Liu, Z.-P. Ni and M.-L. Tong, *Chem.-Eur. J.*, **2012**, *18*, 7357–7361; (c) R. Medishetty, T. T. S. Yap, L. L. Koh and J. J. Vittal, *Chem. Commun.*, **2013**, *49*, 9567.; (d)

R. Medishetty, R. Tandiana, L. L. Koh and J. J. Vittal, *Chem.-Eur. J.*, **2014**, *20*, 1231–1236.; (e) S. Dutta, D.-K. Bučar, E. Elacqua and L. R. Macgillivray, *Chem. Commun.*, **2013**, 49, 1064–1066;

5 (a) D. Liu, Z.-G. Ren, H.-X. Li, J.-P. Lang, N.-Y. Li and B. F. Abrahams, *Angew. Chem. Int. Ed*., **2010**, *49*, 4767–4770; (b) M. H. Mir, L. L. Koh, G. K. Tan and J. J. Vittal, *Angew. Chem. Int. Ed.*, **2009**, *49*, 390–393.; (c) N. L. Toh, M. Nagarathinam and J. J. Vittal, *Angew. Chem. Int. Ed.*, **2005**, *44*, 2237–2241; (d) R. Medishetty, L. L. Koh, G. K. Kole and J. J. Vittal, *Angew. Chem. Int. Ed.*, **2011**, *50*, 10949-10952; (e) I.-H. Park, R. Medishetty, J.-Y. Kim, S. S. Lee and J. J. Vittal, *Angew. Chem. Int. Ed*., **2014**, *53*, 5591–5595; (f) A. Hazra, S. Bonakala, K. K. Bejagam, S. Balasubramanian and T. K. Maji, *Chem.-Eur. J.*, **2016**, *22*, 7792–7799; (g) A. Chanthapally, W. T. Oh and J. J. Vittal, *Chem. Commun.*, **2014**, *50*, 451–453; (h) I.-H. Park, A. Chanthapally, H.-H. Lee, H. S. Quah, S. S. Lee and J. J. Vittal, *Chem. Commun.*, **2014**, *50*, 3665; (i) Y.-C. Ou, W.-T. Liu, J.-Y. Li, G.-G. Zhang, J. Wang and M.-L. Tong, *Chem. Commun.*, **2011**, *47*, 9384; (j) H. Sato, R. Matsuda, M. H. Mir and S. Kitagawa, *Chem. Commun.*, **2012**, *48*, 7919; (k) F.-L. Hu, S.-L. Wang, J.-P. Lang and B. F. Abrahams, *Scientific Reports*, **2014**, *4*, 6815; (ml G.-L. Li, W.-D. Yin, G.-Z. Liu, L.-F. Ma, L.-L. Huang, L. Li and L.-Y. Wang, *Inorg. Chem. Commun.*, **2014**, *43*, 165–168; (m) Y.-B. Shu, N. Tu, H.-T. Shi, Y.-G. Yin and W.-S. Liu, *Dalton Trans.*, **2015**, *44*, 7131–7134; (n) D. Liu, N.-Y. Li and J.-P. Lang, *Dalton Trans.*, **2011**, *40*, 2170–2172; (o) R. Medishetty, Z. Bai, H. Yang, M. W. Wong and J. J. Vittal, *Cryst. Growth Des.*, **2015**, *15*, 4055–4061; (p) M.-H. Xie, X.-L. Yang and C.-D. Wu, *Chem.-Eur. J.*, **2011**, *17*, 11424–11427; (q) G. K. Kole, A. M. P. Peedikakkal, B. M. F. Toh and J. J. Vittal, *Chem.-Eur. J.*, **2013**, *19*, 3962–3968.

6 (a) A. Hazra, S. Bonakala, K. K. Bejagam, S. Balasubramanian and T. K. Maji, *Chem.-Eur. J.*, **2016**, *22*, 7792–7799; (b) M. L. Foo, R. Matsuda, Y. Hijikata, R. Krishna, H. Sato, S. Horike, A. Hori, J. Duan, Y. Sato, Y. Kubota, M. Takata and S. Kitagawa, *J. Am. Chem. Soc.*, **2016**, *138*, 3022–3030.

7 B. Chen, G. Qian, "*Metal–Organic Frameworks for Photonics Applications*", Springer, Berlin, **2014**.

8 G. M. J. Schmidt, *Pure Appl. Chem.*, **1971**, *27*, 647–678

9 (a) G. Marras, P. Metrangolo, F. Meyer, T. Pilati, G. Resnati and A. Vij, *New J. Chem.*, **2006**, *30*, 1397–1402; (b) G. W.; Dunn, A. R.; Henling, L. M.; Ziller, J. W.; Lobkovsky, E. B.; Grubbs, R. H. *J. Am. Chem. Soc.* **1998**, *120*, 3641; (c)S. P. Gromov, A. I. Vedernikov, N. A. Lobova, L. G. Kuz'mina, S. N. Dmitrieva, Yu. A. Strelenko and J. A. K. Howard, *J. Org. Chem.*, **2014**, *79*, 11416 (d) Gromov, S. P.; Vedernikov, A. I.; Kuz'mina, L. G.; Lobova, N. A.; Basok, S. S.; Strelenko, Yu. A.; Alfimov, M. V. Russ. *Chem. Bull., Int. Ed.*, **2009**, *58*, 108C; (e) M. Linares and A. Briceño, *New J. Chem.*, **2010**, *34*, 587–590; (f) M. A. Sinnwell and L. R. MacGillivray,

Angew. Chem., Int. Ed., **2016**, *55*, 3477–3480.

10 S. Vaday; H. C. Geiger, B. Cleary, J Perlstein, D. G. Whitten, *J. Phys. Chem. B*, **1997**, *101*, 321-329.

11 Z. Dogan, R. Paulini, J. A. Rojas Stütz, S. Narayana and C. Richert, *J. Am. Chem. Soc.*, **2004**, *126*, 4762.

12 (a) F. A. Cotton, C. A. Murillo and R. A. Walton, "*Multiple Bonds Between Metal Atoms*", Springer Science and Business Media, New York, 3rd edn, **2005**; (b) E. B. Royar and S. D. Robinson, *Platinum Metals Rev.*, **1982**, *26*, 65–69.

13 The channel entrance size was estimated by considering the Van der Waals radii of constituent atoms, and the atoms at axial ligands are omitted for the calculation.

14 A. Schaate, P. Roy, T. Preußе, S. J. Lohmeier, A. Godt and P. Behrens, *Chem.–Eur. J.*, **2011**, *17*, 9320–9325

15 G. M. Sheldrick, *Program for Crystal Structure Refinement*, University of Göttingen, Germany, **199**7.

Chapter 4

Reactivity of complexes with diazo compounds and triazoles

Introduction

Development of facial synthetic method to obtain complicated chemical structures is still demanded for the areas of total syntheses and pharmaceuticals. One of the most attractive ways to answer the demand is selective C-H functionalization of inactivated C-H bonds. In the past several decades, two different strategies to deal with the demand have been developed.[1,2] One is C-H activation via oxidative addition of C-H bond to a highly reactive metal complex which is difficult to be regenerated for completion of a catalytic cycle. [1a-e] Another strategy is utilization of metal-carbenoid for C-H insertion.[1f-i] Unlike the former strategy, metal carbenoids doesn't include metal/C-H interactions. Moreover, there is an advantage that metal carbenoids generated form the reaction with diazo compound can be regenerated easily to proceed a catalytic process. With respect to metal-carbenoid-induced C-H insertion, Rh(II) complexes have been emerged as the most effective catalysts[1f,1h,2] while Cu(I) complexes is also effective.[3] That's why numerous Rh(II) complexes with a variety of ligands have been developed so far.[2] However, most of them are homogeneous catalysts and practical applications is still restricted due to their instability and difficulty of product separation from the catalysts. To solve the problems, several approaches to produce heterogeneous catalysts have been developed[4] (e.g. polymer supported,[4a-d] silica supported,[4e] MOFs or PCPs[4f]). Among them, MOFs or PCPs with catalytic sites so called self-supported catalyst in this context has advantage over other immobilized catalyst in terms of highly-dense catalytic sites and controlled arrangement of catalytic sites.

Recently, we have succeeded in construction of porous framework based on Rh(II) paddle-wheel dimer the catalytic sites of which are exposed to the pores.[5] Hence, investigation of the reactivity of the porous framework might be interesting. In order to examine the reactivity, diazo compounds and [1,2,3]triazolo[1,5-a]pyridine derivatives were employed in this study. While diazo compounds react with Rh(II) paddle-wheel complex rapidly to form Rh carbenoid species,[6] [1,2,3]triazolo[1,5-a]pyridine derivatives exhibit diazo-azomethine/1,2,3-triazole tautomerism[7] and 1,2,3-triazole can coordinate at its axial sites before the reaction. Therefore, there is a chance to construct porous framework with the substrates at axial sites of Rh complexes.

Reactivity of Rh(II) complexes with diazo compounds

Preparation of catalyst and diazo compound

$Rh_2(ppeb)_4(THF)_2$ (**3-THF**) was recrystallized from THF/Et_2O mixed solution. The crystals were collected by filtration and dried crystalline powder was used for the reaction in hexanes or pentane. PXRD pattern after drying of catalyst indicates structural transformation arising from removal of the solvent molecules (Figure 1). The crystal packing after transformation is unclear, but as mentioned in chapter 2, at least the crystalline powder has porosity indicated by regeneration of **3-THF** when exposed to THF and CO_2 absorption property.[5] It should be noted that we previously obtained $Rh_2(ppeb)_4(THF)_2$ crystal with C_4 symmetrical packing (**3-THF-*C*$_4$**) crystallized from THF solution in globe box and presence of excess amount of 2-diazo-2-(4-methoxyphenyl)acetate (Table 1, Figure 1). But simulated PXRD pattern of **3-THF-*C*$_4$** is also different from that of dried **3-THF** (Figure 2).

As donor/acceptor carbenoid precursors which show good reactivity in carbenoid mediated reactions,[2] methyl (4-bromophenyl) diazoacetate and 2,2,2-trichloroethyl 2-(4-bromophenyl)-2-diazoacetate was prepared according to reported procedure.[2d]

Table 1. Crystallographic data and structural refinements for **3-THF** and **3-THF-*C*$_4$**.

Compound	**3-THF**	**3-THF-*C*$_4$**
Formula	$Rh_2O_{10}C_{68}H_{32}F_{20}$	$RhO_6C_{38}H_{16}F_{10}$
Formura weight	1594.76	861.42
Temperature (˚C)	-150	-150
Crystal color, habit	green, stick	green, platelet
Crystal system	monoclinic	triclinic
Space group	*C2/m* (#12)	*P*-1 (#2)
a (Å)	18.6449(7)	11.0168(3)
b (Å)	27.2267(14)	12.4821(4)
c (Å)	8.8932(4)	13.4165(4)
α (deg)	90	105.3108(10)
β (deg)	107.4822(12)	96.3626(9)
γ (deg)	90	94.8338(10)
V (Å^3)	4306.0(3)	1756.06(9)
Z	2	2
R_1	0.0660	0.0366
wR_2	0.1742	0.1042
Goodness of fit on F^2	1.135	1.116

[a] $R_1 = \Sigma||F_o| - |F_c||/ \Sigma|F_o|$. [b] $wR_2 = [\Sigma(w(F_o^2 - F_c^2)^2) / \Sigma w(F_o^2)^2]^{1/2}$.

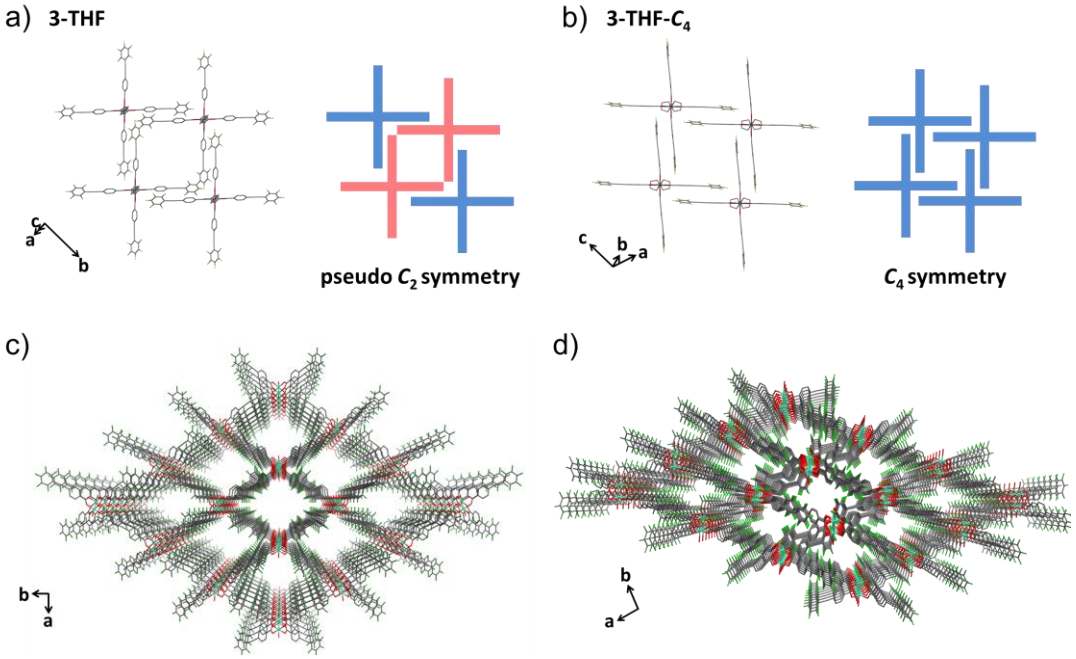

Figure 1. Crystal structural comparison of **3-THF** and **3-THF-*C*$_4$**. 2-D sheet structure of **3-THF** (a) and **3-THF-*C*$_4$** (b). Hydrogen atoms are omitted for clarity. Crystal packing of **3-THF** (c) and **3-THF-*C*$_4$** (d) along the c axis. Hydrogen atoms, and carbon atoms of THF at the axial positions and crystal solvent molecules observed in the channels are omitted for clarity. O = red, C = grey, F = pale green, Rh = sea green.

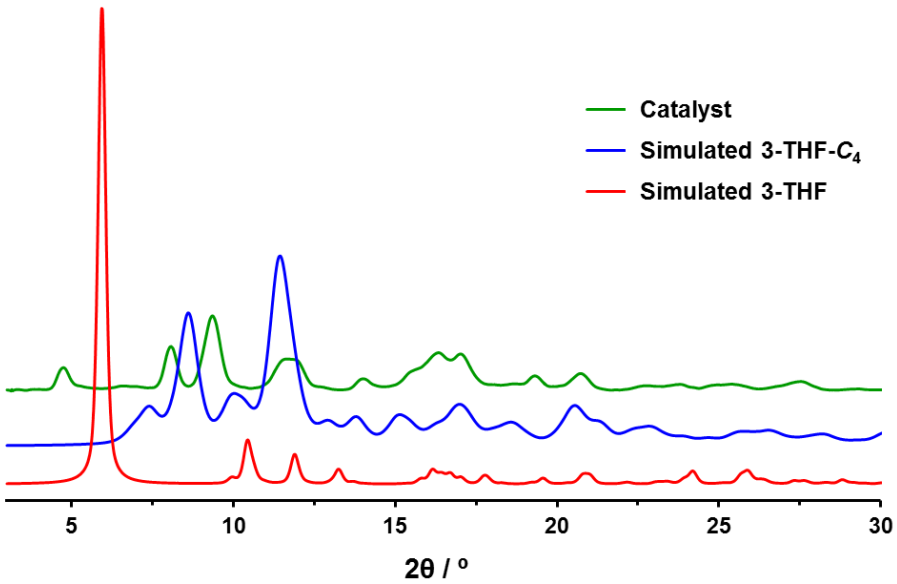

Figure 2. Simulated XRD patterns of for **3-THF** (red) and **3-THF-*C*$_4$** (blue) and PXRD pattern of **3-THF** after drying in a vacuum (green).

Cyclopropanation of styrene

Firstly, cyclopropanation of styrene was chosen to evaluate catalytic activity of $Rh_2(ppeb)_4$ (Table 1). To check leaching of catalyst, several controlled experiments were performed. As shown in Figure 3, $Rh_2(ppeb)_4$ doesn't dissolve in hexanes, but it can dissolve in styrene. Therefore, the reaction in hexanes isn't heterogeneous condition completely. Between entries 1-3, there are no significant difference. In all entries, good diastereomeric ratio which was higher than 11:1 was obtained. About enantiomeric excess, all entries gave racemic mixtures which reflect that the catalyst or its crystal packing doesn't have any chirality. About the solubility of the catalyst in 4-ethyltolune, it can be dissolved in the substrate slightly

Scheme 1. Cyclopropanation of styrene catalysed by $Rh_2(ppeb)_4$.

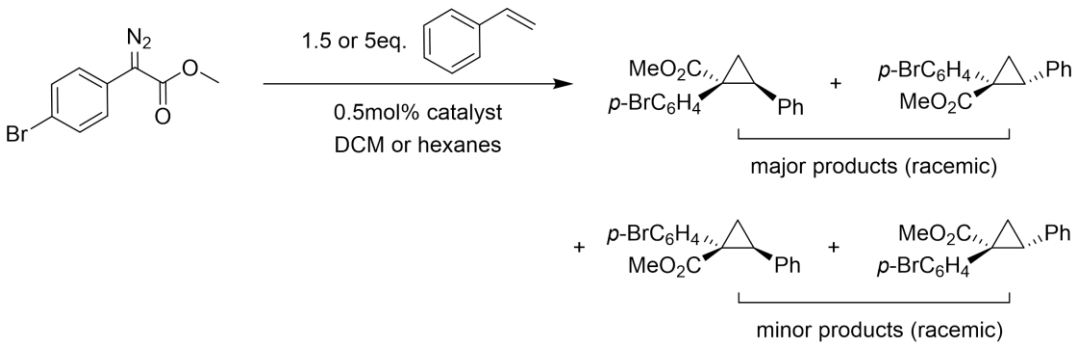

Entry	Solvent	styrene	Temp.	Time(h)	dr	yield
1	DCM	5 eq.	r.t.	1	50:1	79%
2	Hexanes	5 eq.	r.t.	1	100:1	88%
3[a]	Hexanes	1.5 eq.	r.t.	1	11-50:1	57-84%

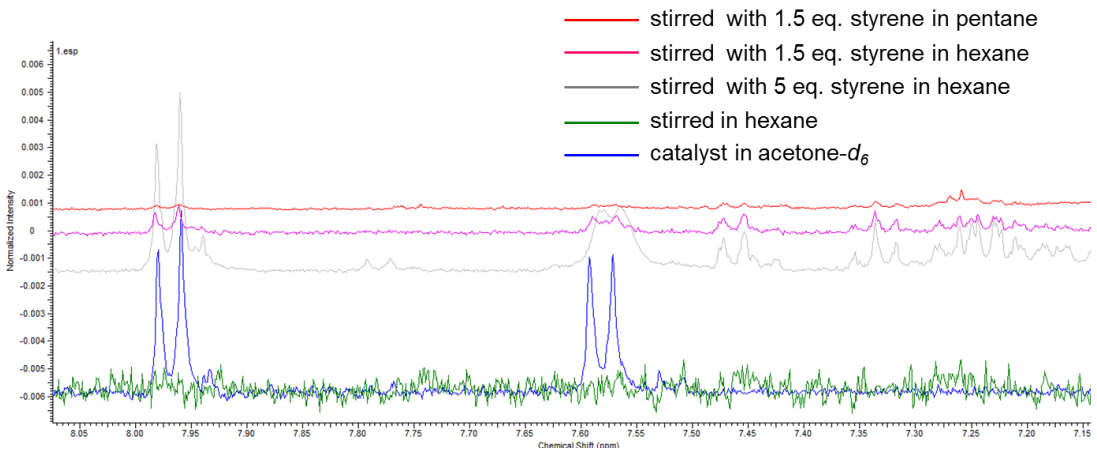

Figure 3. Leaching test of the catalyst into hexanes and styrene.

C-H functionalization of 4-ethyltoluene

Since $Rh_2(ppeb)_4(THF)_2$ has a porous structure, we hypothesized that such a reaction field could influence the site selectivity of the C-H functionalization. Then C-H functionalization of 4-ethyltoluene was conducted (Table 3). $Rh_2(ppeb)_4$ catalyzed reaction of 4-ethyltoluene favors C-H functionalization at the secondary benzylic site (Scheme 5). From an electronic point of view, tertiary carbon can stabilize positive charge build-up best in the transition state. Therefore, the tendency of the reactivity would be 3º > 2º > 1º. However, from a steric perspective, reactivity of the substrates is anticipated to follow the tendency 1º > 2º > 3º.[2e] So, the site selectivity of $Rh_2(ppeb)_4$ is moderate. In the case of 2,2,2-trichloroethyl 2-(4-bromophenyl)-2-diazoacetate as carbene precursor, the yield increased dramatically probably due to the robustness of TCE ester compared to methyl ester.[2d] 4-Ethyltoluene also dissolves the catalyst like styrene, so heterogeneous catalytic activity could not be evaluated (Figure 5).

Table 3. C-H insertion into 4-ethyltolune catalysed by $Rh_2(ppeb)_4$.

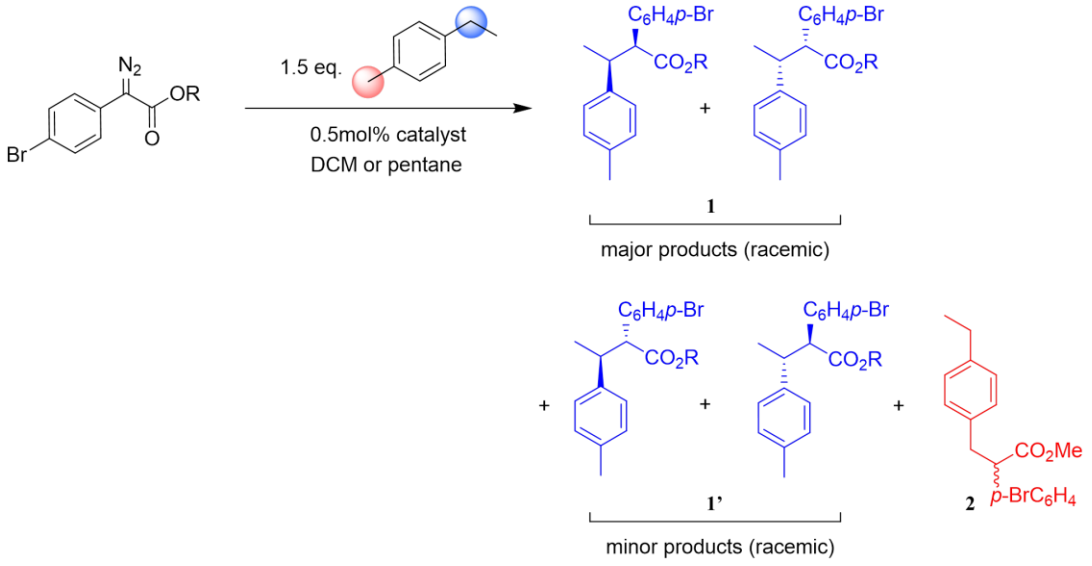

Entry	R	Solvent	substrate	Temp.	Time(h)	Ratio of 1+1':2	dr of 1	Yield
1	Me	DCM	1.5 eq.	r.t.	8	**1** only	3:1	11%
2	Me	DCM	1.5 eq.	reflux	1	**1** only	3:1	23%
3	Me	Pentane	1.5 eq.	r.t.	1	**1** only	2.6:1	2%
4	CH_2Cl_3	DCM	1.5 eq.	reflux	1	14:1	4.4:1	70%

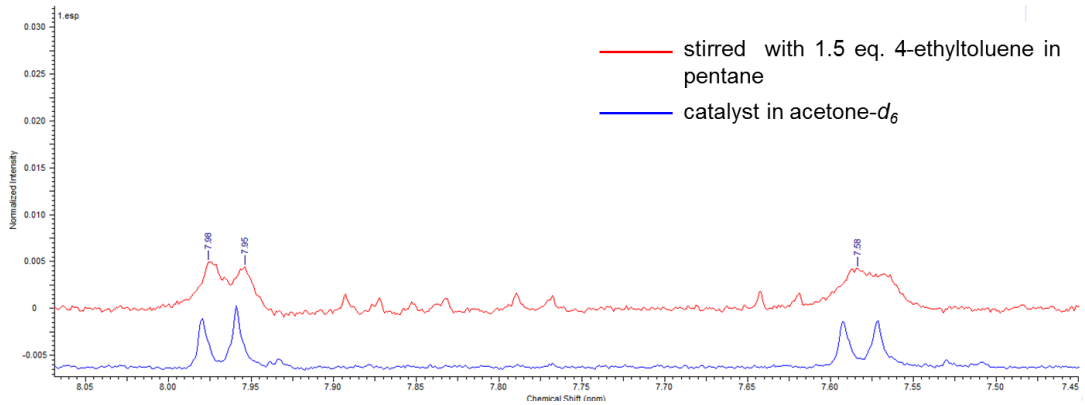

Figure 4. Leaching test of the catalyst into 4-ethyltoluene.

C-H functionalization of (*E*)-2-hexene

To see whether the same trend would be seen for allylic C-H functionalization, C-H functionalization of (*E*)-2-hexene was also conducted (Table 4). As shown in scheme 5, $Rh_2(ppeb)_4$ catalyst prefers to give the secondary C-H insertion product. In the case of the reaction in hexanes, the secondary C-H insertion product was also obtained, but wecouldn't isolate the product by silica-gel column chromatography probably due to the similarity of the polarity of side products. Side products can be attributed to C-H insertion into hexanes by ^{1}H NMR spectrum. Regarding solubility of the catalyst in the substrate, leaching test suggested that not only aromatic substrate but also allylic substrate can dissolve the catalyst (Figure 5).

Table 4. C-H insertion into (*E*)-2-hexene catalysed by $Rh_2(ppeb)_4$.

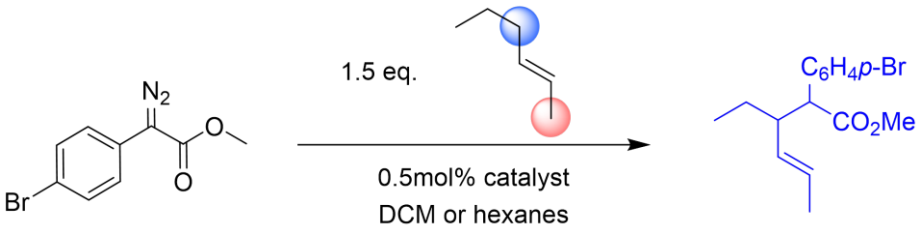

Entry	Solvent	substrate	Temp.	Time(h)	dr	Yield
1	DCM	1.2 eq.	reflux	1.5	1.4:1	54%
2	Hexanes	1.2 eq.	48°C	1.5	-	mess

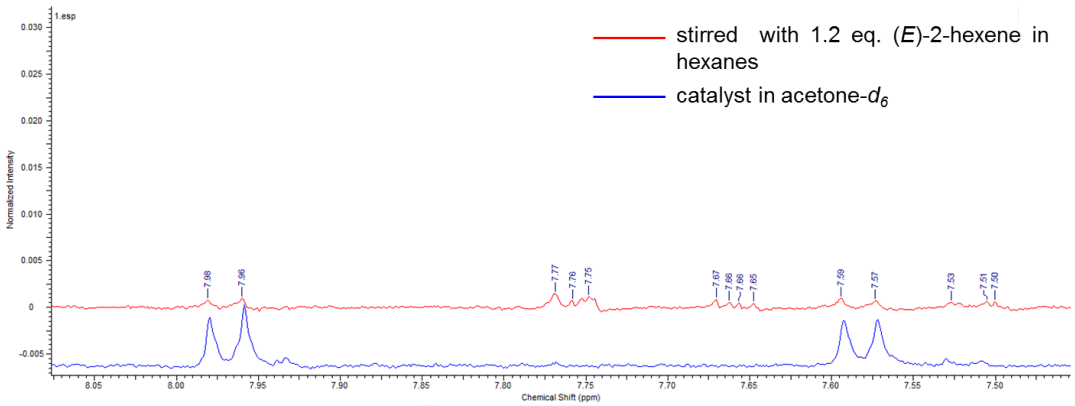

Figure 5. Leaching test of the catalyst into (E)-2-hexene.

Reactivity of Rh(II) complexes with triazoles

Syntheses of TR1 and its reactivity with Rh(II) complex

$Rh_2(ppeb)_4$ can catalyze cyclopropanation or some C-H insertion reactions and the catalyst gave secondary insertion product mainly to show the moderate reactivity in the C-H insertion reactions. What is a problem in the reaction of $Rh_2(ppeb)_4$ with diazo compounds is we cannot utilize the catalyst in heterogeneous condition because of leaching of the catalyst into substrate. Thereby, we thought if we could construct porous framework with the carbene precursor incorporated prospectively, reaction in the pore would be possible. For this strategy, we focused on triazoles as alternative carbene precursors. As mentioned in the introduction, [1,2,3]triazolo[1,5-a]pyridine derivatives exhibit diazo-azomethine/1,2,3-triazole tautomerism and diazo-azomethine tautomer can be more favorable accompanied with several factors such as temperature increase.[7] Additionaly, 1,2,3-triazole can coordinate as N-donor ligand at the axial site of Rh catalyst in priority to other solvent molecules except that with N-donor. Thus, for the second choice, methyl 7-chloro [1,2,3]triazolo[1,5-a]pyridine-3-carboxylate (**TR1**) which shows relatively high reactivity compared to other derivatives due to the chloro group at C7[8] was chosen (Scheme 1). As we expected, reaction of **TR1** with Et_2O catalyzed by $Rh_2(ppeb)_4$ gave C-H inserted product (scheme 2), but **TR1** was found to be too reactive to form adduct with Rh dimer. Actually, the reaction mixture didn't change its color from green to purple although Rh dimer with N-donor axial ligands show purple color as known as solvatochromic behavior of Rh dimer.[9]

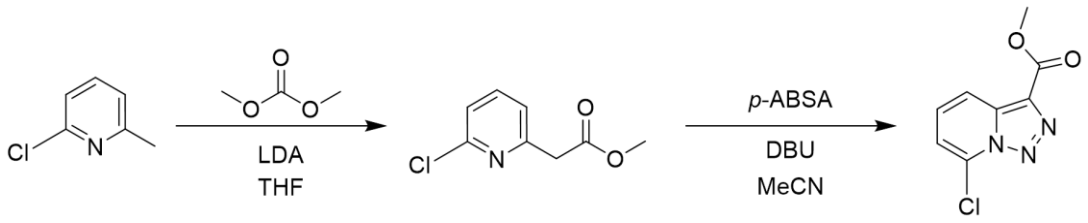

Scheme 1. Synthesis of **TR1**.

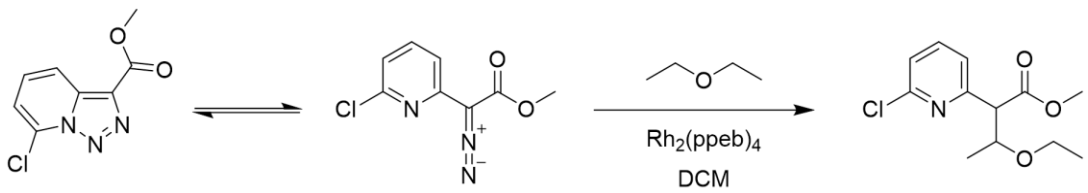

Scheme 2. C-H insertion into Et_2O catalyzed by $Rh_2(ppeb)_4$.

Syntheses of TR2 and TR2 adducts of Rh(II) complex

For the second choice, methyl [1,2,3]triazolo[1,5-a]pyridine-3-carboxylate (**TR2**) was chosen because its 1,2,3-triazole tautomer is enough stable to coordinate at the axial sites of Rh dimer and several carbenoid mediated reactions have been reported.[8] **TR2** was synthesized by following the literature[8a] as shown in scheme 3. Subsequently, **TR2** adducts of Rh_2 (ppeb)$_4$ were obtained by various recrystallization conditions (Table 5).

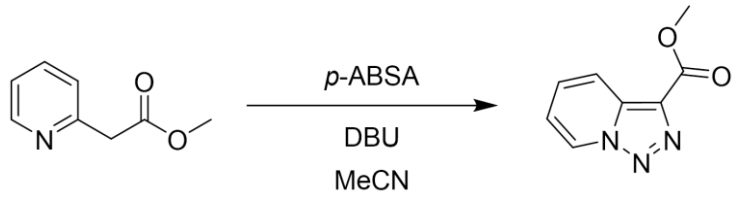

Scheme 1. Synthesis of **TR2**.

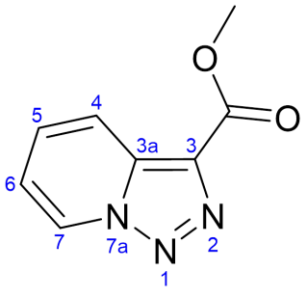

Chart 1. Chemical structure and numbering of **TR2**. Rh_2(ppeb)$_4$.

Table 5. Crystllization conditions for **TR2** adducts of Rh_2(ppeb)$_4$.

Entry	Good solvent for Rh_2ppeb$_4$	Good solvent for triazole	Poor solvent	Crystal color	Crystal structure
1	Et_2O	1,1,2,2-tetrachloroethane	cyclohexane	purple	Similar to 3-TR2
2			*n*-hexane	purple	3-TR2
3			MeOH	purple	3-TR2X
4			*n*-pentane	purple	Similar to 3-TR2
5		1,1,2-trichloroethane	MeOH	green, purple	Not suitable for X-ray analysis
6			^{t}BuOMe	purple	Not suitable for X-ray analysis
7		1,2-dichloroethane	^{i}Pr$_2$O	purple	Similar to 3-TR2
8		$CHCl_3$	pentane	purple	Similar to 3-TR2

Crystal structures of TR2 adducts of Rh(II) complex

3-TR2 was obtained from mixed solution of Et_2O/*n*-hexane/1,1,2,2-tetrachloroethane and in the crystal structure, two **TR2** coordinated at the axial sites of $Rh_2(ppeb)_4$ with nitrogen 1 and hexane was incorporated as crystallization solvent. In the Cambridge Structure Database,[11] [1,2,3]triazolo[1,5-a]pyridine derivatives usually coordinate with nitrogen 2 and no metal complex which is coordinated with only nitrogen 1 of those derivatives has been reported so far.

In the crystal packing structure of **3-TR2**, four of two $ppeb^-$ ligands interacted well with the ligands of adjacent Rh dimer via Ar-Ar^F interaction to form 1-D chain structure (Figure 6b), but other two $ppeb^-$ ligands interact with perfluorophenyl ring and **TR2** via Ar-Ar^F interaction and π-π interaction as described in Figure 6. That's why we obtained not channel structure but 0-dimentional porous structure. Surprisingly, crystals of $Rh_2(ppeb)_4$ with two **TR2** at the axial sites obtained from entry 1, 2, 4, 7, 8 (Table 5) always gave same crystal packing although sometimes crystallization solvents were not included and disorder of the ligands were observed, instead (Figure 7). Therefore, interaction between $ppeb^-$ ligand and **TR2** seems to be highly favored. From these results, it is suggested that axial ligands with aromaticity and high planarity can participate in the self-assembly process and the influence is not too small to be neglected.

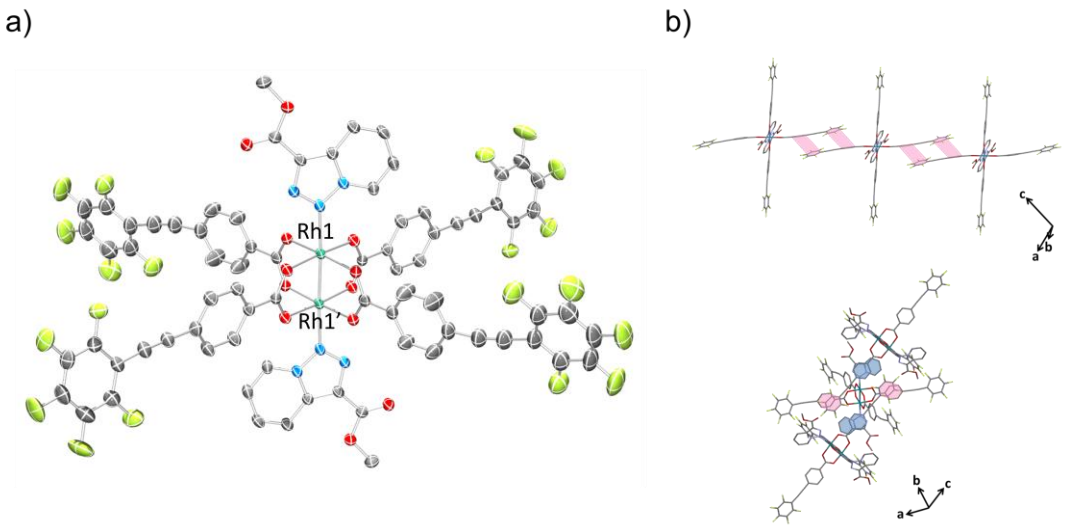

Figure 6. (a) An ORTEP drawing of **3-TR2** (50% probability ellipsoids). Hydrogen atoms and crystal solvent molecules are omitted for clarity. (b) 1-D chain structure of **3-TR2** and π-π interaction between ppeb^{-} and **TR2**. Ar–Ar^{F} interactions and π–π interactions are shown in red and blue lines respectively. Hydrogen atoms and crystal solvent molecules observed are omitted for clarity.

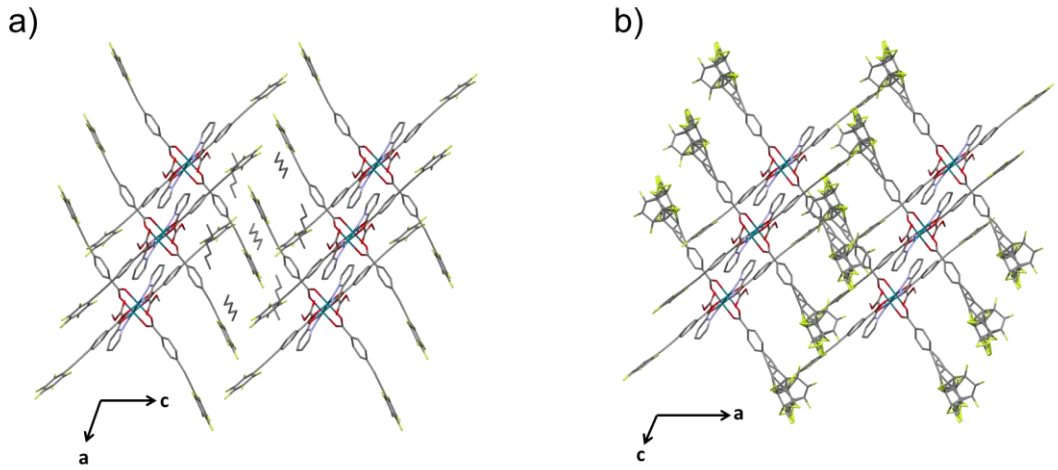

Figure 7. Structural comparison of **3-TR2** crystallized from (a) Et2O/*n*-hexane/1,1,2,2-tetrachloroethane and (b) Et2O/*n*-pentane/1,1,2,2-tetrachloroethane.

In Entry 3, unsymmetrical structure Rh dimer, $Rh_2(ppeb)_4$(**TR2**)(X) (**3-TR2X**) was accidentally obtained as purple crystals. In the crystal structure, Rh dimer had two different axial ligands (Figure 8a). One is **TR2** and another one is unidentified molecule. Unidentified molecule is possibly decomposed product of acetonitrile in solvent purification equipment because acetonitrile used for the synthesis of **TR2** seems to contain some impurity judging from strange smell. Interstingly, the crystal packing structure of **3-TR2X** possesses 2-D sheet structure constructed by Ar-Ar^F interaction (Figure 8b). The estimated average angle between the phenylene and perfluorophenyl rings was 11.5°, which was relatively low compared to 3-THF and 3-PN (18.3° and 14.7° respectively). This resulted in no π-π interaction between 2-D sheets like 1-AD probably due to the bulkiness of an unidentified axial ligand and 1-D channel structure was obtained (Figure 8c).

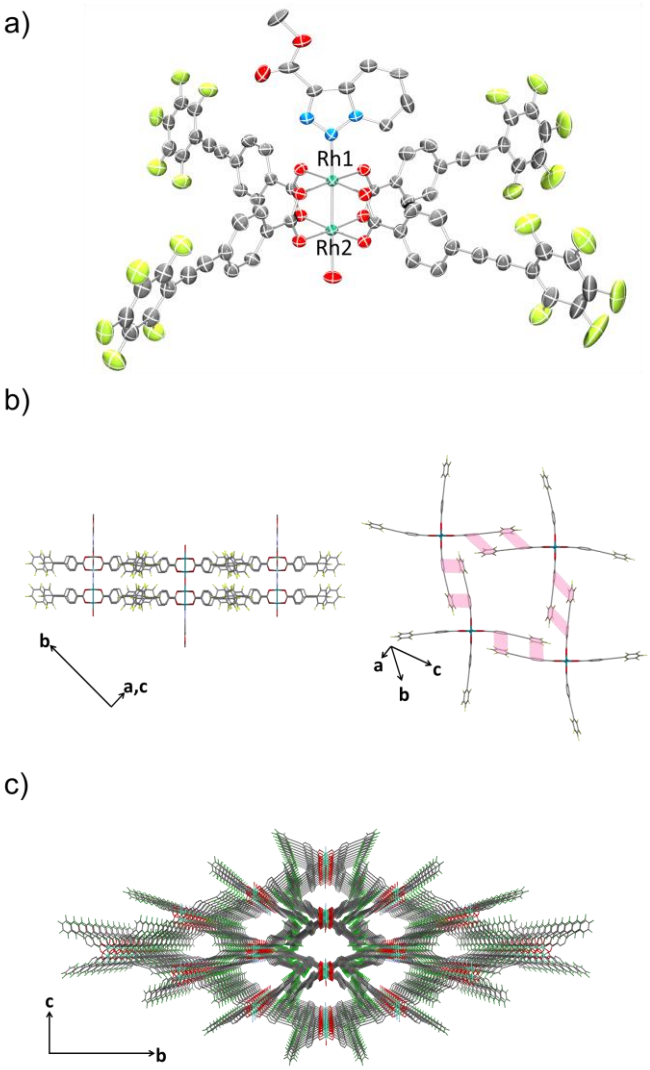

Figure 8. (a) An ORTEP drawing of **3-TR2X** (50% probability ellipsoids). Hydrogen atoms and crystal solvent molecules are omitted for clarity. (b) 2-D sheet structure of **3-TR2X**. Ar–Ar^F interactions is shown in red and blue lines respectively. Hydrogen atoms, carbon atoms and nitrogen atoms of **TR2** at the axial positions and crystal solvent molecules observed in the channels are partially omitted for clarity. (c) Crystal packing of **3-TR2X** along the a axis. Hydrogen atoms, carbon atoms and nitrogen atoms of **TR2** at the axial positions and crystal solvent molecules observed in the channels are partially omitted for clarity. O = red, C = grey, F = pale green, Rh = sea green.

Consequently, two strategies to construct channel structure were conceived. First one is introduction of bulky substituent into triazole to disturb π-π interaction between triazole and $ppeb^-$ ligand. The other is construction of unsymmetrical structure by using two different kinds of axial ligands. For the second strategy, to confirm the possibility to synthesize unsymmetrical $Rh_2(ppeb)_4$ by design, ^1H NMR measurements were performed. Firstly, ^1H NMR spectrum of in situ generated **TR2** and pyridine adducts by addition of 2 equivalent of axial ligands were measured (Figure 9, 10) and compared to $Rh_2(ppeb)_4$ with 1 equivalent of each (Figure 11). As a result, the spectra matched neither triazole adducts nor pyridine adducts and indicated the formation of $Rh_2(ppeb)_4$ with one **TR2** and one pyridine as axial ligands. We didn't mention about this part further in this thesis, but unsymmetrical structure can be obtained in a rational way.

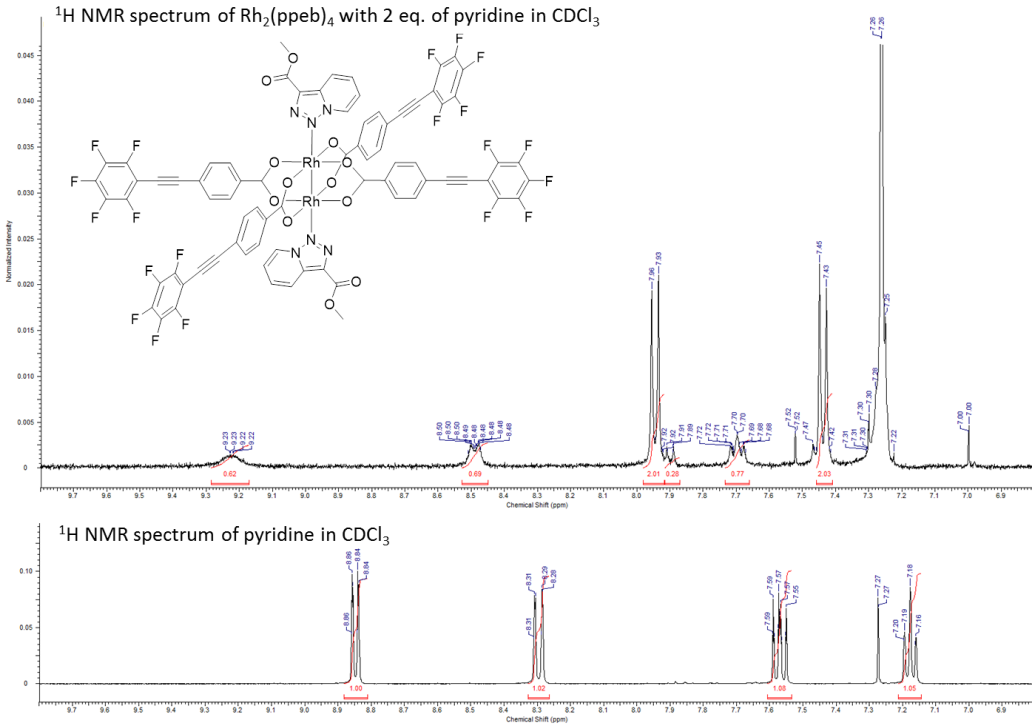

Figure 9. ^{1}H NMR spectra of (top) $Rh_2(ppeb)_4$ with 2 eq. of **TR2** and (bottom) **TR2**.

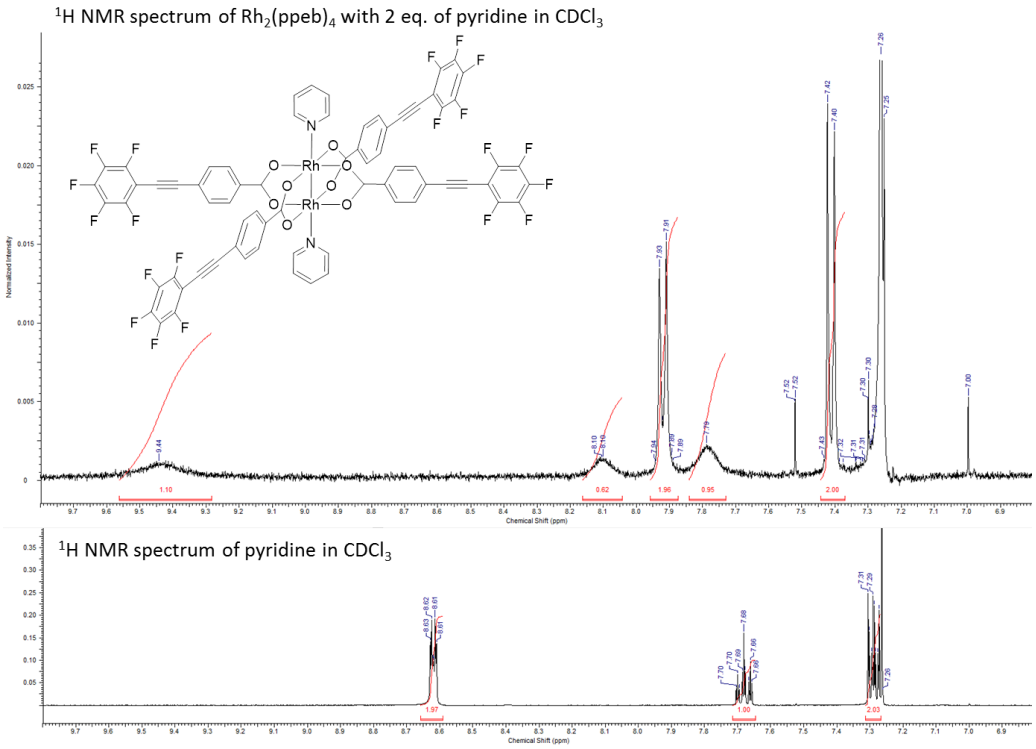

Figure 10. ^{1}H NMR spectra of (top) $Rh_2(ppeb)_4$ with 2 eq. of pyridine and (bottom) pyridine.

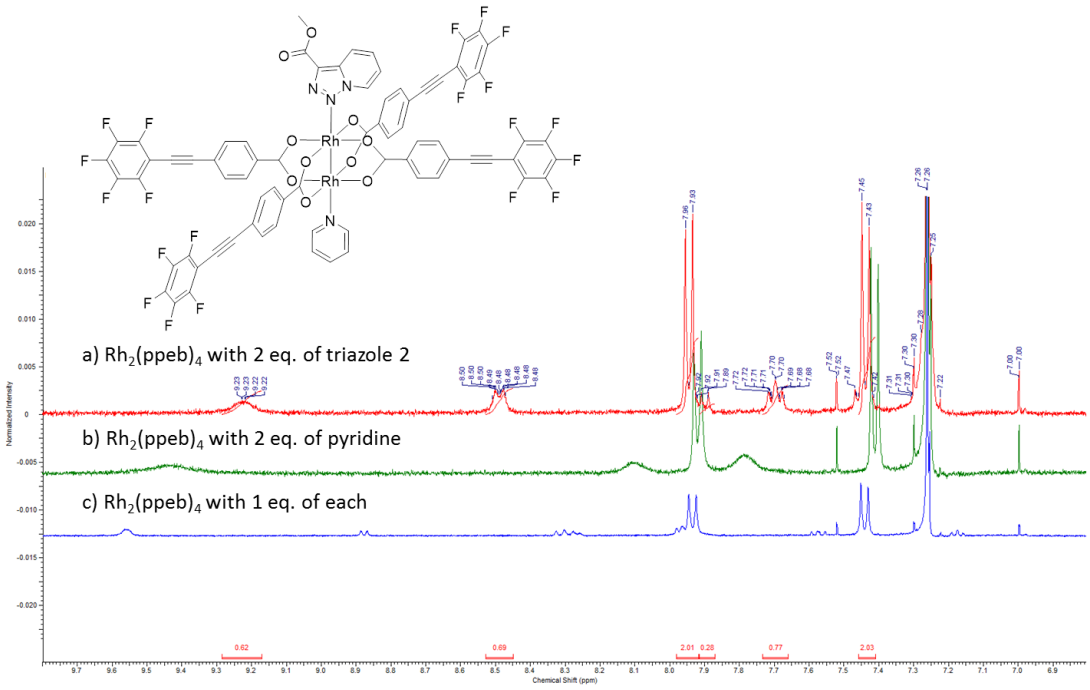

Figure 11. ^{1}H NMR spectra of $Rh_2(ppeb)_4$ with (a) 2 eq. of **TR2** (b) 2 eq. of pyridine and (c) 1 eq. of each.

Syntheses of triazole with bulky substituent

Based on the first strategy, *tert*-butyl group was chosen as a bulky substituent and *tert*-butyl [1,2,3]triazolo[1,5-a]pyridine-3-carboxylate, **TR3** was newly designed (Chart 2). Synthesis of the precursor, *tert*-butyl pyridin-2-ylacetate was synthesized according to reported procedure.[12] Then, by the diazo transfer reaction, **TR3** was obtained with 17% total synthetic yield (scheme 3).

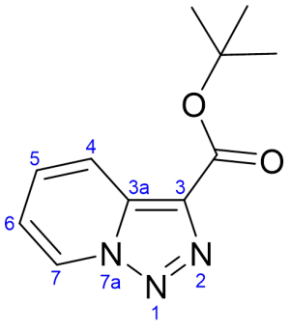

Chart 2. Chemical structure and numbering of **TR3**.

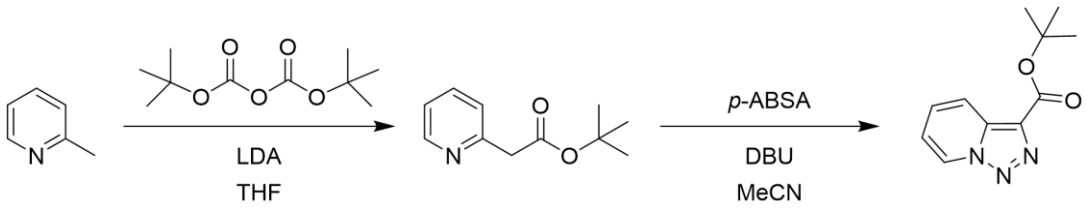

Scheme 3. Synthesis of **TR3**.

Crystal structures of TR3 adducts of Rh(II) complex

3-TR3-1 was obtained from mixed solution of Et_2O/1,1,2-trichloroethane/$^{i}Pr_2O$ and in the crystal structure, two **TR3** coordinated at the axial sites of $Rh_2(ppeb)_4$ with nitrogen 2 and nitrogen 1 denoted as A-Rh_2 and B-Rh_2 respectively. Very interestingly, two Rh dimers were observed independently, and one $Rh_2(ppeb)_4$ had a symmetrical structure, A-Rh_2-A, and another one had a unsymmetrical structure, A-Rh_2-B as shown in Figure 12a.

In the crystal packing structure of **3-TR3-1**, π-π interaction between **TR3** and $ppeb^-$ ligand was successfully inhibited due to the existence of bulky *tert*-butyl substituent as anticipated. Consequently, all of $ppeb^-$ ligands interacted well with each other to form 2-D sheets via Ar-Ar^F interactions (Figure 12b). Furthermore, stacking of 2-D sheets resulted in 1-D channel structure like **3-THF** or **3-PN** (Figure 12 c).[5] The mean interplanar separation between phenylene and perfluorophenyl rings was 3.13(18) Å, and the channel entrance size was estimated to be 13.4 x 12.9 $Å^2$.[13] In the channel, two facing axial ligands always have A···B or A···A (A = **TR3** coordinating with nitrogen 2, B = **TR3** coordinating with nitrogen 1) combination to avoid interference of two axial ligands (Figure 13). Regarding guest molecules included in the pore, the diffused Q peaks indicated the existence of $^{i}Pr_2O$ and **TR3** although they were removed from the data set using the SQUEEZE routine of PLATON and refined further using the data generated to decrease the R value. It should be noted that **3-TR3-1** was also obtained from mixed solution of Et_2O/1,1,2-trichloroethane/^{t}BuOMe and cell parameters were almost same as when $^{i}Pr_2O$ was used.

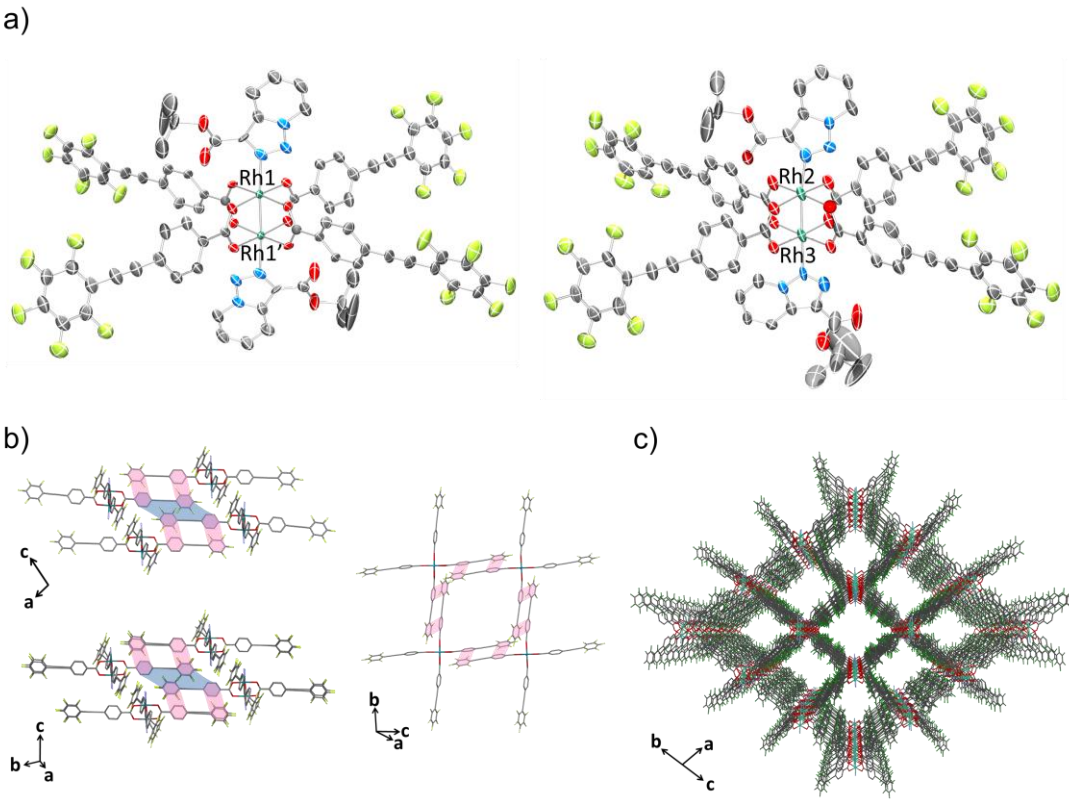

Figure 12. (a) ORTEP drawings of **3-TR3-1** (50% probability ellipsoids). Hydrogen atoms and crystal solvent molecules are omitted for clarity. (b) 2-D sheet structure of **3-TR3-1**. Ar–Ar^{F} interactions is shown in red and blue lines respectively. Hydrogen atoms, carbon atoms and nitrogen atoms of **TR3** at the axial positions and crystal solvent molecules observed in the channels are partially omitted for clarity. (c) Crystal packing of **3-TR3-1** along the channel direction. Hydrogen atoms, carbon atoms and nitrogen atoms of **TR3** at the axial positions and crystal solvent molecules observed in the channels are partially omitted for clarity. O = red, C = grey, F = pale green, Rh = sea green.

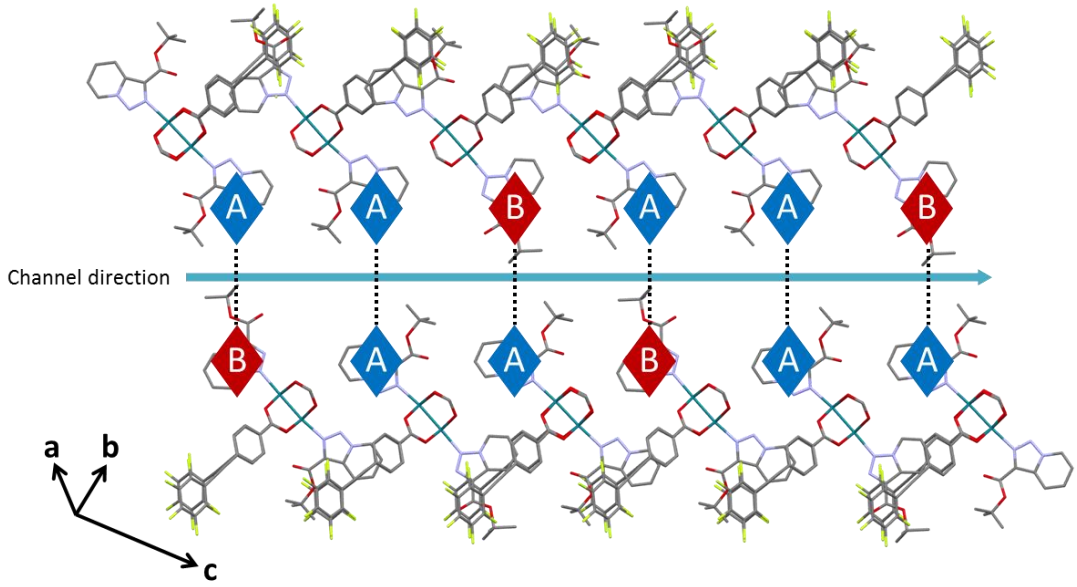

Figure 13. Facing axial ligands in the channel of **3-TR3-1**. Coordinating **TR3** with N2 and N1 are denoted as A and B, respectively.

Crystal structure of **3-TR3-2** which is differ from **3-TR3-1** was obtained from mixed solution of Et_2O/*n*-pentane/1,1,2-trichloroethane and in this case, **TR3** coordinated at the axial sites of $Rh_2(ppeb)_4$ with nitrogen 2 and nitrogen 1 and only A-Rh_2-B type structure was observed (Figure 14a).

In this case, the 1-D channel was also obtained (Figure 14c) and the channel entrance size was estimated to be 10.5 x 7.2 $Å^2$. In the channel, inclusion of *n*-pentane as guest molecules was observed and two facing axial ligands always have A···B combination to avoid interference of two axial ligands (Figure 15). **3-TR3-2** was also obtained from mixed solution of Et_2O/1,1,2-trichloroethane/*n*-hexane and cell parameters were almost same as when *n*-hexane was used.

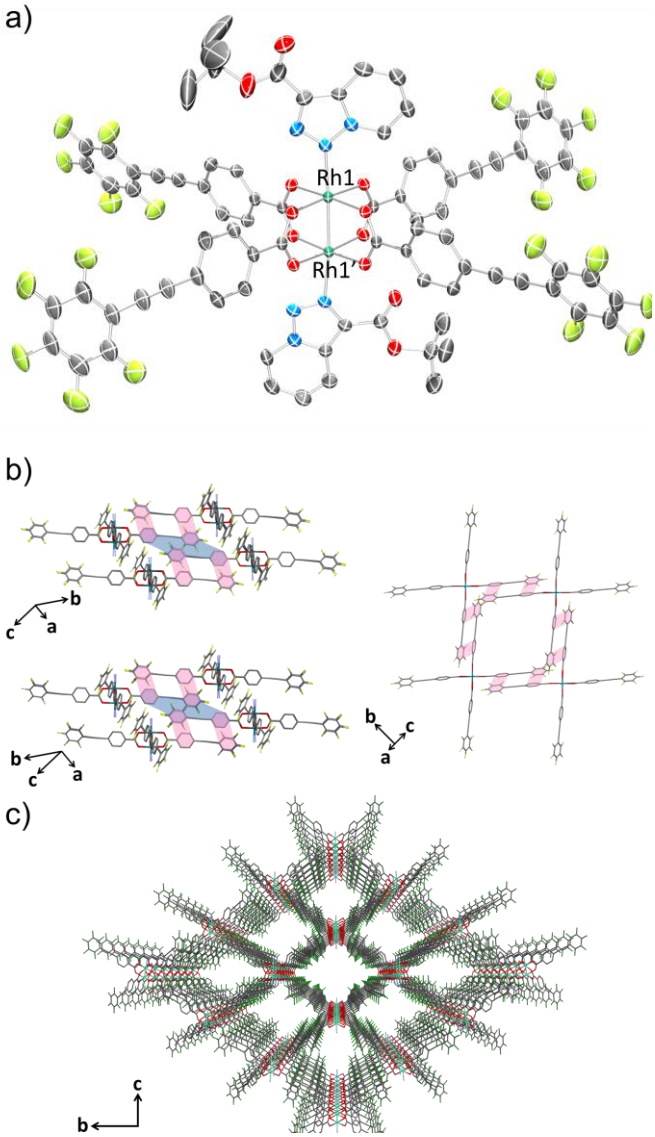

Figure 14. (a) ORTEP drawings of **3-TR3-2** (50% probability ellipsoids). Hydrogen atoms and crystal solvent molecules are omitted for clarity. (b) 2-D sheet structure of **3-TR3-2**. Ar–Ar^{F} interactions are shown in red and blue lines respectively. Hydrogen atoms, carbon atoms and nitrogen atoms of **TR3** at the axial positions and crystal solvent molecules observed in the channels are partially omitted for clarity. (c) Crystal packing of **3-TR3-2** along the channel direction. Hydrogen atoms, carbon atoms and nitrogen atoms of **TR3** at the axial positions and crystal solvent molecules observed in the channels are partially omitted for clarity. O = red, C = grey, F = pale green, Rh = sea green.

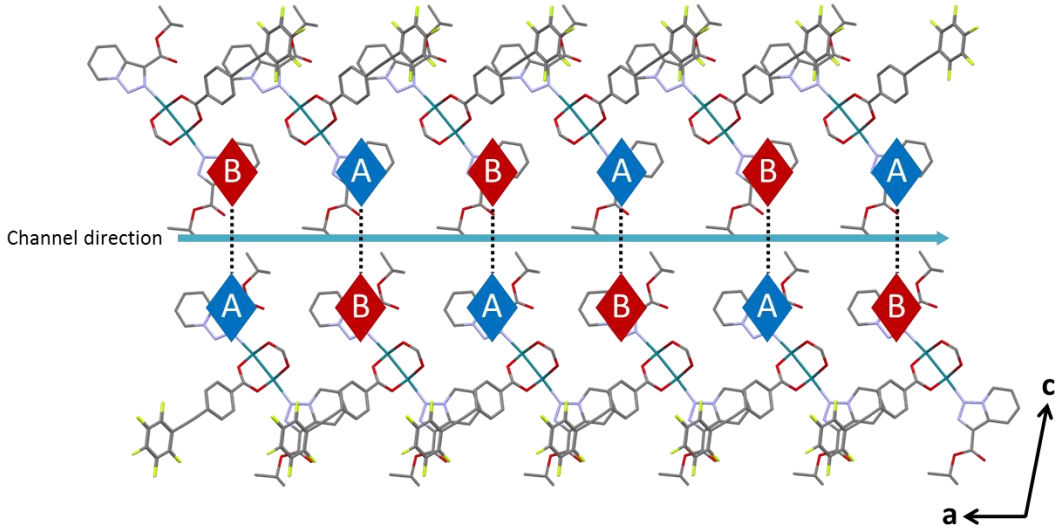

Figure 15. Facing axial ligands in the channel of **3-TR3-2**. Coordinating **TR3** with N2 and N1 are denoted as A and B, respectively.

Et_2O/EtOH/1,1,2-trichloroethane gave unexpected structure **3-TR3-3** which had B-Rh_2-B type structure. What is surprising is that B-Rh_2-B type structure still can form 1-D channel structure derived from the stacking of 2-D sheets constructed via Ar-Ar^F interactions. As shown in Figure16c, π-plane of **TR3** is inclined from Rh-Rh bond to avoid the interference of the two axial ligands. In addition, two facing axial ligands always have B···B combination as described in Figure 17. The channel entrance size was estimated to be 13.5 x 10.6 $Å^2$. In the channel, inclusion of EtOH and water as guest molecules was observed and one of EtOH molecules is hydrogen bonded with **TR3** (Figure 16a) **3-TR3-3** was also obtained from a mixed solution of Et_2O/1,1,2-trichloroethane/MeOH and cell parameters were almost same as when EtOH was used.

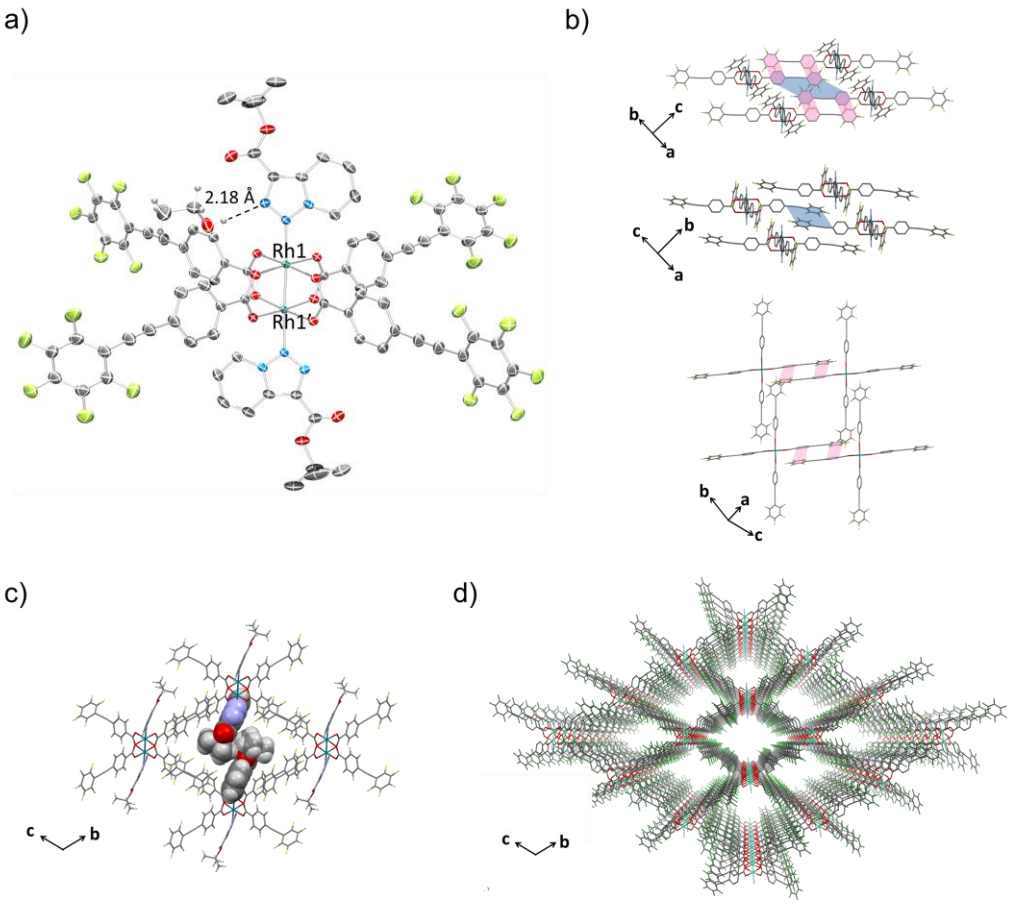

Figure 16. (a) An ORTEP drawing of **3-TR3-3** (50% probability ellipsoids). Hydrogen atoms and crystal solvent molecules are omitted for clarity. (b) 2-D sheet structure of **3-TR3-3**. Ar–Ar^F interactions are shown in red and blue lines respectively. Hydrogen atoms, carbon atoms and nitrogen atoms of **TR3** at the axial positions and crystal solvent molecules observed in the channels are partially omitted for clarity. (c) Facing axial ligands in the channel. (d) Crystal packing of **3-TR3-3** along the channel direction. Hydrogen atoms, carbon atoms and nitrogen atoms of **TR3** at the axial positions and crystal solvent molecules observed in the channels are partially omitted for clarity. O = red, C = grey, F = pale green, Rh = sea green.

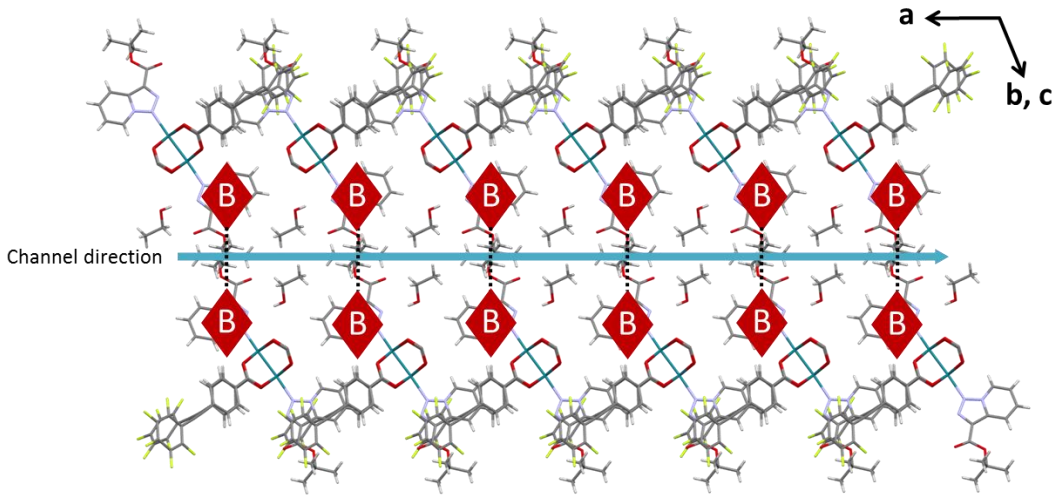

Figure 17. Facing axial ligands in the channel of **3-TR3-2**. Coordinating **TR3** with N1 are denoted as B.

From these results, it is found that crystal packing of $Rh_2(ppeb)_4$ with **TR3** as axial ligands always have 1-D channel structure but there is a tendency for crystal packing to be determined by crystallization solvent. From the perspective of coordination mode of **TR3**, obtained crystal packings can be classified in three types as shown in Figure 18. 3-TR3-1. While the tendency is still controvertible, ethers, alkanes and alcohols give A-Rh_2-A and A-Rh_2-B structure, only A-Rh_2-B structure and B-Rh_2-B structure respectively. Owing to guest-induced change of coordination mode of **TR3**, columnar channel structure which seems to be favorable crystal packing is successfully constructed in any recrystallization condition.

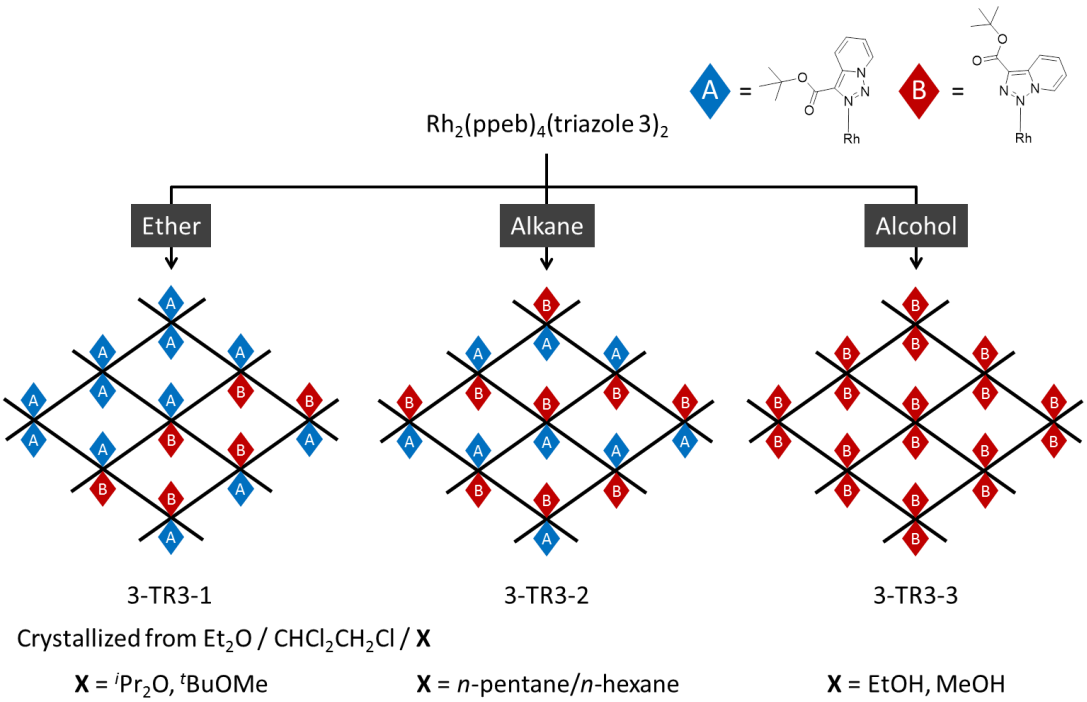

Figure 18. Tendency for **c**rystal packing of **3-TR3** crystallization solvent.

Conclusions

In conclusion, $Rh_2(ppeb)_4$ can catalyze cyclopropanation or some C-H insertion reactions when diazo compounds were used as carbene precursors. In the case of the C-H insertion reactions, inserted secondary C-H insertion products was mainly obtained to show the moderate reactivity of the catalyst. Due to the dissolution of the catalyst in aromatic or allyl substrates, catalytic activity as heterogeneous catalyst could not be evaluated. In order to construct substrate-incorporated porous framework, [1,2,3]triazolo[1,5-a]pyridine derivatives which show diazo-azomethine/1,2,3-triazole tautomerism were chosen as alternative carbene precursors. $Rh_2(ppeb)_4$ with one or two **TR2** axial ligands, **3-TR2** and **3-TR2-X** were obtained and the crystal packing structures of **3-TR2** always show same structures to form 0-dimensional porous structure due to π-π interaction between **TR2** and ppeb- ligand To overcome the problem, **TR3** with bulky *tert*-butyl substituent was synthesized and subsequently **TR3** adduct of $Rh_2(ppeb)_4$ were obtained. Interestingly, in some cases **TR3** coordinated with different position to lead three types of crystal packings depend on crystallization solvent. Furthermore, all of the crystal packings had 1-D channel structure by virtue of the flexible coordination modes of **TR3** and good suppression of π-π interaction between triazole and $ppeb^-$ ligand. We believe that our results presented here could be relevant not only for construction of reaction fields by utilization of intermolecular interactions but also for trapping specific guests molecules. Different reactivities depending on crystal packing structure[14] are also expected. To probe this further, we are currently investigating the reactivity of Rh dimer with triazole in the frameworks and solution.

Experimental section

General Methods

All solvents and reagents are of the highest quality available and used as received. $Rh_2(ppeb)_4$ were prepared by the literature methods.[5] All syntheses were performed under an atmosphere of dry nitrogen or dry argon unless otherwise indicated. Powder X-ray diffraction (PXRD) data were collected on a Bruker D8 APEX II CCD sealed tube diffractometer with graphite monochromated Cu Kα (λ = 1.54178 Å) radiation in transmission mode, since the diffraction was too weak on the powder diffractometer in reflectance geometry.

Measurement Apparatus

Elemental analyses were carried out on a J-SCIENCE LAB MICRO CORDER JM10 elemental analyser. ^1H NMR spectra were acquired on a JEOL JNM-ECS400 spectrometer, where chemical shifts in $CDCl_3$ were referenced to internal tetramethylsilane.

General procedure for cyclopropanation and C-H insertion

An oven- or frame-dried 50 mL round bottom flask containing a Teflon-coated oval stir bar was fitted with a rubber septum and allowed to cool to room temperature under vacuum. At room temperature, substrate and rhodium catalyst (4.0 mg, 2.5 μmol) were added and the flask connected with a water condenser when reflux was needed, which is connected to a vacuum line via a needle inserted through the septum. The flask was evacuated then back-filled with argon (3 times) or flush with argon for one minute to remove the air in the flask. Dichloromethane or alkane (7.5 mL) is introduced via syringe under a positive argon pressure. Then, diazo compound (0.5 mmol) in the given solvent (7.5 mL) is added drop-wise via syringe under the given temperature over 1 hour under argon atmosphere. The diazo residue was rinsed with the same solvent (0.5 mL) and was transferred into the reaction. The resulting solution was stirred another 1 hour. The reaction was cooled to room temperature, concentrated in vacuo and the crude mixture was purified by flash column chromatography (pentane/Et_2O) to afford the product.

Syntheses

Synthesis of *tert*-butyl [1,2,3]triazolo[1,5-a]pyridine-3-carboxylate (TR3)

To a stirred solution of methyl *tert*-butyl pyridin-2-ylacetate (1.17 g, 6.05 mmol) and

DBU (1.0 ml, 6.65 mmol) in 29.3 ml of dry acetonitrile, *p*-ABSA (1.52 g, 6.01 mmol) was added at room temperature in small portions. The resulting yellow solution was stirred overnight and, after removal of solvent dichloromethane was added to the residue. The resulting solution was washed with water and brine, and dried over sodium sulfate. Flash Silica chromatography (3:7 EtOAc/n-pentane) gave the product as white solid. Yield: 888 mg (4.05 mmol, 67%).

Syntheses of 3-TR2, 3-TR2X, 3-TR3-1, 3-TR3-2 and 3-TR3-3: The five kinds of axial ligand substituted complexes were synthesized by the recrystallization of $Rh_2(ppeb)_4(Et_2O)_2$. In all cases, $Rh_2(ppeb)_4(Et_2O)_2$ was firstly dissolved in Et_2O and subsequently chlorinated solvent solution of **TR2** or **TR3** was added until the solution changed its color from green to purple. $Rh_2(ppeb)_4$(**TR2**)$_2$ (**3-TR2**) and $Rh_2(ppeb)_4$(**TR2**)(solvent) (**3-TR2X**) were obtained by slow vapor diffusion of *n*-hexane and MeOH respectively into the solution of $Rh_2(ppeb)_4(Et_2O)_2$ and **TR2** in Et_2O/1,1,2,2-tetrachloroethane. For $Rh_2(ppeb)_4$(**TR3**)$_2$ (**3-TR3-1**, **3-TR3-2**, **3-TR3-3**), the recrystallization was performed by slow vapor diffusion of $^{i}Pr_2O$, *n*-hexane and EtOH respectively into the solution of $Rh_2(ppeb)_4(Et_2O)_2$ and **TR3** in Et_2O/1,1,2-trichloroethane.

X-ray crystallography

All crystals were mounted in a loop. Diffraction data at 123 K were measured on a RAXIS-RAPID Imaging Plate diffractometer equipped with confocal monochromated Mo-Kα radiation and data was processed using RAPID-AUTO (Rigaku). Structures were solved by direct methods and refined by full-matrix least squares techniques on F^2 (*SHELXL-97*).[15] All non-hydrogen atoms were anisotropically refined, while all hydrogen atoms were placed geometrically and refined with a riding model with Uiso constrained to be 1.2 times Ueq of the carrier atom. For **3-TR2X** and **3-TR3-1**, the diffused electron densities resulting from residual solvent molecules or unidentified axial ligand were removed from the data set using the SQUEEZE routine of PLATON and refined further using the data generated.

Crystal data for 3-TR2: $C_{94}H_{72}F_{20}N_6O_{12}Rh_2$, Mr = 2063.4, monoclinic, space group *P* $2_1/a$, (#14), a = 15.5847(7) Å, b = 15.6744(6) Å, c = 19.5443(8) Å, β = 109.567(8)°, V = 4498.6(3) Å^3, Z = 2, T = 123 (2) K, ρ_c = 1.523 gcm^{-3}, μ(Mo-Kα) = 0.473 cm^{-1}, $2\theta_{max}$ = 54.92, λ(Mo-Kα) = 0.710747 Å, 41925 reflections measured, 10264 unique (R_{int} =

0.0706), 7598 (I > 2σ(*I*)) were used to refine 608 parameters, 0 restraints, wR_2 = 0.1398 (I > 2σ(I)), R_1 = 0.0535 (I > 2σ(I)), GOF = 1.011.

Crystal data for 3-TR2X: $C_{90}H_{20}Cl_4F_{20}N_6O_{12}Rh_2$, Mr = 2104.74, monoclinic, space group *P* $2_1/m$, (#11), *a* = 9.9308(16) Å, *b* = 32.969(7) Å, *c* = 13.285(3) Å, β = 98.423(10)°, *V* = 4302.7(15) Å^3, *Z* = 2, *T* = 123 (2) K, ρ_c = 1.625 gcm^{-3}, μ(Mo-Kα) = 0.617 cm^{-1}, 2θ_{max} = 52.76, λ(Mo-Kα) = 0.710747 Å, 41012 reflections measured, 10002 unique (R_{int} = 0.0271), 8942 (*I* > 2σ(*I*)) were used to refine 547 parameters, 0 restraints, wR_2 = 0.2495 (*I* > 2σ(*I*)), R_1 = 0.0838 (*I* > 2σ(*I*)), GOF = 1.055.

Crystal data for 3-TR3-1: $C_{123}H_{63}F_{30}N_9O_{18}Rh_3$, Mr = 2833.5, triclinic, space group $P\bar{1}$, (#2), *a* = 16.4775(5) Å, *b* = 16.9552(6) Å, *c* = 28.8487(9) Å, α = 102.9854(7)°, β = 95.854(7)°, γ = 105.841(7)°, *V* = 7439.8(6) Å^3, *Z* = 2, *T* = 123 (2) K, ρ_c = 1.265 gcm^{-3}, μ(Mo-Kα) = 0.423 cm^{-1}, 2θ_{max} = 54.96, λ(Mo-Kα) = 0.710747 Å, 73289 reflections measured, 33800 unique (R_{int} = 0.0676), 19855 (*I* > 2σ(*I*)) were used to refine 1645 parameters, 0 restraints, wR_2 = 0.3488 (*I* > 2σ(*I*)), R_1 = 0.1101 (*I* > 2σ(*I*)), GOF = 1.142.

Crystal data for 3-TR3-2: $C_{90}H_{66}F_{20}N_6O_{12}Rh_2$, Mr = 2033.33 monoclinic, space group *P* $2_1/m$, (#2), *a* = 9.9310(2) Å, *b* = 25.3084(5) Å, *c* = 18.5618(3) Å, β = 101.001(7)°, *V* = 4579.55(15) Å^3, *Z* = 2, *T* = 123 (2) K, ρ_c = 1.475 gcm^{-3}, μ(Mo-Kα) = 0.464 cm^{-1}, 2θ_{max} = 54.88, λ(Mo-Kα) = 0.710747 Å, 44582 reflections measured, 10656 unique (R_{int} = 0.0355), 7659 (*I* > 2σ(*I*)) were used to refine 643 parameters, 1 restraints, wR_2 = 0.1953 (*I* > 2σ(*I*)), R_1 = 0.0611 (*I* > 2σ(*I*)), GOF = 1.030.

Crystal data for 3-TR3-3: $C_{45}H_{33}F_{10}N_3O_9Rh$, Mr = 1052.65 triclinic, space $P\bar{1}$, (#2), *a* = 10.2672(2) Å, *b* = 15.6478(4) Å, *c* = 16.0106(3) Å, α = 111.348(8)°, β = 101.802(7)°, γ = 102.990(7)°, *V* = 2215.2(2) Å^3, *Z* = 2, *T* = 123 (2) K, ρ_c = 1.578 gcm^{-3}, μ(Mo-Kα) = 0.487 cm^{-1}, 2θ_{max} = 54.94, λ(Mo-Kα) = 0.710747 Å, 21917 reflections measured, 10095 unique (R_{int} = 0.0214), 9184 (*I* > 2σ(*I*)) were used to refine 620 parameters, 0 restraints, wR_2 = 0.1137 (*I* > 2σ(*I*)), R_1 = 0.0416 (*I* > 2σ(*I*)), GOF = 1.082.

References

1 (a) D. A. Colby, R. G. Bergman and J. A. Ellman, *Chem. Rev.*, **2010**, *110*, 624–655; (b) R. Giri, B.-F. Shi, K. M. Engle, N. Maugel and J.-Q. Yu, *Chem. Soc. Rev.*, **2009**, *38*, 3242–3272.; (c) C–H Activation, ed. J.-Q. Yu and Z. Shi, Wiley-VCH Verlag, Heidelberg, **2010**; (d) T.W. Lyons and M. S. Sanford, *Chem. Rev.*, **2010**, *110*, 1147–1169; (e) V. Ritleng, C. Sirlin and M. Pfeffer, *Chem. Rev.*, 2002, 102, 1731–1769. (f) H. M. L. Davies and J. R. Manning, *Nature*, **2008**, *451*, 417–424; (g) M. P. Doyle, R. Duffy, M. Ratnikov and L. Zhou, *Chem. Rev.*, **2010**, *110*, 704–724; (h) H. M. L. Davies and J. R. Denton, *Chem. Soc. Rev.*, **2009**, 38, 3061–3071; (i) H.M. L. Davies and J. Hansen, in *Catalytic Asymmetric Synthesis*, Third ed., Ojima, John Wiley and Sons, Inc., **2010**, pp. 163–226.

2 (a) H. M. L. Davies and R. E. J. Beckwith, *Chem. Rev.*, 2003, *103*, 2861–2904. (b) K. Liao, S. Negretti, D. G. Musaev, J. Bacsa and H. M. L. Davies, *Nature*, **2016**, *533*, 230–234. (c) C. Qin and H. M. L. Davies, *J. Am. Chem. Soc.*, **2014**, *136*, 9792–9796. (d) D. M. Guptill and H. M. L. Davies, *J. Am. Chem. Soc.*, **2014**, *136*, 17718–17721; (e) D. M. Guptill and H. M. L. Davies, *J. Am. Chem. Soc.*, **2014**, *136*, 17718–17721.

3 (a) I. E. Tsyshchuk, D. V. Vorobyeva, A. S. Peregudov and S. N. Osipov, *Eur. J. Org. Chem.*, **2014**, 2480–2486; (b) P. Müller and C. Boléa, Molecules, **2001**, *6*, 258–266; (c) T. Ye and M. A. Mckervey, *Chem. Rev.*, **1994**, *94*, 1091–1160.

4 (a) K. Takeda, T. Oohara, M. Anada, H. Nambu and S. Hashimoto, *Angew. Chem., Int. Ed.*, **2010**, *49*, 6979–6983; (b) T. Oohara, H. Nambu, M. Anada, K. Takeda and S. Hashimoto, Advanced Synthesis & Catalysis, **2012**, *354*, 2331–2338; (c) K. Takeda, T. Oohara, N. Shimada, H. Nambu and S. Hashimoto, *Chem.-Eur. J.*, **2011**, *17*, 13992–13998; (d) H. M. L. Davies, A. M. Walji and T. Nagashima, *J. Am. Chem. Soc.*, **2004**, *126*, 4271–4280. (e) T. Gutmann, J. Liu, N. Rothermel, Y. Xu, E. Jaumann, M. Werner, H. Breitzke, S. T. Sigurdsson and G. Buntkowsky, *Chem.-Eur. J.*, **2015**, *21*, 3798–3805; (f) J. Liu, C. Fasel, P. Braga-Groszewicz, N. Rothermel, A. S. L. Thankamony, G. Sauer, Y. Xu, T. Gutmann and G. Buntkowsky, Catal. Sci. Technol., **2016**, *6*, 7830–7840.; (g) J. Liu, A. Plog, P. Groszewicz, L. Zhao, Y. Xu, H. Breitzke, A. Stark, R. Hoffmann, T. Gutmann, K. Zhang and G. Buntkowsky, *Chem.-Eur. J.*, **2015**, *21*, 12414–12420; (h) N. R. Candeias, C. A. M. Afonso and P. M. P. Gois, *Org. Biomol. Chem.*, **2012**, *10*, 3357.

5 T. Itoh, M. Kondo, H. Sakamoto, K. Wakabayashi, M. Kanaike, K. Itami and S. Masaoka, *Dalton Trans.*, **2015**, *44*, 15334–15342.

6 K. P. Kornecki, J. F. Briones, V. Boyarskikh, F. Fullilove, J. Autschbach, K. E. Schrote, K. M. Lancaster, H. M. L. Davies, J. F. Berry, *Science*, **2013**, *342*, 351-354.

7 W. Dehaen and V. A. Bakulev, "*Chemistry of 1,2,3-triazoles*", Springer, Cham, 2015.

8 (a) S. Chuprakov, F. W. Hwang, V. Gevorgyan, *Angew. Chem., Int. Ed.*, **2007**, *46*, 4757; (b) H. M. L. Davies and R. J. Townsend, *J. Org. Chem.*, **2001**, *66*, 6595–6603; (c) B. Chattopadhyay

and V. Gevorgyan, *Angew. Chem., Int. Ed.*, **2011**, *51*, 862–872.

9 S. A. Johnson, H. R. Hunt and H. M. Neumann, *Inorg. Chem.*, **1963**, *2*, 960–962.

10 Y. Shi, A. V. Gulevich and V. Gevorgyan, *Angew. Chem., Int. Ed.*, **2014**, *53*, 14191–14195.

11 C. R. Groom, I. J. Bruno, M. P. Lightfoot and S. C. Ward, Acta Cryst., **2016**, *B72*, 171-179.

12 R. Frank, et al., *PCT Int. Appl.*, 2013013817, 31 Jan **2013**

13 The channel entrance size was estimated by considering the Van der Waals radii of constituent atoms, and the atoms at axial ligands are omitted for the calculation.

14 R. Ding, C. Huang, J. Lu, J. Wang, C. Song, J. Wu, H. Hou and Y. Fan, *Inorg. Chem.*, **2015**, *54*, 1405–1413.

15 G. M. Sheldrick, *Program for Crystal Structure Refinement*, University of Göttingen, Germany, 1997.

Concluding Remarks

In this thesis, we addressed construction of porous frameworks based on Rh(II) paddle-wheel complex with reactive sites by usage of Ar-Ar^F interaction. For this subject, Rh(II) paddle-wheel complexes which have ligands with multipoint Ar-Ar^F interaction sites were synthesized and their crystal packing, structural transformations, porous properties and reactivities with diazo compounds and triazoles were studied.

In chapter 1, the usability of multipoint Ar-Ar^F interactions for the self-assembly of paddle-wheel unit was studied. I- and cross-shaped complexes with a novel ligand which has arene and perfluoroarene moieties bridged by C≡C bond were synthesized. Molecular arrangements of them in crystal packing were controlled well by multipoint Ar-Ar^F interactions. As a result, I- and cross-shaped complexes gave one- or two-dimensional structures respectively at room temperature as expected. Moreover, in the case of cross-shaped complex, the solvent accessible channel structure with open axial sites which is hardly observed in discrete paddle-wheel units was found. The results presented in this chapter suggested the possibility that Ar-Ar^F interactions can be used to assemble paddle-wheel units of various metal ions with open axial sites at room temperature regardless of substitution activity.

In chapter 2, the construction of porous frameworks by the self-assembly of substitution-inert Rh(II) dimer units with active sites via multipoint Ar-Ar^F interactions and their porous properties were studied. Rh(II) paddle-wheel complexes with multipoint Ar-Ar^F interaction sites, $Rh_2(ppeb)_4(X)_2$ (X = THF (**3-THF**), 3-pentanone (**3-PN**), and 1-adamantylamine (**3-AD**)), were newly synthesized. In their crystal packings, porous frameworks with a solvent accessible channel were successfully obtained by multipoint Ar-Ar^F interactions to show the versatility of our strategy for the self-assembly of paddle-wheel dimer units. Active sites of Rh dimer units were exposed to the channel, and by the comparison of those three complexes, the size and the structure of the axial ligands induced structural differences were observed. It was also found that the porous properties of these frameworks can be affected by the coordination ability of axial ligands. Besides, **3-THF** and **3-PN** which have labile axial ligands showed reversible crystal to crystal structural transformation in response to the ligand substitution.

In chapter 3, the construction of porous frameworks with Rh(II) dimer units with with (*E*)-ppvb$^-$ ligands have both multipoint Ar-Ar^F interaction sites and photo chemically reactive site were studied. Before the synthesis of the Rh(II) complexes, photodimerizarion of (*E*)-Hppvb were examined. The crystal packing of (*E*)-Hppvb crystallized from DMF exhibited ideal molecular arrangements for photodimerization controlled by Ar-Ar^F interaction. As a consequence, [2+2] photo dimerization reaction proceeded quantitatively at crystalline state by irradiation of UV-light. Then, three Rh(II) paddle-wheel complexes, $Rh_2((E)\text{-ppvb})_4(X)_2$ (X = THF (**4-THF**), 2-butanone (**4-BN**), and pyridine (**4-PY**), were synthesized. Among them, the crystal packing structures of **4-THF** and **4-BN** were successfully determined by multipoint Ar-Ar^F interactions and arrangements of C=C bond in the ligands seemed to be suitable for photodimerization. However, photo polymerized products of Rh dimers were not obtained by UV-light irradiation using Hg lamp probably due to quenching of excited state of the ligand by Rh center.

In chapter 4, reactivity of $Rh_2(ppeb)_4$ with diazo compounds and incorporation of triazoles at its axial sites were studied. In terms of the reactivity with diazo compounds, $Rh_2(ppeb)_4$ showed moderate reactivity and mainly C-H insertion into the secondary carbon was observed in the case of C-H insertion reactions. Heterogeneous catalytic activity of porous framework of $Rh_2(ppeb)_4$ could not be appraised because of the dissolution of the catalyst in aromatic or allyl substrates. Aiming for incorporation of carbene precursors into axial sites of Rh dimer in porous frameworks, [1,2,3]triazolo[1,5-a]pyridine derivatives which exhibit diazo-azomethine/1,2,3-triazole tautomerism were employed. $Rh_2(ppeb)_4$ with two **TR2** which has methyl ester moiety gave 0-dimensional porous structure because multipoint Ar-Ar^F interaction of the ligand was disturbed by π-π interaction between **TR2** and ppeb$^-$ ligand. This problem was solved by employing **TR3** with bulky *tert*-butyl substituent. Owing to the bulky substituent, π-π interaction between triazole and ppeb- ligand was successfully avoided to give 1-D columnar channel structure. Additionally, flexible coordination modes of **TR3** was also observed while not observed in the case of **TR2**.

In conclusion, substitution-inert Rh(II) dimer units were successfully assembled to afford porous frameworks with 1-D columnar structure. In those frameworks, multipoint Ar-Ar^F interaction worked effectively as a supramolecular synthon and active sites of Rh dimer units were exposed to the channel. The crystal packing structures or porous properties can be affected by the size or coordination ability of axial ligands.

Furthermore, it is proved that triazoles as carbene precursors can be incorporated into the axial site of Rh dimers. These survey results would be a new strategy to construct a new class of porous materials composed of substitution inert metal complexes with open metal sites.

Acknowledgements

The presented thesis is the summary of the author's studies from April 2012 to March 2017 at the Department of Structural Molecular Science, School of Physical Science, the Graduate University for Advanced Studies (SOKENDAI) under the direction of Dr. Shigeyuki Masaoka, Associate Professor of SOKENDAI.

I express his deepest gratitude to Associate Professor Shigeyuki Masaoka for his significant guidance, continuous encouragement and valuable discussion. I could learn a lot from him about passion to science, how to establish my own research field, and how to emphasize my research impact. I am deeply grateful to Assistant Professor Mio Kondo for her warm-hearted encouragement, instructive direction and invaluable discussion. I could learn a lot from her about how to proceed with a research and how to instruct and encourage students. There are no words to describe how grateful I am. I would like to thank Designated Assistant Professor Dr. Masaya Okamura in Nagoya University for giving me comprehensive knowledge of chemistry and beneficial advices

I gratefully acknowledge Professor Kenichiro Itami and Designated Assistant Professor Hirotoshi Sakamoto in Nagoya University for the measurement of the powder x-ray diffraction and gas adsorption, and many helpful advices.

I express his sincere thanks to Assistant Professor Dr. Masaki Yoshida in Hokkaido University

I am deeply grateful to Professor Tetsuro Murahashi and Assistant Professor Koji Yamamoto in Tokyo Institute of Technology for the measurement of single crystal X-ray diffraction.

I am deeply grateful to Mr. Seiji Makita in Institute for Molecular Science for the measurement of elemental analysis.

I am deeply grateful to Ms. Michiko Nakano and Ms. Haruyo Nagao in Institute for Molecular Science for the measurement of ^{1}H and ^{19}F NMR spectroscopy.

I express sincere appreciation to our members in Institute for Molecular Science, Dr. Vijayendran K. K. Praneeth, Researcher in NARD institute, ltd. Dr. Go Nakamura,

Researcher in Toyota Central R&D Lab Mr. Masakazu Murase, Mr. Yuki Okabe, Ms. Pondchanok Chinapang, Mr. Ke Liu, Ms. Arisa Fukatsu, Ms. Yukino Fukahori, Mr. Sze Koon Lee, Mr. Takafumi Enomoto, Mr. Hitoshi Izu, Mr. Riku Ushijima, Ms. Chihiro Matsui, Ms. Reiko Kuga, Ms. Mari Kanaike, Ms. Kaori Wakabayashi, Ms. Akane Shibata and Ms. Miho matsuda for many advices about research, valuable discussion, heartfelt encouragement and friendship during his time in the lab. I also wish to express sincere thanks to my co-workers, Mr. Teramoto Masahiro in Tokyo Institute of Technology and the foreign student from ParisTech, Ms. Marine Simoen. I also grateful to Ms. Mayuko Taniwake and Ms. Kyoko Nogawa for their secretarial support.

I am deeply grateful to Professor Tada Mizuki, Assistant Professor Satoshi Muratsugu in Nagoya University, Professor Nobuhiro Kosugi, Assistant Professor Hiroyuki Yamane, and Assistant Professor Masanari Nagasaka in the Institute for molecular Science for kindly support in the lab rotation.

I also gratefully acknowledge Professor Toshi Nagata in Meijo University, Professor Hidehiro Sakurai in Osaka University, Assistant Professor Shuhei Higashibayashi, Associate Professor Norie Momiyama, Assistant Professor Atsuto Izumiseki, Assistant Professor Takuya, Kurahashi in the Institute for Molecular Science, Assistant Professor Koji Yamamoto in Tokyo Institute of Technology, and the other members and invited speakers in the joint seminar for a enlightening discussion of chemistry.

I would like to thank Professor Huw M. L. Davies, his group members and Dr. John Bacsa, crystallographer in Emory University for the evaluation of catalytic activity of may compound, many helpful advices and invaluable experiences through the internship.

I gratefully acknowledge the financial support of the Research Fellowships of the Japan Society for the Promotion of Science for Young Scientists.

Finally, I offer thanks to my parents, Morio Itoh and Hiromi Itoh, and my brother Toshiaki Itoh, and my sister Yukako Itoh, and my girlfriend Yuka Kameda for their continuous, warm-hearted encouragement.

List of Publications

Chapter 1

"Arene-perfluorarene Interactions for Crystal Engineering of Metal Complexes: Controlled Self-assembly of Paddle-wheel Dimers"
Takahiro Itoh, Mio Kondo, Mari Kanaike and Shigeyuki Masaoka
CrystEngComm, **2013**, *15*, 6122–6126.
(Included in this thesis)

Chapter 2

"Porous Frameworks Constructed by Non-Covalent Linking of Substitution-Inert Metal Complexes"
Takahiro Itoh, Mio Kondo, Hirotoshi Sakamoto, Kaori Wakabayashi, Mari Kanaike, Kenichiro Itami and Shigeyuki Masaoka
Dalton transactions, **2015**, *44*, 15334–15342.
(Included in this thesis)

Chapter 3

Takahiro Itoh, Mio Kondo, Marine Simoen, Masahiro Teramoto and Shigeyuki Masaoka
Manuscript in preparation.

Chapter 4

Takahiro Itoh, Mio Kondo and Shigeyuki Masaoka
Manuscript in preparation.

Other Publications

"Dispersed Ru Nanoclusters Transformed from a Grafted Trinuclear Ru Complex on SiO_2 for Selective Alcohol Oxidation"
Satoshi Muratsugu, Min Hwee Lim, **Takahiro Itoh**, Wipavee Thumrongpatanarks, Mio Kondo, Shigeyuki Masaoka, T. S. Andy Hor and Mizuki Tada
Dalton Transactions, **2013**, *42*, 12611-12619.